MICROGLIA RESPONSES IN A RAT MODEL OF CHRONIC SLEEP RESTRICTION

by

Shannon E. Hall

Submitted in partial fulfillment of the requirements
for the degree of Doctor of Philosophy

at

Dalhousie University
Halifax, Nova Scotia
August 2020

© Copyright by Shannon E. Hall, 2020

TABLE OF CONTENTS

LIST OF TABLES

LIST OF FIGURES

ABSTRACT

Recent research suggests that the brain and body adapt to chronic sleep restriction (CSR) resulting in only modest attempts to recover lost sleep and negatively impacting health over time. Microglia, the immune cells of the brain, are possible mediators of this adaptation to CSR, yet their responses to CSR in key keep/wake regulatory brain regions remained to be characterized. Therefore, I investigated microglia responses to CSR using a rat model featuring slowly rotating wheels (3 h on/1 h off). Adult male rats were sleep restricted for 3, 27 or 99 h, or 99 h followed by 6 days of undisturbed recovery sleep along with several time-matched housing and activity control groups.

First, using the microglia marker ionized calcium-binding adaptor molecule-1 (Iba1), I found that the number of Iba1-immuoreactive cells and the density of Iba1 immunoreactivity were increased in 4/10 brain regions involved in sleep/wake regulation and cognition after 27 and/or 99 h of CSR. Neither microglia proliferation nor impaired blood–brain barrier permeability appeared to contribute to the increased Iba1 immunoreactivity. In the frontal cortex and lateral hypothalamus, two brain regions that showed increased Iba1 in response to CSR, Iba1+ microglia appeared ramified in all treatment groups with no effect of CSR.

Next, I demonstrated using qRT-PCR that after 27 h, but not 99 h, of CSR, mRNA levels of the anti-inflammatory cytokine interleukin-10 were increased in the frontal cortex. Pro-inflammatory cytokine mRNA levels (tumor necrosis factor-α, interleukin-1β, and interleukin-6) were unchanged. Furthermore, cortical microglia were not immunoreactive for several inflammatory markers but were immunoreactive for the P2Y12 receptor. Collectively, these results suggest a homeostatic microglia phenotype.

Finally, I investigated the functional role of CSR-responsive microglia by examining the structural relationship of microglia with two major populations of sleep/wake-regulatory neurons, namely melanin-concentrating hormone (MCH) and orexin (ORX) neurons in the lateral hypothalamus. Microglia were found in close contact with both MCH and ORX neurons and this microglia–neuron contact remained unaltered following CSR.

These results suggest that microglia respond to CSR while remaining in a physiological state and may contribute to the previously reported homeostatic and adaptive responses to CSR.

LIST OF ABBREVIATIONS USED

ABC	Avidin-biotin-horseradish peroxidase complex
ANOVA	Analysis of variance
Arg1	Arginase-1
B2M	Beta-2-microglobulin
BDNF	Brain-derived neurotrophic factor
BrdU	Bromodeoxyuridine
CNS	Central nervous system
CSR	Chronic sleep restriction
COX-2	Cyclooxygenase-2
DAB/Ni	Diaminobenzidine/nickel
EC	Exercise control
EEG	Electroencephalogram
EB	Evans Blue
FITC	Fluorescein isothiocyanate
GAPDH	Glyceraldehyde-3-phosphate dehydrogenase
GFAP	Glial fibrillary acidic protein
GABA	γ-aminobutyric acid
HPRT	Hypoxanthine phosphoribosyltransferase
Iba1	Ionized calcium-binding adaptor molecule-1
IL6	Interleukin-6
IL10	Interleukin-10
IL1β	Interleukin-1β
IP	Intraperitoneal
Ir	Immunoreactive
LPS	Lipopolysaccharide
LW	Locked wheel
MCH	Melanin-concentrating hormone
MR	Mannose receptor
NREM	Non-rapid eye movement
ORX	Orexin (also known as hypocretin)
PeF/LH	Perifornical lateral hypothalamic area
PrL	Prelimbic cortex
qRT-PCR	Quantitative reverse transcriptase-polymerase chain reaction
REC	Recovery
sc-RNAseq	Single-cell RNA sequencing
SD	Sleep deprived
SEM	Standard error of the mean
SR	Sleep restriction
TBS	Tris-buffered saline
TNFα	Tumor necrosis factor-α
REM	Rapid eye movement

ACKNOWLEDGEMENTS

I'd like to express my sincerest gratitude to my supervisor, **Dr. Kazue Semba**. Thank you for welcoming me into your lab all those years ago. Your wealth of knowledge is astounding, and your constructive criticisms pushed me to sharpen my thinking and improve my scientific writing. Thank you for giving me the freedom to pursue my passions both within and outside of the lab, as well as for all of the opportunities to travel and grow as a scientist. I will never forget my time as a member of the Semba Lab family.

To **Dr. Samüel Deurveilher**, I thank you for your endless guidance and patience. You are an incredible teacher and your expertise was invaluable for the development and implementation of my research questions. Thank you for always being available to talk, give advice, and lend a hand.

Joan Burns, thank you for providing your technical expertise and for the many, many hours training me in immunohistochemistry and animal handling. You were always there to help me troubleshoot and never failed to put a smile on my face when times were tough – I will miss our lab chats!

Thank you to **Dr. Ying Zhang** for chairing my committee meetings and for the feedback during my defence; to **Dr. Turgay Akay** for participating on my comprehensive exam committee; to **Dr. William Baldridge** for filling in on my committee when needed and being a caring and supportive Department Head; to **Dr. Mark Opp** for graciously acting as my external examiner and for helping me see the 'big picture' of my research.

I am very thankful to **Dr. George Robertson** for sharing his knowledge and expertise, as well as for his insightful comments during my committee meetings and thesis defence. Thank you for providing the space and equipment for qRT-PCR. Additional thanks to Robertson Lab members **Alix Lammie** and **Elizabeth Belland** for teaching me qRT-PCR methodology and for ample help with troubleshooting.

Thank you to members of the Semba Lab, **Eleri McEachern**, **Brock Saumure,** and **Natalie Barthel,** for their help with data acquisition and analysis. It was a pleasure working with all of you! Additional thanks to **Dr. Chantalle Briggs** for her expertise in apposition analysis and for being a great friend both within and outside of the lab. Thank you to **Kristin Ko** for her support of my research over the years and for being a great source of positivity. **Maxine Profitt**, I am forever grateful to have met you in the Semba lab! From the fun times in lab, to the continuous support during thesis writing – I am so thankful for you. To **Liam Rice**, **Qendresa Sahiti**, **Cameron Stanley**, **Foroozan Keshavarzi**, and **Iona Stylianides**, thank you for your assistance with data analysis and for giving me my first experience as a research supervisor! Thank you to past and present Semba Lab members: Tatjana Golovin, Jess Wallingford, Madjou Bah, Andrew Baldin, Michael Antonchuk, Stephanie Shewchuk, Jesse Langille, Mikaela Friedrich, Greg Warren, Kevin Bradley, and Tareq Yousef.

Special thanks to **Stephen Whitefield** and **Brianne Lindsay** for lending their expertise and assistance with microscopy. **Dr. Ellen Parker**, **Dr. Alon Friedman**, and **Kay Murphy**, thank you for your insightful discussions of blood-brain barrier permeability and for providing brain tissue for antibody testing. On the same note, thank you to **Dr. Drew DeBay** for also providing brain tissue to test antibodies. Thank you to **Dr. Dan Marsh** for access to an extra microscope, **Dr. John Frampton** for access to a microplate reader, and **Dr. Angelo Iulianella** for access to a NanoDrop. To members of the **Dalhousie Animal Care Staff**, thank you for supporting my animal research and the special care you took looking after my animals and answering my questions.

To my partner **Cody Higgins**, you are an endless source of love and support. You are my biggest cheerleader and I don't think I could've made it through the homestretch without you. I appreciate the support you've given me to follow my passions and I'm so incredibly lucky to have you in my life.

I couldn't have completed this work without the endless love and support from my family – my parents **Ron** and **Ginny Hall**, my sister **Katie Hall** and her husband **Alex Kehoe**. I appreciate you always encouraging and motivating me. You are always there for me and support me in everything I do. I wouldn't be who I am today without you and I feel so lucky to have such an incredible family support system. I love you.

Thank you to my wonderful friends – thank you for being an endless source of support, encouragement, and inspiration. **Julia Harrison** (thank you for also being my thesis writing guru!), **Ali Muise-Hennessey**, **Adelle Marshall**, **Kaitlyn Keller**, **Maral Aali**, **Olivier D. Laflamme**, **Antonios Diab**, **Emily Capaldo**, **Jess Clark**, members of FMGSS and MNGSS, and all of the amazing humans I've met in grad school – I'm so grateful to have met you and for the memories we've made.

I'd also like to acknowledge those that provided financial assistance to support me and my research: **Dalhousie Faculty of Graduate Studies**, **Dalhousie Department of Medical Neuroscience**, **Canadian Institutes of Health Research**, and **Dalhousie Medical Research Foundation.**

CHAPTER 1

INTRODUCTION

1.1 Sleep Loss in Society

1.1.1 Impacts of sleep loss

Despite several proposed theories with substantial supporting evidence, the function of sleep remains a controversial topic. What is agreed upon, however, is that sleep is an essential physiological process that is crucial for healthy functioning of the brain and body (Banks & Dinges, 2007). Despite this, modern society has embraced a "24/7" culture, resulting in extended work hours and around-the-clock societal and professional pressures that often come about at the expense of sleep (Walker, 2019). Various medical conditions and sleep disorders also affect one's ability to obtain sufficient amounts of sleep (Banks & Dinges, 2007). Therefore, a great number of people in modern society habitually get less sleep than the recommended 7-9 h per day (Chaput, Wong, & Michaud, 2017).

Sleep loss has profound societal and economic consequences. A strong association has been found between subjective sleepiness in drivers and the risk of motor vehicle accidents (Bioulac et al., 2017), including an increased risk of injury or death in the event of an accident (Connor et al., 2002). Likewise, extended work hours and prolonged wakefulness can lead to an increased risk of traffic accidents (McEwen & Gianaros, 2011). Habitual sleep loss also places a substantial economic burden on the health care system. Insufficient sleep is estimated to cost the Canadian economy more than $20 billion yearly due to lost productivity, workplace absences, increased accident risk, and increased health care costs (Hafner, Stepanek, Taylor, Troxel, & van Stolk, 2016). Participants who met the diagnostic criteria for insomnia have been found to report more work absences, decreased productivity, and instances of chronic health problems than those categorized as "good sleepers" (Daley, Morin, LeBlanc, Gregoire, & Savard, 2009). It was also

found that individuals reporting poor sleep took more medication and made more health care visits than good sleepers (Linton & Bryngelsson, 2000).

1.1.2 Chronic sleep restriction (CSR)

Common forms of sleep loss include acute sleep deprivation, sleep fragmentation, and chronic sleep restriction (CSR). Acute sleep deprivation occurs when sleep is eliminated for a single, prolonged (i.e., 24 h) period of time (Short & Banks, 2014). Sleep fragmentation results from repeated awakenings that interrupt sleep, a phenomenon associated with many sleep and health disorders (Reynolds & Banks, 2010). CSR occurs when sleep is reduced below optimal levels for long periods of time (i.e., days, weeks, or years) and is the most common form of sleep loss experienced in everyday life (Basner, Rao, Goel, & Dinges, 2013).

CSR impacts a wide range of physiological functions resulting in an increased risk of metabolic dysfunction, including obesity and diabetes (Colwell & Matveyenko, 2014), disordered mood (Haack & Mullington, 2005), cardiovascular dysfunction (Faraut, Boudjeltia, Vanhamme, & Kerkhofs, 2012), and altered immune responses (Vgontzas et al., 2005).

In addition to physiological functions, CSR profoundly affects behavioural alertness and cognition. Deficits in sustained attention, learning and memory, and higher-order processes such as decision making are observed in response to CSR (Reviewed in (McCoy & Strecker, 2011)). Sustained attention performance, commonly assessed using the psychomotor vigilance task, is very sensitive to sleep loss and severely deteriorates over consecutive days of CSR (Dorrian, Rogers, & Dinges, 2005; Van Dongen, Maislin, Mullington, & Dinges, 2003). Individuals that sleep <7 h/night on consecutive nights also show impaired sustained attention and working memory functions (Van Dongen et al., 2003). Interestingly, subjective reports of sleepiness do

not match the accumulation of deficits in cognitive performance observed following CSR. Subjects rate themselves as only moderately sleepy, despite showing progressive impairment on tests of behavioural alertness (Belenky et al., 2003; Van Dongen et al., 2003).

It is important to understand the mechanisms in the brain and body that are involved in the physiological and behavioural impacts of CSR, in order to develop targeted strategies and treatments for those suffering from chronic sleep loss. Animal models are advantageous for studying the complexities of biological functions and have been an essential tool in sleep research to understand the impacts of CSR, as discussed below.

1.2 Rat Models of CSR

1.2.1 The '20/4' protocol

Several rodent models have been developed and used to study CSR that feature alternating periods of sleep deprivation and sleep opportunity (Deurveilher & Semba, 2019). Apparatuses such as disk-over-water platforms (Everson & Szabo, 2009; Leemburg et al., 2010), treadmills (Bjorness, Kelly, Gao, Poffenberger, & Greene, 2009; Clasadonte, McIver, Schmitt, Halassa, & Haydon, 2014) and slowly rotating activity wheels (Deurveilher, Rusak, & Semba, 2012; Meerlo, Koehl, van der Borght, & Turek, 2002) have been used to achieve periods of sleep deprivation. Alternatively, gentle stimulation and/or environmental enrichment may also be used (Bellesi et al., 2017; Zhang et al., 2014). Several sleep restriction studies feature alternating, single, daily periods of sleep deprivation and sleep opportunity. A commonly used paradigm is the "20/4" CSR protocol in which animals are sleep-deprived daily for 20 h followed by 4 h of sleep opportunity, over several days (Y. Kim, Laposky, Bergmann, & Turek, 2007; Leemburg et al., 2010). Although the "20/4" CSR model has been useful in studying the neurobiological and

physiological effects of cumulative sleep loss, this protocol does not reflect the polyphasic sleep cycle of rats. Sleep patterns in nocturnal rodents are not consolidated within a single period but rather are distributed across 24 h, with a higher concentration of sleep spent in the light (inactive) than dark (active) phase (Trachsel, Tobler, Achermann, & Borbely, 1991).

1.2.2 The '3/1' protocol

To better reflect the polyphasic sleep cycle of rats, a "3/1" CSR model was developed in our lab that features slowly rotating programmable activity wheels (Deurveilher et al., 2012). In this model, sleep is restricted through cycles of 3 h of sleep deprivation, at which time the wheel slowly rotates, followed by 1 h of sleep opportunity, during which the wheel remains stationary, for 4 continuous days resulting in a total of 18 h sleep deprivation and 6 h sleep opportunity per day. The 3/1 CSR protocol reduces total daily sleep time by 60% compared to baseline levels and initiates both immediate and adaptive changes in sleep patterns (Figure 1; (Deurveilher et al., 2012)), as discussed further in Section 1.3.3. As periods of sleep opportunity occur periodically throughout a 24 h period, this model allows for the study of interactions between homeostatic and circadian processes.

It has been suggested that sleep need may accumulate faster in rats than in humans (Rechtschaffen, 1998) and experimental evidence suggests that a day in the lifespan of an adult rat is equivalent to approximately 35 human days (Sengupta, 2013). Therefore, the 4-day period of CSR imposed by the 3/1 protocol is equivalent to just over 4.5 human months, thus making it an effective model of CSR in rats.

In response to the 3/1 protocol, we have observed changes in sleep patterns (Deurveilher et al., 2012) as well as brain levels of brain-derived neurotrophic factor (BDNF) (Wallingford,

Deurveilher, Currie, Fawcett, & Semba, 2014) and FosB family proteins (Hall, Deurveilher, Ko, Burns, & Semba, 2017), impaired performance on a task of sustained attention (Deurveilher, Bush, Rusak, Eskes, & Semba, 2015) and elevated heart rate and body temperatures (Bah et al., 2014).

1.3 Circadian, Homeostatic, and Allostatic Sleep Regulation

1.3.1 Sleep/wake states

Wakefulness is characterized by high frequency, low amplitude electroencephalogram (EEG) activity (Scammell, Arrigoni, & Lipton, 2017). During sleep, individuals alternate between cycles of non-rapid eye movement (NREM) and rapid eye movement (REM) sleep (Scammell et al., 2017). NREM sleep consists of three stages in humans, ranging from "light" to "deep" sleep, with synchronous, low amplitude EEG delta activity (i.e., slow wave sleep) characterizing the deepest stage. REM sleep is distinguished by high frequency, low amplitude EEG activity in conjunction with skeletal muscle atonia and rapid horizontal eye movements (Scammell et al., 2017).

1.3.2 Circadian and homeostatic processes

The timing and duration of sleep are determined by the interactions between circadian and homeostatic processes, according to the two-process model (Borbely, 1982). The circadian process is governed by the principal circadian clock located in the suprachiasmatic nucleus of the hypothalamus in mammals (Moore, 2007). This endogenous clock is based on transcription/translation feedback loops of clock genes and has a period of approximately 24 h. The circadian clock is normally entrained to the light/dark cycle via the photic input it receives

from the retina. Through its neuronal and non-neuronal output pathways, the principal circadian clock influences virtually all functions in the body including sleep. Thus, the clock modulates sleep/wake timing, creating a rest-activity rhythm that is normally entrained to the light/dark cycle of the environment (Borbely, Daan, Wirz-Justice, & Deboer, 2016; Mistlberger, 2005). Markers of the circadian process include core body temperature and melatonin secretion rhythms (Dijk & Duffy, 1999; Scammell et al., 2017). While circadian rhythms in humans result in a single monophasic sleep period, sleep in many animals, including rodents, is polyphasic with alternating cycles of short sleep and wake bouts throughout a 24 h period, yet with greater occurrences of sleep in the inactive phase (Mistlberger & Rusak, 2005).

The homeostatic process monitors sleep propensity and homeostatic mechanisms maintain the physiological processes underlying sleep by offsetting departures from normal sleep levels. Homeostatic pressure or "sleep need" builds during periods of wake and dissipates during sleep. NREM sleep EEG delta power is a commonly used marker of sleep intensity based on sleep need (Borbely & Achermann, 1999). Recent research has further suggested the decay of the intensity of EEG delta power as a measure of the resolution of sleep need (Greene, Bjorness, & Suzuki, 2017). BDNF and adenosine have been suggested as molecular substrates of sleep pressure or need (Greene et al., 2017; Huber, Tononi, & Cirelli, 2007).

1.3.3 Allostatic process

In addition to circadian and homeostatic processes, a third aspect of sleep regulation has been proposed and is referred to as allostasis (McEwen & Stellar, 1993). Studies using animal models found that homeostatic sleep/wake mechanisms respond to CSR differently than to acute sleep deprivation. During recovery sleep following acute sleep deprivation, robust increases are

observed in NREM sleep and NREM EEG delta power (a measure of sleep intensity) (Borbély & Neuhaus, 1979). In contrast, several studies using different sleep restriction protocols in rats, including our own 3/1 CSR protocol, have shown that CSR is followed by only moderate sleep recovery and transient increases in NREM EEG delta power (Clasadonte et al., 2014; Deurveilher et al., 2012; Y. Kim et al., 2007; Leemburg et al., 2010; Stephenson, Caron, & Famina, 2015), suggesting adaptation to repeated sleep restriction. Using our rat 3/1 CSR protocol, NREM EEG delta power initially increased after one day of CSR but gradually declined over the following three days of CSR, albeit remaining above baseline levels; there was no recovery of lost NREM sleep delta power during the subsequent 2 days of recovery. Both NREM and REM sleep amounts showed only modest recovery after two days of recovery sleep, reflecting cumulative sleep deficits (Deurveilher et al., 2012). These results indicate that the 3/1 protocol induced both homeostatic and allostatic compensatory processes over 4 days of CSR (see Figure 1).

There is far less evidence for adaptive responses to CSR in humans. However, one study examined changes in sustained attention performance in humans using the psychomotor vigilance task, a reaction task measuring a subject's sustained attention as well as speed and accuracy in responding to a randomly presented visual stimulus, following 7 days of CSR (Belenky et al., 2003). Subjects that received 9 h of sleep per night showed baseline levels of response speed and lapses, while those that received only 3 h of sleep per night showed increased reaction time and greater lapses. Subjects that received either 7 or 5 h of sleep per night showed an initial degradation in their performance, followed by stabilization at this reduced level. While task performance improved in response to 3 days of recovery sleep in subjects that received 3 h of sleep per night, recovery remained incomplete (Belenky et al., 2003). In another study, NREM

EEG patterns were also found to exhibit an initial acute response (increase) to sleep restriction, followed by insignificant further increases over the two weeks of CSR, providing evidence of CSR-induced changes and adaptation in sleep patterns (Van Dongen et al., 2003). Collectively, these results provide evidence that sleep/wake-regulatory systems adapt to CSR.

Adaptive responses to CSR are consistent with the concept of allostasis – the adjustment of homeostatic processes in response to changing environmental conditions (Goldstein & McEwen, 2002). Allostasis is thought to be controlled by a non-linear (i.e., reciprocally regulated) network of mediators, including glucocorticoids, parasympathetic and sympathetic nervous system activity, and cytokines, that are involved in the body's stress response (McEwen, 2006). Prolonged activation of these mediators can result in an 'allostatic load' characterized by the cumulative 'wear and tear' on internal systems from continuous adaptation (McEwen & Karatsoreos, 2015). CSR likely contributes to an allostatic load, resulting in altered sleep/wake regulation and negatively impacting cognition and health (Laposky, Bass, Kohsaka, & Turek, 2008).

The neurobiological basis of allostatic adaptation to CSR, and subsequent allostatic load, remains largely unexplored. However, recent studies from our lab suggest that the molecular markers of chronic neuronal activation FosB/ΔFosB (Hall et al., 2017) and BDNF, a neurotrophic factor involved in the regulation of NREM sleep EEG delta activity (Wallingford et al., 2014), may be involved in these allostatic mechanisms. To study the neurobiological mechanisms underlying CSR-induced changes in sleep patterns, it is important to understand the neural circuitry involved in sleep/wake regulation, as discussed below.

1.4 Neurobiology of Sleep and Wake

1.4.1 Brief overview of the sleep/wake circuit

Alternating states of sleep and wakefulness are controlled by a widely distributed network of mutually antagonistic sleep- and wake-active neurons in the brain stem, hypothalamus, thalamus, and basal forebrain (Fuller, Gooley, & Saper, 2006; Jones, 2020; Saper, 2013; Scammell et al., 2017). Mutual inhibition between these neuronal groups results in a "flip-flop" switch, controlling transitions between sleep and wakefulness (Scammell et al., 2017). Cortical arousal is achieved through the activity of several well-established neuronal groups with specific neurotransmitters.

Monoaminergic and glutamatergic signaling from several wake-promoting nuclei heavily contributes to promoting wakefulness. These include but are not limited to noradrenergic neurons in the locus coeruleus, serotonergic neurons in the dorsal and median raphe nuclei, and glutamatergic neurons in the parabrachial nucleus (Saper, 2013). Ascending axonal projections from these neuronal populations extend through the lateral hypothalamus, which contains overlapping populations of mutually inhibitory sleep/wake-regulatory neurons, including wake-promoting orexin (ORX; also known as hypocretin)-containing neurons and sleep-promoting melanin-concentrating hormone (MCH)-containing neurons (Broberger, De Lecea, Sutcliffe, & Hokfelt, 1998). The role of these neurons in sleep/wake regulation is discussed below.

1.4.2 ORX and MCH neurons

ORX neurons are maximally active during wake and promote arousal (Lee, Hassani, & Jones, 2005; Sakurai, Mieda, & Tsujino, 2010; Takahashi, Lin, & Sakai, 2008). They send dense projections that excite the ascending arousal system, including the monoaminergic neuronal

groups in the locus coeruleus and dorsal raphe nucleus (Peyron et al., 1998). In contrast, MCH neurons fire maximally during REM sleep and are inactive during wake (Hassani, Lee, & Jones, 2009; Tsunematsu et al., 2014) and send projections to inhibit wake-promoting monoaminergic nuclei groups (Saper, 2013). Thus, alternate activation of these neuronal populations occurs in response to sleep loss: ORX neurons are more greatly activated during sleep deprivation, while MCH neurons are activated during sleep recovery (Modirrousta, Mainville, & Jones, 2005). ORX neurons send inhibitory signaling to MCH neurons (Apergis-Schoute et al., 2015) which, in turn, have an inhibitory effect on ORX neurons (Rao et al., 2008), thus creating a negative feedback interaction with the function of fine tuning the output from the lateral hypothalamus. ORX neurons send activating projections to the cortex to produce cortical arousal (de Lecea, 2012), while projections from MCH neurons, along with γ-aminobutyric acid (GABA)-ergic input from other sleep-promoting brain regions, inhibit neurons in the arousal system to induce sleep (Saper, 2013).

The neuroanatomical connections between sleep/wake-regulatory brain regions are fundamental for understanding the control of sleep and wakefulness. However, various molecules mainly of non-neuronal origins also play important roles in regulating sleep and wakefulness, including immune signaling molecules such as cytokines (see below).

1.5 Sleep-Immune Interactions

There is clear evidence for an interaction between the sleep and immune systems, in that immune challenges (e.g., infection) alter sleep, and sleep loss causes immune dysfunction (Imeri & Opp, 2009; Ingiosi, Opp, & Krueger, 2013; Krueger, Majde, & Rector, 2011; Krueger, Obal, Fang, Kubota, & Taishi, 2001). These observations led to the discovery of endogenous sleep-

regulating immune substances in the central nervous system (CNS) (Krueger et al., 2001). For example, the pro-inflammatory cytokines interleukin-1β (IL1β) and tumor necrosis factor-α (TNFα) have been implicated as regulators of physiological sleep. Administration of exogenous IL1β and TNFα was found to increase NREM sleep amounts in animals (Krueger, Walter, Dinarello, Wolff, & Chedid, 1984; Shoham, Davenne, Cady, Dinarello, & Krueger, 1987), while spontaneous NREM sleep was inhibited when the signaling of these cytokines was interfered with or blocked using antibodies or receptor antagonists (Imeri, Bianchi, & Opp, 2006; Opp & Krueger, 1994). Expression of IL1β and TNFα was discovered in sleep/wake-regulatory neuronal populations (Breder, Dinarello, & Saper, 1988; Breder, Tsujimoto, Terano, Scott, & Saper, 1993). In addition, brain levels of IL1β and TNFα mRNA show diurnal variations with peak expression coinciding with the onset of sleep, when NREM sleep propensity is maximized (Floyd & Krueger, 1997; Taishi, Bredow, Guha-Thakurta, Obal, & Krueger, 1997). Furthermore, the anti-inflammatory cytokine interleukin-10 (IL10) has the opposite effect on sleep. A study conducted in rabbits found that administration of exogenous IL10 during the light phase (sleep period) inhibited NREM sleep (Kushikata, Fang, & Krueger, 1999), possibly through its inhibitory effects on TNFα and IL1β expression (Krueger et al., 2001).

In addition to changes during spontaneous sleep, cytokine expression is altered in response to sleep loss. For example, sleep deprivation for 48 and 72 h increased TNFα, IL1β, interleukin-6 (IL6) and interleukin-8 protein levels in the rat hippocampus, while reducing IL10 protein expression (Wadhwa et al., 2017). Additionally, IL1β and TNFα mRNA and proteins levels are elevated in the rat cortex, hippocampus, and/or basal forebrain following CSR for 5 days (Zielinski et al., 2014) and 21 days (Manchanda, Singh, Kaur, & Kaur, 2018) in rats.

Collectively, these studies have delineated a clear role for cytokines in contributing to physiological sleep regulation and in responses to sleep loss. Microglia are the primary producers of cytokines in the CNS (Delpech et al., 2015; Kettenmann, Hanisch, Noda, & Verkhratsky, 2011) and are therefore of particular interest for studying the neuroimmune response to sleep loss.

1.6 Microglia: Immune and Homeostatic Functions

1.6.1 Microglia: A brief introduction

Microglia were first characterized in detail in the early 20th century by Pío del Río-Hortega and determined to be morphologically distinct from other brain glia, such as astrocytes and oligodendrocytes, leading Río-Hortega to call them microglia (Del Rio-Hortega Bereciartu, 2020). Many advances since their discovery have resulted in an enormous level of insight into microglia origins and functions in both the healthy and diseased brain.

Microglia are derived from primordial myeloid cell progenitors in the yolk sac (Ginhoux et al., 2010), a developmental lineage that is ontogenetically distinct from other brain glia, as well as other CNS macrophages (Prinz, Jung, & Priller, 2019). Microglia populate all areas of the adult brain with individual cells occupying distinct, non-overlapping territories (Kettenmann et al., 2011). In the non-pathologic brain, microglia morphology is characterized by a small cell body with long, highly branched processes (Karperien, Ahammer, & Jelinek, 2013).

Microglia are capable of self-renewal and are maintained throughout life by local proliferation (Bruttger et al., 2015). Indeed, fate mapping has revealed that, following pharmacological depletion, microglial repopulation derives from the proliferation of residual microglia, as opposed to microglia progenitor cells (Huang et al., 2018).

Recent research has uncovered brain regional differences in microglia density, turnover rates, morphology, and molecular signatures (Tan, Yuan, & Tian, 2020), establishing microglia as a versatile, heterogenous population. Despite this acknowledged heterogeneity, more research is needed to understand the functional consequences of region-specific microglial features.

1.6.2 Microglia as regulators of neuroimmune responses

Originally, microglia were thought to be in a "resting" state in the normal brain and become "activated" in response to pathology. As the resident immune cells of the CNS, the role of microglia in brain disease progression and in responding to brain injury or infection is well-characterized (summarized in Figure 1.2). Microglia respond to pathological changes in the brain by thickening and retracting their processes and enlarging their cell bodies, reflecting an immunologically activated state (Karperien et al., 2013). "Activated" microglia were thought to polarize within a spectrum between a classical "M1" activation state and an alternative "M2" activation state (Orihuela, McPherson, & Harry, 2016). 'Classically activated' microglia are considered mediators of pro-inflammatory responses, such as antigen presentation, pathogen removal, and adaptive immune response initiation. In contrast, 'alternatively activated' microglia resolve inflammatory processes through tissue remodeling, angiogenesis, and the production of anti-inflammatory molecules (Orihuela et al., 2016). During microglia inflammatory responses, peripheral macrophages can be recruited to the CNS; while remaining distinct from resident microglia, these infiltrating macrophages may provide additional neurotrophic support or aid in disease resolution (Butovsky & Weiner, 2018; London, Cohen, & Schwartz, 2013).

Notably, the validity of "M1" and "M2" categorization has been questioned by recent advances in neuroimaging and genetic phenotyping, particularly at the single-cell level

(Hammond et al., 2019). The latter technology has led to the discovery of new microglia-specific genes and transcriptional signatures during various disease states (Ransohoff, 2016). It is now recognized that microglia responses fail to conform to the dichotomous "M1" and "M2" classification and instead show disease-specific changes in morphology and function, as well as a diversity of roles in the non-diseased brain (Masuda, Sankowski, Staszewski, & Prinz, 2020).

1.6.3 Microglia as regulators of brain homeostasis

Microglia in the healthy brain are anything but "resting" cells, with roles extending from maintaining brain homeostasis to contributing to neural circuit maturation and plasticity (Wake, Moorhouse, Miyamoto, & Nabekura, 2013) (Figure 1.2A). Non-immunologically activated (i.e., homeostatic) microglia continuously extend and retract their highly motile processes to survey the local brain environment, revealing physiological microglia as 'attentive housekeepers' in the adult brain (Davalos et al., 2005; Nimmerjahn, Kirchhoff, & Helmchen, 2005). During development, microglia engulf synaptic material and, thus, are major contributors to synaptic pruning through several signalling pathways, including complement-, fractalkine-, and purinergic-dependent pathways (Paolicelli & Gross, 2011; Schafer et al., 2012; Sipe et al., 2016; Weinhard et al., 2018). In the mature brain, microglia regulate neurogenesis in the hippocampal dentate gyrus by phagocytosing apoptotic neuron progenitors and releasing soluble substances that affect neural progenitor proliferation (Choi, Cho, Hoyt, Naegele, & Obrietan, 2008; Sierra et al., 2010). Microglia also contribute to the plasticity of neuronal circuits by interacting with neuronal elements, such as axons, spines, and synapses (Tremblay et al., 2011; Wake, Moorhouse, Jinno, Kohsaka, & Nabekura, 2009), in a neuronal activity-dependent manner (Tremblay et al., 2011). Indeed, it is suggested that microglia sense synaptic activity as they

express a variety of neurotransmitter receptors (e.g., monoamine and glutamate receptors; (Pocock & Kettenmann, 2007)) and closely contact neurons with both their cell bodies and processes (Baalman et al., 2015; Wogram et al., 2016).

Increased occurrences of microglia–synapse contact may contribute to neuronal firing synchronization. A recent study found that under anesthesia microglia process contact on a synapse led to increased activity at that specific synapse and increased the synchronization of local neuron population activity (Akiyoshi et al., 2018). Additionally, 3D electron microscopy of immunologically activated microglia revealed the close apposition of microglia processes around cortical neuron cell bodies that resulted in the displacement of inhibitory synapses on the neuron soma and increased neuronal firing synchronization (Z. Chen et al., 2014). Microglia contact may also occur for neuroprotective purposes. In response to neuroinjury, microglia processes increase their somatic coverage of damaged, but still viable, cortical neurons via purinergic P2Y12 receptor signaling (Cserep et al., 2020). Homeostatic microglia have also been found to closely appose neurons in the cortex and hippocampus in a similar manner (Baalman et al., 2015; Wogram et al., 2016). The specific purpose of this type of microglia–neuron contact is unknown but may serve a neuroprotective function.

1.6.4 Ionized calcium-binding adaptor molecule-1 (Iba1) as a microglial marker

Various immunohistochemical markers have been identified and characterized that discriminate microglia from other brain cells and/or provide information on microglia activity state. One of the first discovered and most commonly used markers is ionized calcium-binding adaptor molecule-1 (Iba1), a microglia/macrophage-specific protein involved in calcium homeostasis, actin-bundling activity, and cytoskeletal reorganization (Kettenmann et al., 2011;

Ohsawa, Imai, Sasaki, & Kohsaka, 2004). Iba1 is expressed by microglia in all activity states and is upregulated in response to a variety of stimuli, including chronic stress (Hinwood, Morandini, Day, & Walker, 2012), neurodegenerative disease (Xu et al., 2017), brain injury (Ito, Tanaka, Suzuki, Dembo, & Fukuuchi, 2001), and infection (Kondo, Kohsaka, & Okabe, 2011). However, Iba1 is expressed by both microglia and other brain macrophages and is limited in its ability to provide information on microglia activity state. Therefore, additional markers are needed to discriminate microglia from other macrophages and to provide insight on microglia function. A list of the microglia immunohistochemical markers used in the experiments described in this thesis can be found in Appendix A, Table A.1.

1.7 Sleep and Microglia

1.7.1 Microglia activity across the light/dark cycle

Diurnal changes in microglia process extension/retraction and subsequent interactions with synapses have been observed in the rodent cortex. Mouse cortical microglia are shown to extend their processes during the dark (active) phase and retract them during the light (inactive) phase (Hayashi et al., 2013). These diurnal changes in process extension and retraction were associated with a greater incidence of microglia-synapse contact during the dark compared to the light phase that was found to be dependent on P2Y12 receptor expression (Hayashi et al., 2013). In the adult rat prefrontal cortex, phagocytosis of synapses by microglia was enhanced at the onset of the light phase compared to the onset of the dark phase (Choudhury et al., 2020).

1.7.2. Microglia activity during wakefulness

Studies using *in vivo* two-photon imaging in awake mice have provided important insights into microglia dynamics. During wake, microglia processes are highly motile, moving through continuous cycles of extension and retraction and making frequent contact with neuronal synapses (Nimmerjahn et al., 2005). These microglia–synapse interactions have been shown to result in increased activity at the contacted synapse, leading to increased synchrony of local neuron firing (Akiyoshi et al., 2018).

Several recent studies investigating microglia process dynamics in wake versus anaesthesia in mice have observed a reduction in microglia surveillance activities during wake compared to anaesthesia conditions (Liu et al., 2019; Stowell et al., 2019; Sun et al., 2019); it is not known whether these alterations in microglia surveillance under wake versus anaesthesia conditions exhibit diurnal changes. Two of these studies implicated noradrenergic signaling in the inhibition of microglia process motility during wake (Liu et al., 2019; Stowell et al., 2019). Noradrenaline is a potent neuromodulator of wakefulness and arousal (Berridge, Schmeichel, & Espana, 2012), therefore these studies not only emphasize the importance of studying microglia dynamics during wake/sleep cycles in non-anaesthetized animals, but also reveal a role for the wake-related neurotransmitter noradrenaline in the regulation of microglia surveillance activities.

1.7.3 Microglia responses to sleep loss

Microglia have been shown to respond to sleep loss, with a particular focus on cognitive-related brain regions in earlier studies. Microglia increased in number and displayed larger cell bodies with thickened processes in the hippocampus after 5 days of sleep fragmentation in rats (Hsu et al., 2003). An increased number of microglia was also found in the mouse hippocampus

at least one week after 24 h of sleep disruption (B. Zhu et al., 2012) and in the hypothalamus of mice fed a high fat diet after 3 or 9 days of sleep fragmentation (Ho, Ducich, Nguyen, & Opp, 2018). Following 48 and 72 h of sleep deprivation in rats, microglia increased in number in the hippocampus in parallel with increased levels of pro-inflammatory cytokines (Wadhwa et al., 2017). Furthermore, administration of minocycline, an anti-inflammatory compound that attenuates microglia pro-inflammatory responses, has been shown to suppress acute sleep deprivation-induced increases in sleep need (Wisor, Schmidt, & Clegern, 2011), suggesting a role of microglia in sleep/wake regulation. It should be noted, however, that minocycline is not a microglia-specific inhibitor and could also act through other mechanisms to suppress sleep deprivation-induced sleep need.

More recent studies have shown that microglia–synapse interactions are altered in response to sleep loss. CSR for 4.5 days was shown to enhance microglial engulfment of presynaptic glutamatergic terminals in the adolescent mouse cortex in the absence of obvious signs of neuroinflammation (Bellesi et al., 2017). In contrast, another study observed that microglial phagocytosis of post-synaptic elements was reduced in the adolescent mouse hippocampus following 72 h of sleep deprivation (Tuan & Lee, 2019). In the latter study, sleep deprivation also reduced hippocampal mRNA levels of several microglia-specific proteins including fractalkine and P2Y12 receptors as well as CD11b (Tuan & Lee, 2019), possibly indicating an early-stage inflammatory response.

Collectively, these studies indicate that microglia respond to sleep loss, but much remains to be investigated to understand its nature and mechanisms. Furthermore, microglial regional heterogeneity suggests that microglia may display different sensitivities to sleep loss in different

brain regions and, until now, microglia responses to sleep loss in key sleep/wake-regulatory brain regions had remained uncharacterized.

1.8 Rationales and Hypotheses

While recent studies have shed light on microglial responses to sleep loss, relatively little is known on microglia responses in specific sleep/wake-regulatory brain regions or the role microglia play in sleep/wake regulation. The objective of this thesis was to characterize the microglia response to the 3/1 CSR protocol in rats in order to evaluate their possible role in contributing to the altered, long-lasting sleep responses to CSR. I examined the microglia response to CSR in several brain regions involved in sleep/wake-regulatory and cognitive functions using three approaches (Studies 1−3), all using the 3/1 CSR protocol. The rationale and hypotheses are stated below for each of the three studies. The **principle hypothesis** is that microglia in sleep/wake- and cognitive-related brain areas respond to CSR by altering their morphology, phenotype, and their physical interactions with neurons.

1.8.1 Study 1: Iba1 immunoreactivity following CSR and subsequent recovery

If microglia are a part of the neurobiological mechanisms underlying the homeostatic and/or allostatic responses to CSR, then they may change their expression of Iba1, a well-established marker specific to microglia/macrophages and known to be upregulated in a variety of microglial responses (see Section 1.6.4). I hypothesized that:

1) **Iba1 levels would increase in brain regions involved in sleep/wake, limbic, and/or autonomic regulation in response to CSR,**

2) **Iba1 levels would remain elevated following recovery sleep after CSR,**
3) **Microglia morphology would be altered following CSR to reflect their functional state, and**
4) **Microglia will proliferate and/or peripheral macrophages will be recruited into the brain in response to CSR.**

To test these hypotheses, I examined brain tissue from rats that were sleep restricted for either 3 h, ~1 day (27 h), or ~4 days (99 h) of the 3/1 CSR protocol, sleep restricted for 99 h followed by 6 days of recovery sleep, or left undisturbed (controls). Iba1 immunoreactivity was evaluated in 10 different brain regions, using light microscopy. Microglia proliferation was examined using the cell division marker and Iba1 and blood-brain barrier permeability was assessed using fluorescent tracer injections.

1.8.2 Study 2: Characterization of microglia phenotype in response to CSR

Microglia responses to various stimuli are known to be accompanied by changes in their molecular phenotype (see Section 1.6.2), including the expression of immune-regulating molecules (see Section 1.5). Given the microglia response to CSR observed in Study 1, I hypothesized that:

5) **CSR would induce changes in mRNA expression of inflammatory cytokines in the frontal cortex, and**
6) **The molecular phenotype of microglia would be affected by CSR.**

To test these hypotheses, I measured brain levels of several inflammatory cytokines using quantitative reverse transcriptase-polymerase chain reaction (qRT-PCR) on frontal cortex tissue of rats that were sleep restricted for either 27 or 99 h of CSR, or left undisturbed (controls). Additionally, I used qualitative dual immunohistochemistry to assess inflammatory and homeostatic markers of microglia molecular phenotype.

1.8.3 Study 3: Microglia contacts on ORX and MCH neurons in the lateral hypothalamus following CSR

Physical interactions between microglia and specific populations of sleep/wake-regulatory neurons remain to be characterized. Therefore, I asked whether microglia contact wake-active ORX and sleep-active MCH neurons in the PeF/LH and, if so, whether CSR would alter these contacts in a cell type-specific fashion. Specifically, I hypothesized that:

7) Microglia contact ORX and MCH neurons in a neuronal activation state-dependent manner, and

8) Microglia-neuron contacts in the PeF/LH are altered, and occur in a cell type-specific manner, in response to CSR.

To test these hypotheses, I examined brain tissue from rats that were sleep restricted for either 27 or 99 h, exercise control rats, and undisturbed control rats. I performed quantitative immunofluorescence analysis with microglia, neuropeptides, and neuronal activation markers using confocal microscopy and measured microglia-neuron appositions (processes and cell bodies) within the PeF/LH.

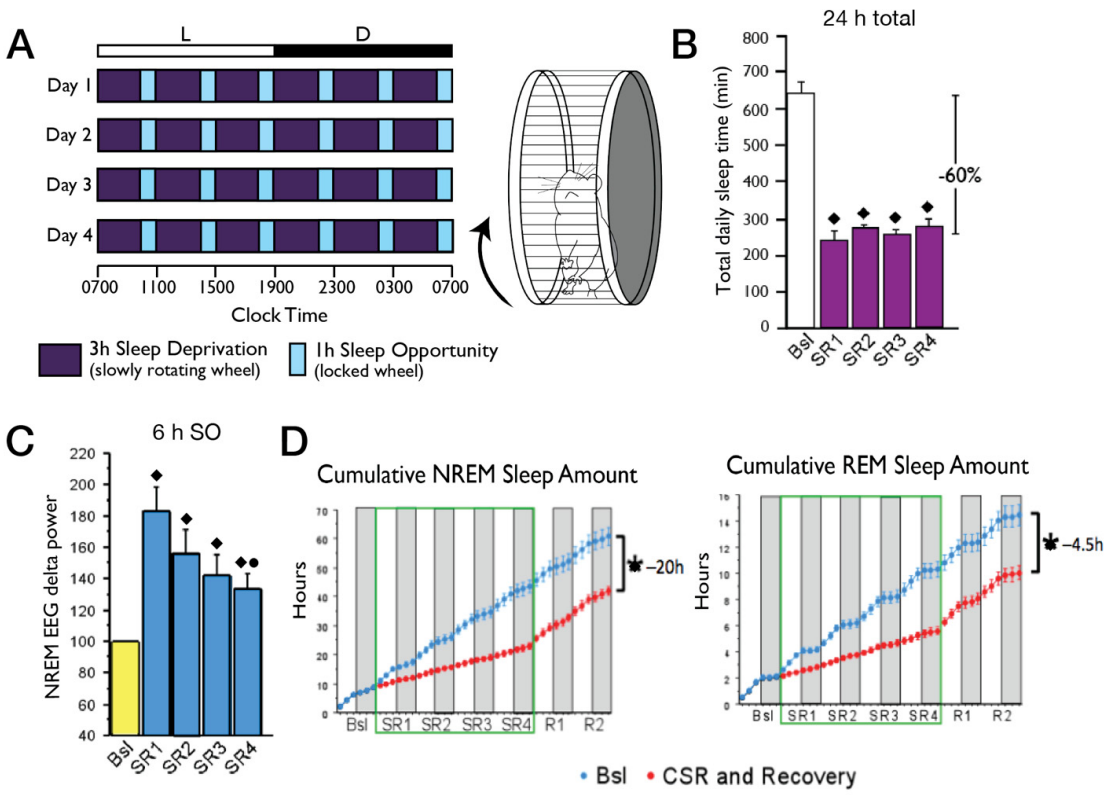

Figure 1.1. Homeostatic and adaptive sleep responses to the "3/1" protocol of chronic sleep restriction (CSR). In the 3/1 CSR model (A), sleep is restricted through repeating cycles of 3 h of sleep deprivation, at which time the motorized activity wheel slowly rotates, followed by 1 h of sleep opportunity where the activity wheel remains locked. Over the four days of CSR (SR1–4), total daily sleep time (B) was reduced by ~60% as compared to baseline levels (Bsl). Total daily sleep time includes both non-rapid eye movement (NREM) and rapid eye movement (REM) sleep during both the 3 h sleep deprivation and 1 h of sleep opportunity. NREM electroencephalogram (EEG) delta (0.5−4 Hz) power (C) during the daily 6 h of sleep opportunity was increased on the first day of CSR (SR1), followed by a gradual decline over the next three days (SR2–4), indicating that the 3/1 protocol induced both homeostatic and adaptive (allostatic) compensatory EEG responses over the 4 days of CSR. In D, cumulative NREM (*left*)

and REM (*right*) sleep amounts in 4-h intervals are shown for Bsl, SR1−4, and 2 days of recovery (R1 and 2) in red, and over the corresponding 6 days in the absence of CSR (i.e., predicted values) in blue. NREM sleep amount that was lost during the 4 days of CSR was not regained during the two days of recovery sleep (R1, R2), resulting in a cumulative deficit of 20 h at the end of R2. REM sleep amount also showed only modest recovery during the two days of recovery sleep, resulting in a cumulative deficit of 4.5 h at the end of R2. In D, the gray shading indicates the 12-h dark phase. Means + SEM (B,C) or means ± SEM (D) are shown (n = 5/group). ♦ and • , Significantly different from baseline and SR1, respectively ($p < 0.05$). (Adapted from (Deurveilher et al., 2012)).

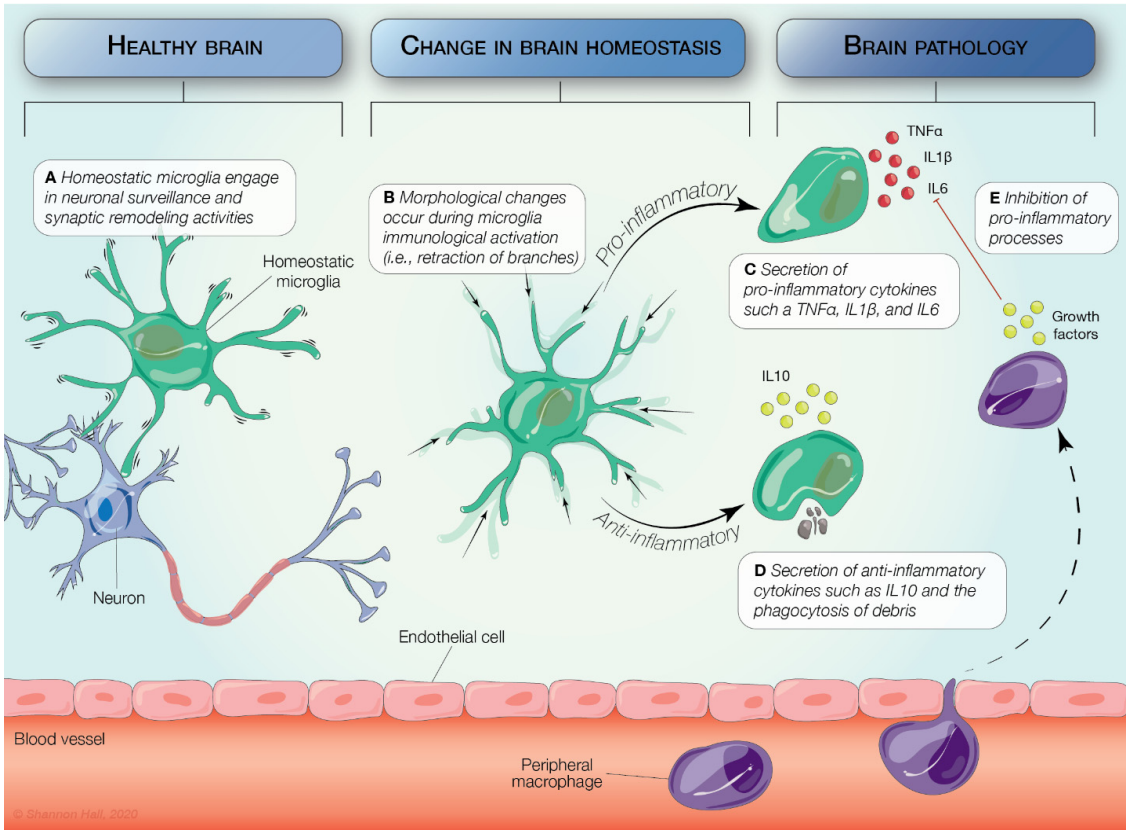

Figure 1.2. Multiple roles of microglia in the brain in healthy and pathological conditions. In the healthy brain (A), microglia exhibit a ramified morphology with a relatively small cell body and contribute to brain homeostasis by participating in phagocytosis, neuronal surveillance, and synaptic remodeling (Wake et al., 2013). In response to a change in brain homeostasis (B) that occurs during brain pathology such as injury or infection, microglia become immunologically activated, enlarge their cell bodies and retract their branches to assume an "ameboid" morphology (Karperien et al., 2013). Immunologically activated microglia upregulate their expression of a variety of molecules including inflammatory cytokines. Depending on the type of signal received, microglia can produce pro-inflammatory cytokines (e.g., interleukin [IL]-1β,

tumor necrosis factor [TNF]−α, and IL6; C) to mediate the initiation of adaptive immune responses, antigen presentation, and pathogen removal, or produce anti-inflammatory cytokines (e.g., IL10; D) to mediate tissue remodeling, angiogenesis, and the resolution of inflammation (Butovsky & Weiner, 2018). Under pathological conditions, peripherally derived macrophages can be recruited to the brain through the blood-brain barrier due to increased permeability and provide additional neurotrophic support to microglia through the inhibition (red line) of pro-inflammatory responses (E) (London et al., 2013).

CHAPTER 2

IBA1 IMMUNOREACTIVITY FOLLOWING CSR AND SUBSEQUENT RECOVERY

Parts of the text, figures, and tables in this chapter have been published in Hall, S., Deurveilher, S., Robertson, G.S., Semba, K. Homeostatic state of microglia in a rat model of chronic sleep restriction, SLEEP, 2020, 1–16, and are reproduced by permission of Oxford University Press.

2.1 Introduction

Chronic sleep restriction (CSR), characterized by habitual sleep insufficiency, is common in today's "24/7" society and negatively impacts cognition, mood, and health (Aldabal & Bahammam, 2011; Banks & Dinges, 2007; Ingiosi et al., 2013). Rodent models of CSR have shown that CSR affects brain function at both cellular and molecular levels, impairing neuronal functions, and even causing neuronal loss (Zhao et al., 2017). Microglia play an important role in brain function in both health and disease (S. U. Kim & de Vellis), and it is possible that these innate immune cells, in addition to neurons and other glial cells, are involved in the physiological and cognitive responses to CSR.

Microglia are the resident macrophages of the central nervous system and play an essential role in mediating inflammation and promoting tissue repair (Streit, Mrak, & Griffin, 2004) as well as in synaptic plasticity (Delpech et al., 2015; Kierdorf & Prinz, 2017). There is growing evidence that microglia are involved in sleep regulation (Ingiosi et al., 2013; Wisor et al., 2011). Microglia activation after sleep loss has been reported in brain areas associated with cognitive functions (Bellesi et al., 2017; Hsu et al., 2003; Tuan & Lee, 2019; Wadhwa et al., 2018; Xie et al., 2020; B. Zhu et al., 2012). For example, microglia increased in number and displayed larger cell bodies with thickened processes in the rat hippocampus after 5 days of sleep fragmentation (Hsu et al., 2003). In addition, following 4.5 days of CSR, microglia adopted a less ramified morphology suggestive of immunological activation and were detected phagocytosing presynaptic terminals in the adolescent mouse cortex (Bellesi et al., 2017). Whether CSR activates microglia in brain regions that regulate sleep/wake cycles is unknown.

In this study, we investigated microglia responses to 4 days of our 3/1 CSR protocol in sleep/wake, limbic, and autonomic regions in the rat brain using immunohistochemistry for the well-established microglia/macrophage-specific marker ionized calcium-binding adaptor molecule-1 (Iba1). We evaluated the numbers of Iba1-immunoreactive (ir) microglia and the density of Iba1 immunoreactivity (**Experiment 1**), as well as the morphology of Iba1-ir microglia (**Experiment 2**), in the selected brain regions after 3 h, ~1 day (27 h) and ~4 days (99 h) of the 3/1 CSR protocol, and after 6 days of unrestricted sleep following 99 h of CSR. As we found time-dependent and region-specific increases in Iba1 immunoreactivity in response to CSR (see Section 2.3.1.1), we investigated possible mechanisms by examining for proliferation of existing microglia using double-labelling for Iba1 and the cell division maker bromodeoxyuridine (**Experiment 3**) and for peripheral macrophage recruitment across the blood-brain barrier using the fluorescent tracers sodium fluorescein and Evans Blue dye (**Experiment 4**).

In addition, in Experiment 1, we examined the astrocyte responses to CSR using immunohistochemistry for the astrocyte-specific marker glial fibrillary acidic protein (GFAP) in a subset of brain regions examined for Iba1 immunoreactivity.

2.2 Methods

2.2.1 Animals

Adult male Wistar rats (n = 69; Charles River Canada, St. Constant, QC), 300–350 g on arrival, were initially housed in pairs in a colony room under a 12 h:12 h light/dark cycle (lights on at 07:00 am) at 23 ± 1°C, with food and water available ad libitum. Our previous studies using the same 3/1 CSR protocol used only male rats, due to the requirement of stable

background in sleep patterns (without reproductive hormone-dependent fluctuations) over at least 1 or 2 weeks (Deurveilher et al., 2015; Deurveilher et al., 2012; Hall et al., 2017; Wallingford et al., 2014). Due to similar requirements, we limited the present study to male rats. All animals were handled in accordance with the guidelines of the Canadian Council on Animal Care, and the animal handling protocols were approved by the Dalhousie University Committee on Laboratory Animals.

Four experiments were conducted. In Experiments 1−4 (see below), rats were randomly assigned to two to eight experimental groups and run in multiple cohorts of six rats at a time (except in Experiment 3; four or six rats per cohort).

2.2.2 The 3/1 CSR protocol

The sleep restriction (SR) protocol involved housing rats individually in programmable, motorized activity wheels, as described previously (Deurveilher et al., 2012). Briefly, sleep was restricted by continuous cycles of 3 h of sleep deprivation, imposed by the slow rotation of the activity wheel (~2.5 m/min), followed by 1 h of sleep opportunity when the wheel remained stationary; the protocol (the first sleep deprivation period) began at the onset of the light phase, i.e. 07:00 am. Control rats were housed in the same wheel-chambers, but their activity wheels were always locked to allow undisturbed sleep (locked wheel or LW condition).

All rats underwent 4 or 5 days of habituation in LWs prior to their respective experimental protocols (Experiments 1–4). The rats in the CSR condition were additionally habituated to the rotation of the wheels at a speed of approximately 2.5 m/min for 5–20 min once a day during the light phase; the wheels were otherwise locked.

Rats had *ad libitum* access to food and water throughout the experiment. Their body weights were recorded on the last day of habituation and immediately after their respective protocols (Experiments 1–4).

2.2.3 Experiment 1: Iba1 immunohistochemistry

2.2.3.1 Treatment groups

Rats were assigned to eight groups: two SR groups underwent the 3/1 CSR protocol for either 27 h (SR2, $n = 9$) or 99 h (SR5, $n = 8$); a recovery group (REC; $n = 5$) underwent the 3/1 protocol for 99 h followed by 6 days of undisturbed sleep in locked wheels; an acutely (3 h) sleep-deprived group (SD; $n = 4$) and four LW control groups (LW2, $n = 4$; LW5, $n = 4$; LWR, $n = 4$; and LWD, $n = 3$) were housed, and left undisturbed, in locked activity wheels for time intervals matched to those of the SR2, SR5, REC, and SD groups, respectively.

2.2.3.2 Perfusion and brain sectioning

At the end of their respective experimental protocols (i.e. 10:00 am), rats were given an overdose of an anesthetic mixture (208 mg/kg ketamine, 9.6 mg/kg xylazine, and 1.8 mg/kg acepromazine, IP). Animals were perfused intracardially with 100 mL of phosphate-buffered saline (pH 7.4), followed by 400 mL of 4% paraformaldehyde in 0.1 M phosphate buffer (pH 7.4). Brains were post-fixed in the same fixative solution for 4–5 h, followed by cryoprotection in 30% sucrose in 0.01 M phosphate buffer at 4°C for 2–4 days. A freezing microtome was used to cut each brain into five series of 40 μm thick coronal sections, which were collected in 0.05 M Tris-buffered saline (TBS; pH 7.2–7.4).

2.2.3.3 Immunohistochemistry

Single-label immunohistochemistry for Iba1 was performed on one series of sections using a standard avidin–biotin–horseradish peroxidase complex (ABC) method as previously described (Deurveilher, Ryan, Burns, & Semba, 2013), with a polyclonal rabbit anti-Iba1 antibody (1:2,000; Appendix B, Table B.1), a biotinylated donkey anti-rabbit IgG antibody (1:1,000; Jackson Laboratories), ABC (1:200, ABC Elite PK-6100; Vector Laboratories, Burlingame, CA), and diaminobenzidine in the presence of nickel ammonium sulfate and hydrogen peroxide.

Single-label immunohistochemistry for GFAP was performed using a mouse monocolonal anti-GFAP antibody (1:10,000; Millipore, Temecula, CA; see Appendix C, Figure C.1) on a second series of sections using the same protocol as for Iba1 with a biotinylated donkey anti-mouse IgG secondary antibody.

2.2.3.4 Image acquisition

Image capture and analysis were conducted by an examiner (S.H.) who was blind to the treatment conditions. Two adjacent sections within the series (i.e. 200 μm apart) per rat were selected for quantitative analyses of Iba1 immunoreactivity in each of the following 10 brain regions known to be involved in sleep/wake, limbic, and autonomic functions (Scammell et al., 2017): the prelimbic cortex, anterior cingulate cortex, paraventricular hypothalamic nucleus, central amygdala, dentate gyrus of the hippocampus, perifornical lateral hypothalamic area, dorsal raphe nucleus, parabrachial nucleus, locus coeruleus, and the nucleus of the solitary tract (for respective anteroposterior levels, see Appendix D, Table D.1). Unilateral images (1,300 × 1,030 pixels) of each region were captured using a 10× (cell counts) or 20× (densitometry and morphology) objective lens on a bright-field microscope (Zeiss AxioPlan MOT II) equipped with an AxioCam camera, with identical exposure and illumination settings for all images.

2.2.3.5 Densitometry and cell counts

The density of Iba1 immunoreactivity and counts of Iba1- immunoreactive (ir) cells were obtained for each brain region unilaterally in two adjacent sections and averaged for each rat (see Appendix D, Figure D.1 for analysis box sizes and locations).

ImageJ (NIH, Bethesda, MD) was used to set two thresholds for Iba1 in each image, one for density of Iba1 immunoreactivity and the other for cell counts, as follows. For density, the pixel distribution from each image across a gray-scale spectrum ranging from 0 (black) to 255 (white) was first examined to determine the peak background gray value and the highest gray value (i.e. lightest) in the image. The difference between these two values was then subtracted from the peak background gray value to obtain a threshold to define positive Iba1 staining. All gray values below this threshold (i.e. darker) were considered immunopositive. A pilot analysis showed that this procedure adequately highlighted both processes and cell bodies that were visually judged to be stained for Iba1 and also normalized background staining intensity across sections and animals.

The density of Iba1 immunoreactivity in each brain region was then calculated as the percentage of Iba1-ir area, by dividing the number of pixels that were below the threshold gray value by the total number of pixels within the analysis box. Pixels corresponding to blood vessels within the analysis box were excluded from the total pixel count.

For Iba1 cell counts, the threshold was set at 50% of the threshold for density described above, to highlight only Iba1-ir cell bodies, which were typically darkly stained. This setting eliminated processes as they were generally less darkly stained than cell bodies. The total number of Iba1-ir cells within respective analysis boxes was automatically counted in ImageJ, after excluding elements smaller than 20 μm^2.

2.2.3.6 GFAP immunohistochemistry

Images of GFAP immunoreactivity were captured as described in Section 2.2.3.4 above. The density of GFAP immunoreactivity was initially assessed in all 10 brain regions that were examined for Iba1 immunoreactivity (unilaterally in two adjacent sections; see Appendix D, Table D.1). However, several brain regions showed little or no GFAP-positive labelling and thus could not be assessed quantitatively. Ultimately, the density of GFAP immunoreactivity was quantitatively assessed in the anterior cingulate cortex, prelimbic cortex, dentate gyrus of the hippocampus, dorsal raphe nucleus, and parabrachial nucleus as described in 2.2.3.5.

2.2.4 Experiment 2: Microglia morphology

2.2.4.1 Treatment groups

Morphology analyses were conducted on Iba1-ir microglia in layers I and II/III of the prelimbic cortex, using sections that had been Iba1-immunostained for cell counts and densitometry in Experiment 1 (see above), for the SR2 (n = 9), SR5 (n = 8), REC (n = 5), LW2 (n = 5), LW5 (n = 4), and LWR (n = 4) groups.

2.2.4.2 Cell selection and Sholl analysis

Layer I and layer II/III were delineated based on additional Iba1-immunostained sections that were counterstained for Nissl in a control rat. A grid of 50 × 50 μm^2 was placed over layer I and layer II/III, and 8–10 Iba1-ir cells in each layer were randomly selected unilaterally in two adjacent sections (200 μm apart) per rat. Only Iba1-ir cells with apparently intact processes that were not obscured by background labeling or other Iba1-ir cells were included in the analyses.

For Sholl analysis, the “concentric circles” plug-in in ImageJ was used to create a series of concentric circles centered at the cell soma and radiating at 5 μm intervals (Hinwood et al., 2013). The “cell counter” plug-in was used to mark each point where an Iba1-ir branch

intersected a given circle. The following six parameters were calculated (Morrison & Filosa, 2013): total number of intersections (between cellular processes and concentric circles), process maximum (maximum number of intersections at one radius), number of primary branches (number of branches that originate from the soma), ramification index (the process maximum divided by the number of primary branches), longest branch length, and cell soma size. The area of the cell soma was calculated using the threshold setting in ImageJ.

2.2.5 Experiment 3: Microglia proliferation

2.2.5.1 Treatment groups

Rats were assigned to SR5 (n = 8) and LW5 (n = 8) groups.

2.2.5.2 CSR and bromodeoxyuridine injections

All rats received IP injections twice daily of 50 mg/kg bromodeoxyuridine (BrdU; Sigma-Aldrich, Oakville, ON) dissolved in saline (Bonde, Ekdahl, & Lindvall, 2006), at 07:00 am and 03:00 pm (corresponding to the beginning of respective 3 h sleep deprivation periods), throughout the CSR or LW condition, with the final injection at 07:00 am on the last day of CSR/LW, for a total of nine injections. Immediately following the completion of their respective experimental protocols at 10:00 am, rats were anesthetized and perfused as described in Section 2.2.3.2.

2.2.5.3 Tissue pretreatment and immunohistochemistry

Sections were incubated in 2N HCl for 30 min at 37°C to denature DNA, neutralized in sodium borate buffer (pH 8.5) for 10 min, and rinsed for 2 × 10 min in 0.05 M TBS, according to (Junek, Rusak, & Semba) with modification. Dual-label immunohistochemistry was conducted as previously described (Junek et al., 2010), using a polyclonal sheep anti-BrdU anti- body

(1:2,000; Appendix B, Table B.1), a polyclonal rabbit anti-Iba1 antibody (see Experiment 1 above), a Cy2-conjugated donkey anti-sheep IgG antibody (1:100; Jackson), and a Cy3-conjugated donkey anti-rabbit IgG antibody (1:400; Jackson). No BrdU immunolabeling was observed in an animal that did not receive BrdU injections. Visual inspection of brain sections confirmed that the tissue pre- treatment did not appear to affect Iba1 immunostaining.

2.2.5.4 Image acquisition and analysis

For unilateral counts of double-labeled Iba1/BrdU-ir cells, two adjacent sections (200 μm apart) per rat were selected in each of the four brain regions that showed significant changes in Iba1 immunoreactivity following CSR (see Section 2.3.1): the prelimbic cortex, central amygdala, perifornical lateral hypothalamic area, and dorsal raphe nucleus. Fluorescent images (2 μm z-stack; 1,024 × 1,024 pixels) were captured using a laser scanning confocal microscope (Zeiss LSM 510 Meta) and a 10× objective lens. The number of double-labeled Iba1/BrdU-ir cells was counted manually in each brain region using the same analysis boxes as described above under Experiment 1.

2.2.6 Experiment 4: Blood–brain barrier permeability

2.2.6.1 Pilot study: Evans Blue and sodium fluorescein dual injections

A pilot study was conducted to assess BBB permeability in the PrL, a brain region which showed an early increase in Iba1 immunoreactivity during CSR (Section 2.3.1), using the commonly used fluorescent tracers Evans Blue dye (EB; 680 nm emission, red) and sodium fluorescein (NaF; 525 nm emission, green) (Gomez-Gonzalez et al., 2013; Yen, Wei, Kuo, & Lai, 2013). While EB binds to albumin in the blood to become a high molecular weight tracer (69,000 Da), NaF is a low molecular weight tracer (376 Da) (Yen et al., 2013).

Animals from LW5 (n = 4) and SR5 (n = 3) groups were anaesthetized as described in Section 2.2.3.2 and given an intracardiac injection of 2% EB followed, 30 mins later, by an intracardiac injection of 0.05% NaF. After an additional 15 min, brains were rinsed with saline for 3 min and immersion-fixed in 4% paraformaldehyde overnight at 4°C.

Brains were cut on a freezing microtome into 50 µm-thick sections through the frontal cortex; sections were mounted on glass slides, and coverslipped. Images were captured using a fluorescence microscope and the integrated fluorescence density (mean gray value x fluorescent area) was quantified in ImageJ. The corrected total fluorescence for NaF and EB was calculated by dividing the integrated density of positive immunofluorescence by the integrated density of the background signal.

2.2.6.2 Treatment groups (main study)

Rats were assigned to SR5 (n = 6) and LW5 (n = 6) groups.

2.2.6.3 Evans Blue injection

Immediately following the SR5 or LW5 protocol (i.e. at 10:00 am), rats were anesthetized with an IP injection of ketamine (104 mg/kg), xylazine (4.8 mg/kg), acepromazine (0.9 mg/kg) mixture, followed by an intracardiac injection of 2 mL/kg of 2% EB (Sigma-Aldrich) in saline. The rats were then placed on a heating pad at 37°C to allow EB to circulate for 10 min under anesthesia (Gomez-Gonzalez et al., 2013); the skin of the rats turned dark blue. Rats were then perfused as described in Section 2.2.3.2. Brains were cut into 40 µm thick coronal sections using a freezing microtome and every fifth Section was stored for the examination of perivascular leakage of EB.

Two additional rats served as controls. One LW5 rat was not injected with EB to serve as an EB-negative control. Another rat was perfused with a mixture of 4% paraformaldehyde and

1% EB following acute cryoinjury to the right frontoparietal cortex (del Valle, Camins, Pallas, Vilaplana, & Pelegri, 2008) to serve as a positive control for EB extravasation.

2.2.6.4 Histology

To visualize blood vessels, brain sections were incubated in fluorescein isothiocyanate (FITC)-conjugated tomato lectin (Sigma-Aldrich, Product #L0401, 20 μg/mL) in 1% bovine serum albumin in 0.05 M TBS for 2 h on a shaker at room temperature. Sections were then rinsed (3 × 10 min), mounted on gelatin-coated slides, and cover-slipped.

2.2.6.5 Image acquisition and analysis

Two adjacent sections (200 μm apart) per region per rat were selected for quantitative analyses in the prelimbic cortex and perifornical lateral hypothalamic area (see Appendix D, Table D.1 for analysis box sizes and locations). Unilateral images were captured using a 10× (prelimbic cortex) or 20× (perifornical lateral hypothalamic area) objective lens with an epifluorescence microscope (Zeiss Axiovert 200M) for EB (red) and FITC-conjugated tomato lectin (green).

Perivascular leakage of EB was assessed by subtracting the tomato lectin-positive blood vessels from the EB image, using Photoshop (Adobe). Specifically, each pixel gray value in the tomato lectin image was subtracted from the corresponding pixel gray value in the EB image to create a differential image. Next, using ImageJ, a histogram of the number of pixels at each gray-scale value between 0 (black) and 255 (white) was displayed for each differential image. The threshold value for positive EB fluorescence was defined as the highest gray value measured in the histogram for an EB-negative control image, corresponding to autofluorescence. Next, for each rat, the number of pixels with gray values greater (i.e. lighter) than the threshold was divided by the corrected total number of pixels (i.e. the total number of pixels minus the number

of pixels occupied by blood vessels) in the image to obtain the percentage of EB-positive pixels (i.e. a measure of extravasation) for each differential image.

2.2.7 Statistics

Statistical analyses were conducted using GraphPad Prism 6 (GraphPad Software, Inc., La Jolla, CA). In Experiments 1 and 2, one- or two-way analyses of variance (ANOVA) were performed to compare treatment groups, followed, when applicable, by Fisher's LSD post hoc tests. In Experiments 3 and 4, two-tailed, unpaired Student's *t*-tests or, when the data showed heterogeneity of variance, Mann–Whitney *U*-tests were used. Probability values of <0.05 were considered statistically significant. Data values are expressed as means ± standard error of the mean (SEM).

2.3 Results

2.3.1 Experiment 1: Iba1 immunohistochemistry and Iba1 mRNA levels

2.3.1.1 Iba1 immunohistochemistry

The SD ($n = 4$), SR2 ($n = 9$) and SR5 ($n = 8$) groups underwent 3, 27 and 99 h, respectively, of the 3/1 CSR protocol, while the REC ($n = 4$ or 5) group underwent 99 h of the 3/1 protocol followed by 6 days of recovery sleep. The four non-sleep-deprived control groups LWD, LW2, LW5, and LWR ($n = 3$–5/group) were kept in locked activity wheels for corresponding intervals. The four control groups did not significantly differ between each other in either the number of Iba1-ir cells or the density of Iba1 immunoreactivity in any of the brain regions examined ($p<0.05$); therefore, they were combined into a single control group (LW).

Iba1 immunoreactivity was analyzed in 10 brain regions with sleep/wake, limbic, and autonomic functions. In 4/10 regions examined, including the prelimbic cortex, central amygdala, perifornical lateral hypothalamic area, and dorsal raphe nucleus, the number of Iba1-ir cells and/or the density of Iba1 immunoreactivity changed in response to CSR. Figure 2.1 shows examples of Iba1 immunoreactivity in these four "CSR- responsive" regions. Most microglia in all treatment groups appeared ramified rather than ameboid, with relatively small cell bodies and many fairly long and branching processes (Figure 2.1).

In the prelimbic cortex, the number of Iba1-ir cells (Figure 2.2, A) was higher in the SR2 group than in the LW (+133%, p = 0.0055) and SD (+188%, p = 0.0232) groups, and remained elevated in the SR5 group (+95% vs. LW, p = 0.0494); however, it was statistically at control levels following recovery (REC vs. LW, p = 0.347; $F_{4,35} = 2.96$, p = 0.0330). Similarly, the density of Iba1 immunoreactivity (Figure 2.2, B) was increased in the SR2 (+45% vs. LW, p = 0.0219) and SR5 (+48% vs. LW, p=0.0185) groups, and tended to remain elevated in the REC group (+44% vs. LW, p = 0.0925; Main effect of Group: $F_{4,35} = 2.66$, p = 0.0486).

In the central amygdala, Iba1-ir cell counts (Figure 2.2, D) were increased in the SR5 group (+123% vs. LW, p = 0.0173; +159% vs. SD, p = 0.0288; +147% vs. SR2, p = 0.0145) and returned to control levels after recovery (REC vs. LW, p = 0.277; $F_{4,36} = 2.86$, p = 0.0370). Similarly, the density of Iba1 immunoreactivity (Figure 2.2, E) was significantly increased in the SR5 group (+52% vs. LW, p = 0.0283; +135% vs. SD, p = 0.0098; +85% vs. SR2, p = 0.0114; and +73% vs. REC, p=0.0383), and was at control levels in the REC group (p=0.648 vs. LW; $F_{4,36} = 2.72$, p = 0.0447).

Similar to the central amygdala, the number of Iba1-ir cells in the perifornical lateral hypothalamic area (Figure 2.2, G) was elevated in the SR5 group (+221% vs. LW, p = 0.0007;

+305% vs. SD, p = 0.0070; +175% vs. SR2, p = 0.0043; and +113% vs. REC, p = 0.0374), and returned to control levels after recovery (REC vs. LW, p = 0.48; $F_{4,37} = 3.98$, p = 0.0087). The density of Iba1 immunoreactivity (Figure 2.2H) was not significantly changed by CSR ($F_{4,37} = 1.59$, p = 0.196), although it tended to be increased in the SR5 (+46% vs. LW) and REC (+68% vs. LW) groups (Figure 2.2, H).

In the dorsal raphe nucleus, no significant changes in Iba1-ir cell counts were found following CSR ($F_{4,36} = 2.03$, p = 0.111), although the pattern resembled those in the central amygdala and perifornical lateral hypothalamic area (Figure 2.2, J). However, the density of Iba1 immunoreactivity (Figure 2.2, K) was significantly increased in the SR5 group (+69% vs. LW, p = 0.0039 and +71% vs. SD, p = 0.032) and remained elevated in the REC group (+68% vs. LW, p = 0.0236; $F_{4,36} = 3.39$, p = 0.0187).

Positive correlations were found between the density of Iba1 immunoreactivity and the number of Iba1-ir cells in each of the 4 CSR-responsive brain regions, including the prelimbic cortex (Figure 2.2, C), central amygdala (Figure 2.2, F), perifornical lateral hypothalamic area (Figure 2.2, I), and dorsal raphe nucleus (Figure 2.2, L; r = 0.654–0.851, all $p<0.0001$, n = 40–42).

In the other 6 brain regions examined, there was no significant effect of CSR (Appendix D, Table D.2). Nonetheless, the highest density of Iba1 immunoreactivity and/or number of Iba1-ir cells was observed in the SR2, SR5 or REC groups in all these regions, with a trend for an increase in Iba1 density in the locus coeruleus (p = 0.0752).

2.3.1.2 Iba1 mRNA levels in the frontal cortex

To examine whether increases in Iba1 immunoreactivity following CSR were accompanied with changes in Iba1 expression, Iba1 mRNA levels were quantified in the frontal cortex (which

contains the prelimbic cortex) in an additional cohort of LW (n = 4), SR2 (n = 4), and SR5 (n = 5) animals using qRT-PCR (see Section 3.2.1 for the methods). The LW, SR2, and SR5 groups did not significantly differ in the normalized mRNA levels of Iba1 (H = 2.20, p = 0.36; Appendix E, Figure E.1), indicating that alterations in Iba1 immunoreactivity are related to changes in protein, but not mRNA, levels.

2.3.1.3 GFAP immunohistochemistry

Although microglia are recognized as the primary immune cells of the CNS, astrocytes can also have inflammatory functions during brain pathology (Liddelow & Barres, 2017). Therefore, the density of GFAP immunoreactivity was examined in a subset of brain regions that were examined for Iba1 immunoreactivity. The density of GFAP immunoreactivity, however, was unexpectedly low in the five brain regions examined, with the exception of the hippocampal dentate gyrus, where no group differences were found (Appendix C, Figure C.1). Based on these observations, I concluded that there were problems with the GFAP antibody, and astrocyte responses to the 3/1 CSR protocol in sleep/wake and limbic brain regions should be re-analyzed using a different GFAP antibody.

2.3.1.4 Body weights

The average percent change in body weight from pre-protocol levels varied among the 8 groups ($F_{7,34}$ = 16.79, p<0.0001; Appendix H, Table H.1). Specifically, the 4 control groups progressively gained body weight as expected (LWD: +2.7%, LW2: +3.7%, LW5: +9.5%; and LWR: +22%). The SD group tended to gain weight (+1.8%), while the SR2 and SR5 groups increasingly lost weight (-3.3% and -7.7%, respectively). The REC group lost weight on the last day of CSR (-4.0%) but gained weight during the 6 recovery days (+9.2%).

2.3.2 Experiment 2: Microglia morphology

Since the morphology of microglia changes according to their functional state (Karperien et al., 2013), we quantitatively examined whether CSR induces changes in microglia morphology in the prelimbic cortex, the only region that showed an increase in Iba1 immunoreactivity after both 27 and 99 h of CSR (see Experiment 1 above). Previous studies reported changes in the density and morphology of Iba1-ir microglia in the prelimbic cortex following chronic stress exposure (Hinwood et al., 2012; Tynan et al., 2010). Sholl analyses were conducted on randomly selected Iba1-ir cells in layer I and layer II/III, which are characterized by different cytoarchitecture (*The Rat Nervous System*, 2004), in the SR2 (n = 9), SR5 (n = 8), REC (n = 4 or 5), LW2 (n = 5), LW5 (n = 4), and LWR (n = 4) groups used in Experiment 1. As there was no significant difference between the LW2, LW5, and LWR groups in any of the six morphological parameters analyzed (p=<0.05), these three control groups were combined into a single control group (LW).

The four treatment groups did not significantly differ in any morphological parameters in either of the two cortical layers ($F_{3,58}$ = 0.29–1.84, p = 0.15–0.83), including soma size (Figure 2.3, A), total number of intersections (Figure 2.3, B), ramification index (Figure 2.3, C), process maximum (Appendix F, Figure F.1, A), number of primary branches (Appendix F, Figure F.1, B), and longest branch length (Appendix F, Figure F.1, C). When calculated as a function of distance from the cell soma, the number of intersections of microglia in layer I and layer II/III was also similar across groups (Appendix F, Figure F.1, D and E).

Irrespective of treatment groups, however, microglia were more ramified in layer I than in layer II/III of the prelimbic cortex. There was a main effect of layer for the total number of intersections (Figure 2.3, B), ramification index (Figure 2.3, C), process maximum (Appendix F,

Figure F.1, A), number of primary branches (Appendix F, Figure F.1, B), and longest branch length (Appendix F, F.1, C; $F_{1,58}$ = 7.47–33.76, p <0.0001–0.0083). The main effect of layer did not reach statistical significance for soma size ($F_{1,58}$ = 2.68, p = 0.107; Figure 2.3, A).

As another way to assess for differences in the degree of ramification between the treatment groups, all microglia from all the treatment groups were pooled together, ranked based on their ramification index value, and divided into quartiles (from less ramified to more ramified), separately for layer I (Figure 2.3, D) and layer II/ III (Figure 2.3, E) of the prelimbic cortex. Next, in each layer, the proportion (percentage) of microglia within each quartile was calculated to obtain a population profile for each rat. These profiles were then statistically compared between the four treatment groups. A repeated-measures two-way ANOVA showed no main effect of group or quartile for either layer (p = 0.82–0.99), indicating that there was no significant group difference in the population profile for ramification in response to CSR in either layer of the prelimbic cortex.

2.3.3 Experiment 3: Microglia proliferation

To evaluate the possibility that the proliferation of resident microglia contributed to the observed increase in the number of Iba1-ir cells following CSR (see Section 2.3.1), we assessed for the incorporation of the cell division marker BrdU in Iba1-ir cells using double immunofluorescence, in the prelimbic cortex, central amygdala, perifornical lateral hypothalamic area, and dorsal raphe nucleus in an additional cohort of SR5 (n = 7 or 8) and LW5 (n = 8) animals that received BrdU injections (see Section 2.2.5.2). There were only a few Iba1/BrdU-ir cells in each of these four brain regions in both groups, with no significant group difference (p = 0.16– 0.85; Figure 2.4). As a positive control, BrdU-ir cells were present in the dentate gyrus of

the hippocampus and subventricular zone of the lateral ventricle in both groups (data not shown) (Junek et al., 2010).

Similar to Experiment 1, the SR5 group lost weight from pre-protocol levels (−5.4%) while the LW5 group gained weight (+10.5%; SR5 vs LW5, $p < 0.0001$; Appendix H, Table H.2).

2.3.4 Experiment 4: Blood–brain barrier permeability

2.3.4.1 Pilot study: Evans Blue and sodium fluorescein dual injections

A pilot study was performed to examine blood-brain barrier permeability following CSR in LW5 ($n = 4$) and SR5 ($n = 3$) rats using sequential injections of the fluorescent tracers EB and NaF. Positive fluorescence signal for both EB and NaF in the PrL was very low and remained unchanged following 99 h of CSR (Appendix G, Figure G.1). To verify the technique, a rat that received a cryoinjury to the frontal cortex, which results in increased permeability of the blood-brain barrier (described in Section 2.2.6.3), was used as a positive control. Although EB fluorescence signal was identified in the brain of this animal, NaF fluorescence was not detectable and I was thus able to determine if any technical issue contributed to the lack of NaF extravasation in the PrL after CSR. Therefore, I continued the BBB experiment using EB only, using the procedures described in Section 2.2.6.3.

2.3.4.2 Evans Blue injections

Next, to determine whether or not peripheral macrophage recruitment through the blood–brain barrier contributed to the increases in the number of Iba1-ir cells observed following CSR (see Section 2.3.1), we examined blood–brain barrier permeability by assessing the leakage of the fluorescent dye EB into the brain parenchyma following intracardiac injection in an

additional cohort of SR5 (n = 6) and LW5 (n = 6) animals. Two additional animals served as EB-positive and negative controls (see Section 2.2.6.3 for specific treatment procedures).

As shown in Figure 2.5, A, in the EB-positive control rat, clear extravasation of EB was observed in various brain regions (e.g. cortex, striatum, and hippocampus), while in the EB-negative control rat, no EB fluorescence was visible as expected (not shown). In the LW5 and SR5 groups, no EB fluorescence was seen outside of blood vessels defined by tomato lectin binding in any brain region examined, although some residual EB inside blood vessels was occasionally observed (Figure 2.5, B; white arrowheads).

Consistent with these observations, the quantification of EB extravasation indicated that the percentage of pixels with positive EB fluorescence was 12.6% in the striatum of the EB-positive control but very low (<0.02%) in the LW5 and SR5 groups, with no significant group difference, in the prelimbic cortex ($t10 = 0.67$, $p = 0.51$; Figure 2.5, C) and perifornical lateral hypothalamic area ($U = 6.5$, $p = 0.074$; Figure 2.5, D).

As in Experiments 1 and 2, the SR5 group lost body weight from pre-protocol levels (−10.5%) while the LW5 group gained weight (+5.1%; SR5 vs LW5, $p = 0.0003$; Appendix H, Table H.3).

2.4 Discussion

We show here that 27 and 99 h of the 3/1 CSR protocol increased the number of Iba1-ir microglia and the density of Iba1 immunoreactivity in selected sleep/wake and limbic brain regions in adult rats. These changes, in particular Iba1 density, persisted at least one week following CSR (the only recovery period studied) in most CSR-responsive regions. Despite the observed increases in Iba1 immunoreactivity, microglia morphology examined in the prelimbic

cortex was unaffected by CSR, with no change in cell body size or degree of ramification. Additionally, changes in Iba1 immunoreactivity were not accompanied by evidence of microglia proliferation or peripheral macrophage recruitment across the blood-brain barrier.

CSR caused a gradual loss of body weight compared to pre-protocol levels. This modest weight loss is consistent with previous reports using the same (Deurveilher et al., 2012; Hall et al., 2017; Wallingford et al., 2014) or different (Barf et al., 2012; Everson & Szabo, 2011) CSR protocols in rats. As reported previously in another CSR study (Everson & Szabo, 2011), the weight loss in SR rats may reflect a negative energy balance associated with hyperphagia, although food intake was not measured in the present study.

2.4.1 Methodological considerations and limitations

A control group experiencing the same number of wheel rotations as those in the sleep-restricted groups but with minimal or no sleep deprivation was not included in the present study. Therefore, we cannot rule out that the increased locomotor activity inherent to the CSR protocol contributed, at least in part, to the observed changes in Iba1 immunoreactivity in response to CSR. However, we suspect that this is unlikely for the following reasons: First, Iba1 immunoreactivity was at control levels in all brain regions examined after 3 h of forced wheel rotation (SD group), suggesting no acute effect of locomotor activity on Iba1 immunoreactivity. Second, forced locomotion for 20 min daily over 2 weeks *reduced* ischemia-induced increases in Iba1 immunoreactivity in the rat hippocampus (Lovatel et al., 2014), and voluntary wheel running for 10 days did not alter the number or the morphology of Iba1-ir cells in the mouse hippocampus (Olah et al., 2009).

Another issue to consider is the possibility that stress inherent to the 3/1 CSR protocol contributed to the observed increases in Iba1 immunoreactivity. Previous studies using a 20/4 CSR protocol in rats reported that plasma corticosterone levels were mildly increased at the end of daily 20 h sleep deprivation (using slowly rotating wheels) followed by a return to control levels at the end of the subsequent 4 h sleep opportunity (Barf et al., 2012; Meerlo et al., 2002; Roman, Van der Borght, Leemburg, Van der Zee, & Meerlo, 2005). However, we are inclined to believe that, between the two types of protocol, the 3 h sleep deprivation/1 h sleep opportunity cycle is less stressful and, therefore, would have less of an effect on corticosterone levels, although corticosterone levels were not measured in the present study. Highly stressful experiences such as repeated psychosocial stress for 6 days in mice (Wohleb et al., 2012) or 14 days in rats (Tynan et al., 2010) did produce distinct morphological changes in microglia with hypertrophy combined with shorter, thickened processes consistent with pro-inflammatory activation (Wohleb et al., 2012). Thus, we suppose that the stress associated with the 3/1 CSR protocol was likely mild, although we cannot exclude its possible contribution to the increased Iba1 immunoreactivity following CSR. More plausibly, however, the increases in Iba1 immunoreactivity and the lack of morphological change in microglia suggest a homeostatic or "adaptive" response to CSR (see Chapter 3).

Finally, although the changes in Iba1 immunoreactivity observed in response to CSR in the present study were clear and fairly robust, the use of additional immunohistochemical markers that recognize microglia in all functional phenotypes, such as TMEM119 (Bennett et al., 2016) and CD11b (Roy, Fung, Liu, & Pahan, 2006), would have strengthened our results. In addition, although the absence of changes in Iba1 mRNA levels was confirmed, further analysis of the changes in Iba1 protein levels using enzyme-linked immunosorbent assay (ELISA) or Western

blot analysis is important to validate the observed increases in Iba1 immunoreactivity in response to CSR.

2.4.2 Region-specific increases in Iba1 immunoreactivity in response to CSR

The 3/1 CSR protocol increased Iba1 immunoreactivity with different time courses in 4 out of the 10 examined brain regions with sleep/wake regulatory and limbic functions. In the prelimbic cortex, the number of Iba1-ir cells and/or the density of Iba1 immunoreactivity increased after 27 h of CSR and remained elevated after 99 h of CSR, while in the central amygdala, perifornical lateral hypothalamic area, and dorsal raphe nucleus, increases were observed only after 99 h of CSR.

The increase in Iba1 immunoreactivity, however, was not universal; in fact, 6 out of the 10 brain regions examined in the present study showed no significant changes. These included the lateral parabrachial nucleus and locus coeruleus, which are involved in sleep/wake regulation (Scammell et al., 2017), as well as the anterior cingulate cortex, paraventricular hypothalamic nucleus, nucleus of the solitary tract, and dentate gyrus of the hippocampus. We did not examine microglia morphology in these regions and cannot rule out the possibility that these microglia responded to CSR with morphological changes without changing their Iba1 immunoreactivity. Nonetheless, the lack of change in Iba1 immunoreactivity in the hippocampus in response to CSR is consistent with the previously reported lack of change in the density of Iba1-ir cells in the mouse hippocampus after 72 h of REM sleep deprivation (Tuan & Lee, 2019). However, this result contrasts with previously reported increases in the number of cells immunopositive for Iba1 or another microglial marker OX-42 in the hippocampus after 5 days of sleep fragmentation in rats (Hsu et al., 2003) and after either 1 day or 1 week after 24 h of sleep disruption in mice

(B. Zhu et al., 2012). Collectively, we believe that the regionally different levels or time courses of microglia response likely reflect different functions of these brain areas and different roles microglia play in them.

Although microglia are known to proliferate rapidly in response to a variety of stimuli (Banasr et al., 2007), proliferation (examined using BrdU) did not appear to contribute to the observed increase in the number of Iba1-ir microglia in any of the four CSR-responsive brain regions. Similarly, a previous study reported no evidence of microglia proliferation in response to approximately 2 weeks of chronic stress in stress-related brain regions in rats (Banasr et al., 2007). Additionally, we found no evidence for blood–brain barrier disruption (using EB) in response to CSR, suggesting that macrophage recruitment is an unlikely explanation for the increased number of Iba1-ir cells, despite reports of increased blood–brain barrier permeability to EB and other fluorescent tracers following sleep disruption for 6 days in mice (He et al., 2014) and 10 days in rats (Gomez-Gonzalez et al., 2013; Hurtado-Alvarado, Velazquez-Moctezuma, & Gomez-Gonzalez, 2017). Thus, the observed increases in Iba1-ir cell numbers in response to CSR are most likely due to an upregulation of Iba1 levels in existing microglia, rather than an actual increase in the number of microglial cells. Given the high mobility of microglia (Nimmerjahn et al., 2005; Wake et al., 2013), however, we cannot exclude the possibility that the migration of microglia from adjacent brain regions contributed to the increased numbers of Iba1-ir microglia in the CSR-responsive brain regions.

Despite the increases in Iba1 immunoreactivity in response to CSR, microglia in all CSR-responsive regions retained a ramified phenotype and a relatively small cell body size, indicative of a homeostatic or physiological state. When quantitatively analyzed in the prelimbic cortex, microglia morphometric measures showed no differences between the treatment groups.

Additionally, the values of the morphological parameters analyzed in the current study for the prelimbic cortex are comparable to those reported in rats under control (no CSR) conditions (Hinwood et al., 2013; Morrison & Filosa, 2013). These results are in contrast to the previously reported increased proportion of less ramified microglia in response to 4.5 days of CSR in the frontal cortex of adolescent mice (Bellesi et al., 2017). Differences in species, age, and/or protocols may account for this discrepancy.

2.4.3 Iba1 immunohistochemistry during subsequent recovery from CSR

Although CSR lasted just over 4 days, the increase in the density of Iba1 immunoreactivity persisted for at least one week after CSR in most CSR-responsive regions, while the number of Iba1-ir cells approached control levels. We found no changes in microglia morphology following recovery, as quantified for the prelimbic cortex; therefore, the sustained increases in Iba1 density following recovery are unlikely to be due to changes in microglial morphology. Rather, the elevated Iba1 levels are more likely related to the fact that the detection threshold was lower for densitometry than for cell counts (see Section 2.2.3.5). Thus, we believe that after 6 days of recovery, Iba1 levels were reduced in microglia cell bodies but largely remained elevated in their processes. Such persistent microglia activation could alter microglia responses to subsequent challenges [microglia 'priming'; (Perry & Holmes, 2014)]. Consistent with this possibility, it has been proposed that CSR could prime microglia to increase the brain's vulnerability to a further insult (Bellesi et al., 2017).

2.4.4. Functional significance of increased Iba1 immunohistochemistry

Iba1 is a macrophage-specific actin-bundling protein that helps facilitate the cytoskeletal rearrangements necessary for changes in microglia cell shape, proliferation, phagocytosis, and migration (Ohsawa et al., 2004; Sasaki, Ohsawa, Kanazawa, Kohsaka, & Imai, 2001). Iba1 is shown to be upregulated during neuroinflammation, such as occurs in neurodegenerative diseases (W. Zhu et al., 2017) and brain injury (Ito et al., 2001), thus increases in Iba1 levels following CSR could reflect an immunological activation of microglia. However, microglia morphology remained unaltered in the prelimbic cortex in response to CSR (Experiment 2) and we found no evidence of microglia proliferation (Experiment 3) nor blood-brain barrier impairment (Experiment 4) following CSR. Thus, CSR-induced increases in Iba1 immunoreactivity could reflect a homeostatic, rather than an immune, response of microglia.

A key function of microglia is phagocytosis mediated by phagocytic cups (i.e., bulbous protrusions on the ends of microglia processes that are involved in phagocytosis (Ohsawa, Imai, Kanazawa, Sasaki, & Kohsaka, 2000)). Although microglia in the frontal cortex were not immunoreactive for CD68, a scavenger receptor expressed by microglia which is commonly used as a marker for microglia with phagocytic activities (Perego, Fumagalli, & De Simoni, 2011), following the 3/1 CSR protocol, it has been reported that the phagocytosis of synaptic elements in the mouse cortex was enhanced after 4.5 days of CSR (Bellesi et al., 2017). Further analysis will be useful to determine if phagocytic cups can be identified on microglia during CSR and whether there is evidence of microglia phagocytosis in sleep/wake-regulatory brain regions in response to CSR.

CSR-induced increases in Iba1 immunoreactivity could also be involved in microglia migration (section 2.4.2). Under physiological conditions, microglia cell bodies remain relatively

static, although their processes are highly motile (Nimmerjahn et al., 2005; Wake et al., 2009). However, a recent two-photon imaging study in mice demonstrated that following repeated peripheral injections of LPS, cortical microglia migrate towards blood vessels, and subsequently closely appose blood vessels with their cell bodies (Haruwaka et al., 2019). This microglial response was initially neuroprotective, acting to maintain the integrity of the blood-brain barrier (Haruwaka et al., 2019). Whether increases in Iba1 immunoreactivity are reflective of microglia migration within the 4 CSR-responsive brain regions, or the migration of microglia from adjacent brain regions, in response to CSR is unknown and may have implications for understanding the function of microglia responses to CSR.

In the present study, CSR-induced changes in Iba1 immunoreactivity were observed in two key sleep/wake-regulatory brain regions: the perifornical lateral hypothalamic area, which contains wake-active ORX neurons (Modirrousta et al., 2005), and REM sleep-active MCH neurons (Hassani et al., 2009), and the dorsal raphe nucleus which houses wake-active serotonergic neurons (Fuller et al., 2006). We previously found evidence for increased neuronal activation (indicated by increased ΔFosB/FosB immunoreactivity) in the perifornical lateral hypothalamic area using the same 3/1 CSR protocol (Hall et al., 2017). Thus, microglia in the perifornical lateral hypothalamic area and dorsal raphe nucleus may be responding to the sustained activity of wake-active neurons during sleep deprivation periods and/or of sleep-active neurons during the sleep opportunity periods of the 3/1 CSR protocol.

The relatively early and sustained increase of Iba1 immunoreactivity in the prelimbic cortex, a brain region with a role in sustained attention and working memory requirements for higher-order cognitive tasks (Granon & Poucet, 2000), largely parallels previously observed changes in sustained attention in response to the 3/1 CSR protocol. In a previous study from the

lab, the performance of rats on a psychomotor vigilance task involving sustained attention was found to be initially impaired, then gradually improved, during the same 4-day CSR protocol used in the present study (Deurveilher et al., 2015). It is possible that microglia responses to CSR in the prelimbic cortex, a brain region sensitive to sleep loss (Muzur, Pace-Schott, & Hobson, 2002), could contribute to the adaptive alterations in sustained attention observed during CSR.

CSR-induced increases in Iba1 immunoreactivity was also observed in the central amygdala. These increases may be related to changes in anxiety-related behaviours in response to chronic sleep loss (Silva et al., 2004; Tartar et al., 2009).

2.5 Conclusions

Our data indicate that sleep-restricting rats for 1 to 4 days using the 3/1 CSR protocol resulted in time-dependent and region-specific increases in microglial Iba1 immunoreactivity in selected regions of the rat brain. These increases persisted for at least one week after CSR in most CSR-responsive regions. CSR-induced microglia responses in a subset of sleep/wake and limbic brain regions may be involved in adaptive changes in sleep homeostasis and sustained attention in response to chronic sleep loss. In addition, the sustained microglial activation in response to CSR could alter the way microglia respond to subsequent challenges, thereby increasing brain vulnerability to damage by further insults. The functional significance of elevated Iba1 immunoreactivity during CSR remained unclear, and I addressed this question in Chapter 3, by examining the molecular phenotype of microglia in the CSR-responsive brain regions (see Chapter 3).

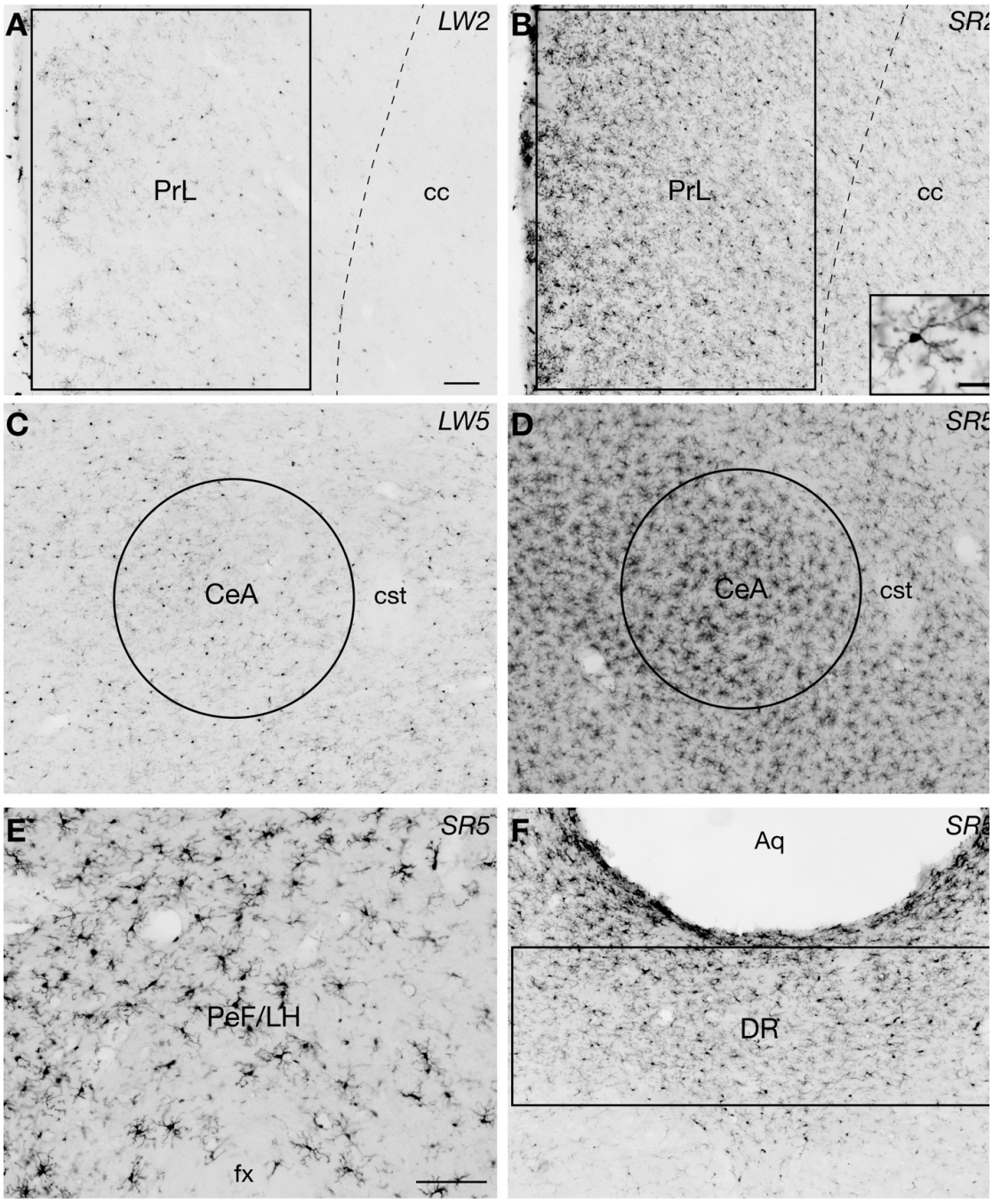
A
LW2
PrL
cc
B
SR2
PrL
cc
C
LW5
CeA
cst
D
SR5
CeA
cst
E
SR5
PeF/LH
fx
F
Aq
SR5
DR

Figure 2.1. Examples of Iba1 immunoreactive (-ir) microglial cells in the four brain regions that showed significant increases in Iba1 immunoreactivity during and following chronic sleep restriction (CSR), including the prelimbic cortex (PrL; A and B including an inset), central amygdala (CeA; C and D), perifornical lateral hypothalamic area (PeF/LH; E), and dorsal raphe nucleus (DR; F). The sections shown in A and C are from rats in the locked wheel control groups LW2 and LW5, respectively. The section shown in B is from a rat in the SR2 group that underwent 27 h of the 3/1 CSR protocol, and the sections shown in D–F are from rats in the SR5 group that underwent 99 h of the same protocol. The size and placement of analysis boxes or circles used for quantification of Iba1 immunoreactivity are shown for each region (in E, the entire image was used for analyses). Aq, cerebral aqueduct; cc, corpus callosum; cst, commissural stria terminalis; fx, fornix. Scale bars = 100 μm (A–F) and 20 μm (inset in B). Reprinted from Hall, S., Deurveilher, S., Robertson, G.S., Semba, K. Homeostatic state of microglia in a rat model of chronic sleep restriction, SLEEP, 2020, 1–16 by permission of Oxford University Press.

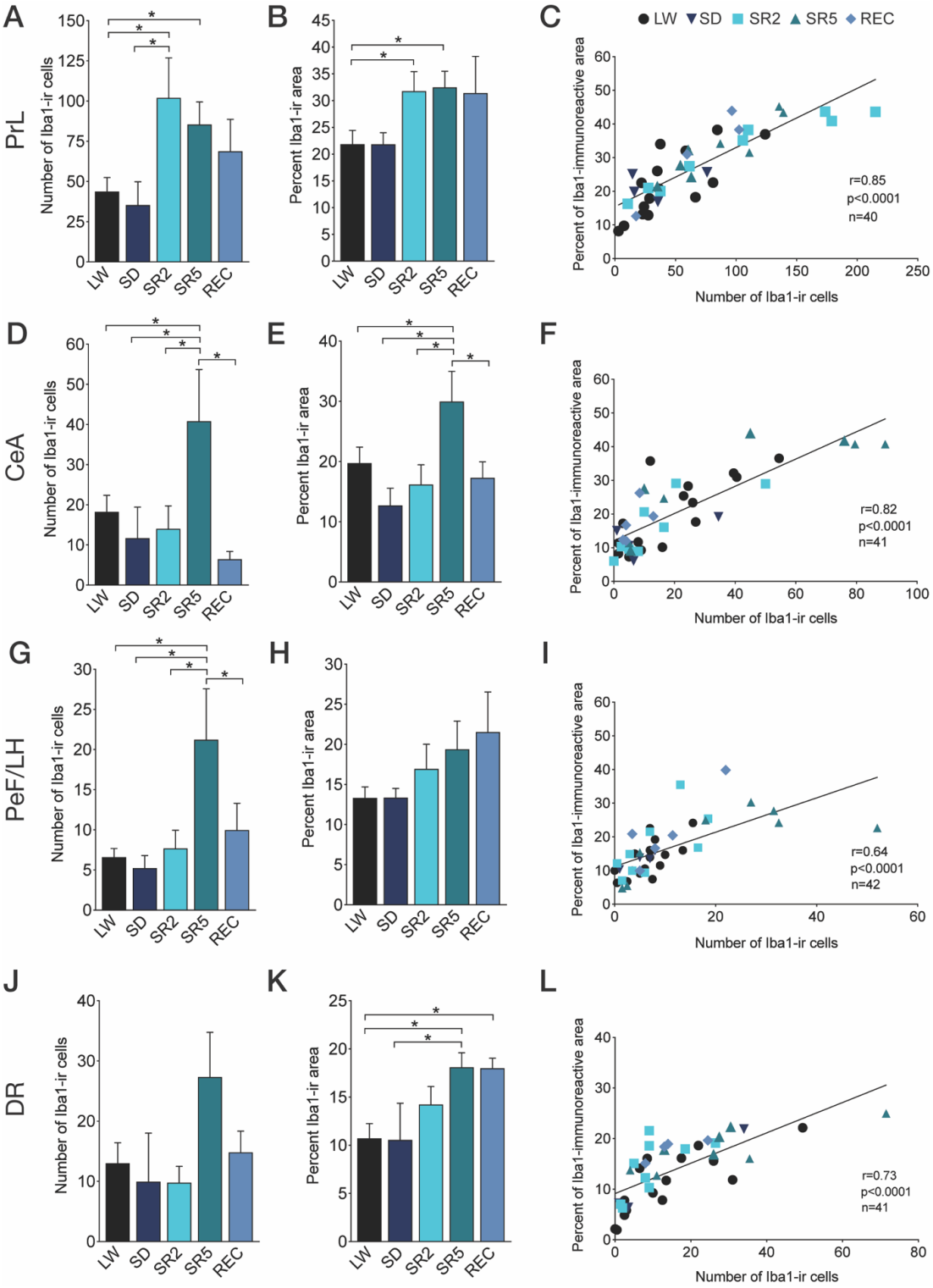
A
PrL
Number of Iba1-ir cells
B
Percent Iba1-ir area
C
LW SD SR2 SR5 REC
Percent of Iba1-immunoreactive area
Number of Iba1-ir cells
r=0.85
p<0.0001
n=40
D
CeA
Number of Iba1-ir cells
E
Percent Iba1-ir area
F
Percent of Iba1-immunoreactive area
Number of Iba1-ir cells
r=0.82
p<0.0001
n=41
G
PeF/LH
Number of Iba1-ir cells
H
Percent Iba1-ir area
I
Percent of Iba1-immunoreactive area
Number of Iba1-ir cells
r=0.64
p<0.0001
n=42
J
DR
Number of Iba1-ir cells
K
Percent Iba1-ir area
L
Percent of Iba1-immunoreactive area
Number of Iba1-ir cells
r=0.73
p<0.0001
n=41
LW SD SR2 SR5 REC

Figure 2.2. The number of Iba1-immunoreactive (ir) cells (*left*), density (percent area) of Iba1 immunoreactivity (*middle*), and scatterplots of number versus density (*right*), in the four brain regions that showed significant increases in Iba1 immunoreactivity in response to CSR, including the prelimbic cortex (PrL; A–C), central amygdala (CeA; D–F), perifornical lateral hypothalamic area (PeF/LH; G–I), and dorsal raphe nucleus (DR; J–L). Data are shown as means + SEM for the LW (n = 15 or 16), SD (n = 4), SR2 (n = 8 or 9), SR5 (n = 8), and REC (n = 4 or 5) groups. The LWD, LW2, LW5, and LWR control groups were combined into a single LW group. Cell counts are obtained from respective analysis boxes and are expressed per section per side of the brain. Regression lines are shown as solid lines. *$p < 0.05$, **$p < 0.01$ (Fischer's LSD post hoc tests).

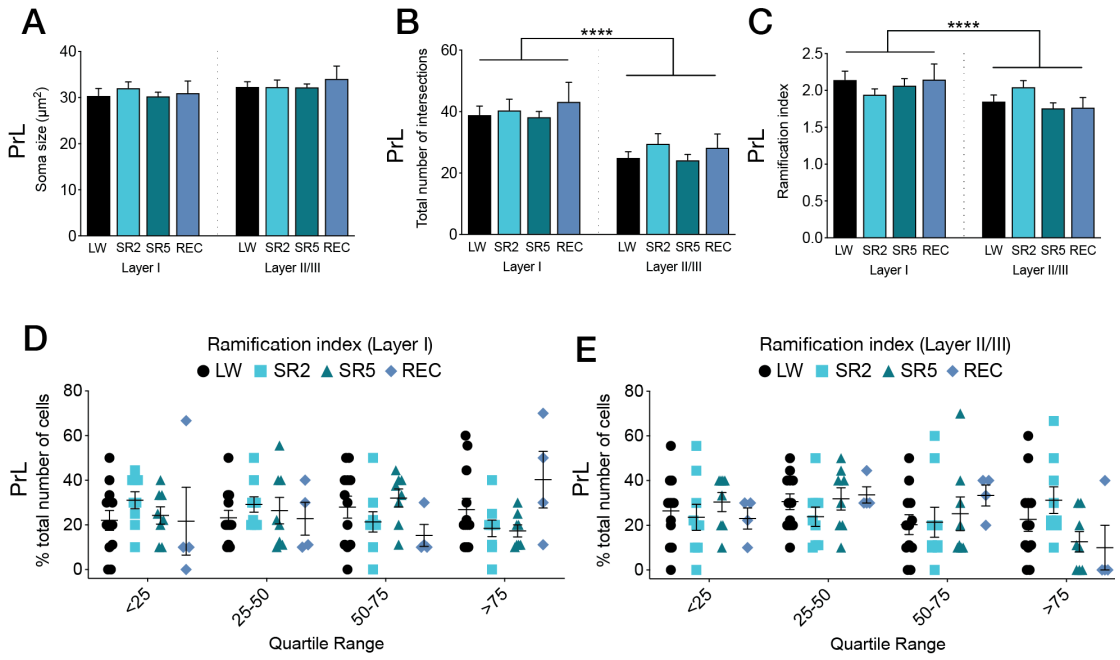

Figure 2.3. Morphological parameters of microglial cells in layers I and II/III of the prelimbic cortex (PrL), which showed a significant increase in Iba1 immunoreactivity after both 27 and 99 h of CSR (see Figure 2.2, A–C). Mean (+SEM) soma size (A), total number of intersections (B), and ramification index (C) are shown for the LW (n = 12), SR2 (n = 9), SR5 (n = 8), and REC (n = 4) groups. Microglia (n = 8–10/layer/rat) were randomly selected for Sholl analyses in each animal (section 2.2.4 in Chapter 2 Experiment 1 for further details). The LW2, LW5, and LWR control groups were combined into a single LW control group. (A–C) There was no significant effect of CSR on soma size (A), total number of intersections (B), or ramification

index (C). However, the total number of intersections (B) was significantly greater in layer I (*left*) than in layer II/III (*right*) across all treatment groups. (D and E) All microglia across animals were pooled, ranked, and divided into quartiles from low to high ramification index, and the proportion of cells in each quartile was calculated for each animal in each treatment group for layer I (D) and layer II/III (E). No significant group difference was found in the proportions of microglia in each quartile in either layer. See Appendix F Figure F.1 for additional morphological parameters analyzed. ****$p < 0.0001$ (main effect of layer, two-way repeated ANOVA).

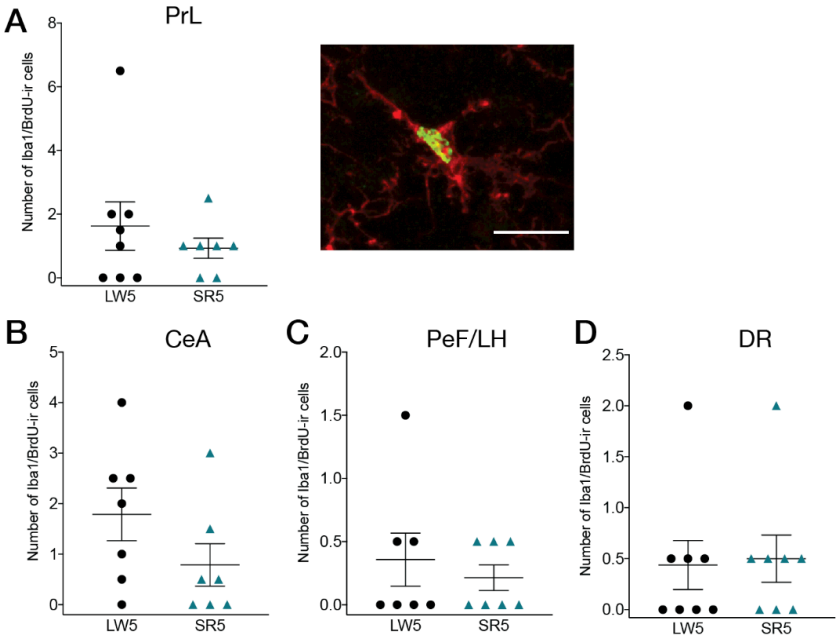

Figure 2.4. Number of double-labelled Iba1 (red)/BrdU (green)-ir microglia cells in the prelimbic cortex (PrL; A), central amygdala (CeA; B), perifornical lateral hypothalamic area (PeF/LH; C), and dorsal raphe nucleus (DR; D), namely, the 4 brain regions that showed an increase in Iba1 immunoreactivity in response to CSR (see Figure 2.2). An example of double-labelled microglia (green nucleus for BrdU, and red cytoplasm for Iba1) in the PrL is shown in A, right. Scale bar = 20 µm. Mean values (± SEM) are shown for the LW5 (n = 7 or 8) and SR5 (n = 7 or 8) groups. Each symbol represents a rat. CSR did not significantly affect the number of double-labeled Iba1/BrdU-ir cells in any of these regions (unpaired t-tests). Reprinted from Hall, S., Deurveilher, S., Robertson, G.S., Semba, K. Homeostatic state of microglia in a rat model of chronic sleep restriction, SLEEP, 2020, 1–16 by permission of Oxford University Press.

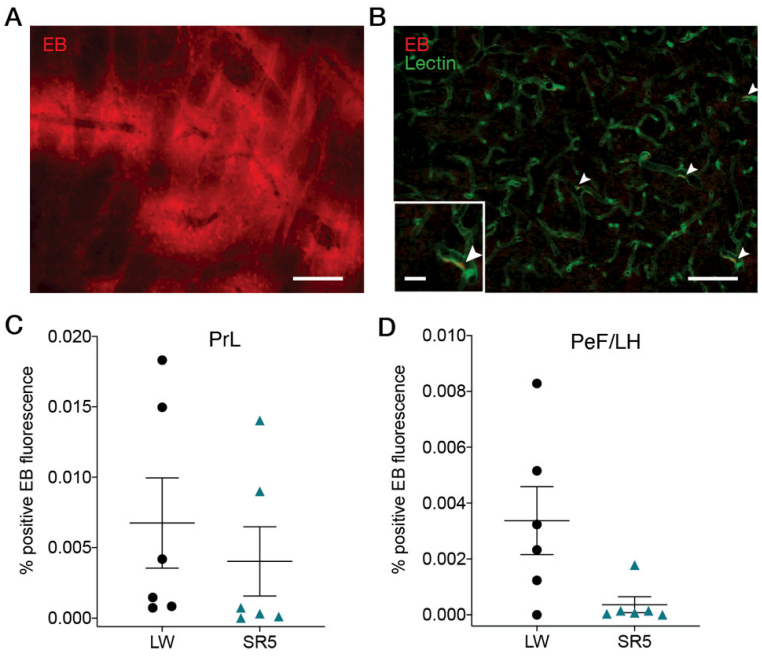

Figure 2.5. Quantification of Evans Blue (EB) dye fluorescence in brain tissue following CSR. (A) Example of a fluorescent microscope image showing EB extravasation (red) in the striatum of a positive control rat with cryoinjury (see section 2.2.6 for details). Scale bar = 150 µm. (B) Example of a fluorescent microscope image in the prelimbic cortex (PrL) of an SR5 rat showing blood vessels identified with tomato lectin-FITC (green) and EB (red). White arrowheads indicate EB remaining inside blood vessels; no EB fluorescence was observed outside of blood vessels. Scale bars = 100 µm and 25 µm (inset). EB fluorescence was quantified in the PrL (C) and perifornical lateral hypothalamic area (PeF/LH; D) for the SR5 (n = 6) and LW5 (n = 6) groups. Each symbol represents a rat. See Experiment 4 in Methods (Section 2.2.6) for calculation of percent positive EB fluorescence area. CSR did not have a significant effect on the percent positive EB fluorescence area in either the PrL or PeF/LH (unpaired t-tests). Reprinted

from Hall, S., Deurveilher, S., Robertson, G.S., Semba, K. Homeostatic state of microglia in a rat model of chronic sleep restriction, SLEEP, 2020, 1–16 by permission of Oxford University Press.

CHAPTER 3

CHARACTERIZATION OF THE IMMUNOLOGICAL PHENOTYPE OF MICROGLIA IN RESPONSE TO CSR

Parts of the text, figures, and tables in this chapter have been published in Hall, S., Deurveilher, S., Robertson, G.S., Semba, K. Homeostatic state of microglia in a rat model of chronic sleep restriction, SLEEP, 2020, 1–16, and are reproduced by permission of Oxford University Press.

3.1 Introduction

Microglia are a heterogeneous population of cells with a diversity of phenotypes and functions in the CNS (Hanisch & Kettenmann, 2007). In the healthy brain, physiological or "homeostatic" microglia modulate neuronal circuitry by regulating neurogenesis, interacting with neuronal elements, and remodeling synapses (Wake et al., 2009). In response to pathological insult or CNS disturbance, microglia can initiate neuroinflammatory responses by changing their molecular phenotype depending on the type of signal received (Butovsky & Weiner, 2018). Immunologically activated microglia produce pro-inflammatory cytokines, such as TNFα, IL1β, and IL6, as well as anti-inflammatory cytokines such as IL10 (Streit, Walter, & Pennell, 1999), in a variety of pathological conditions including brain injury (Donat, Scott, Gentleman, & Sastre, 2017), chronic stress (Hinwood et al., 2013), and neurodegeneration (Smith, Das, Ray, & Banik, 2012). Although reports are conflicting (Bellesi et al., 2017), enhanced brain levels of pro-inflammatory cytokines have been observed after 24 h of sleep disturbance (B. Zhu et al., 2012), 48 and 72 h sleep deprivation (Wadhwa et al., 2017), as well as after 5 and 21 days of CSR (Manchanda et al., 2018; Zielinski et al., 2014). Importantly, pro- and anti-inflammatory cytokines are also known to regulate physiological sleep, with pro-inflammatory cytokines typically promoting sleep and anti-inflammatory cytokines inhibiting sleep (Imeri & Opp, 2009; Krueger et al., 2011).

The results reported in Chapter 2 demonstrated that 1 or 4 days of the 3/1 CSR protocol increased the number of Iba1-ir microglia and the density of Iba1 immunoreactivity in select brain regions involved in sleep/wake-regulatory and limbic functions, including the prelimbic

cortex (PrL) and perifornical lateral hypothalamic area (PeF/LH). Iba1 is constitutively expressed by microglia and is upregulated in response to perturbations in brain homeostasis, such as that occurs during neuroinflammation (Ito et al., 2001; Kondo et al., 2011; W. Zhu et al., 2017). Although we found no evidence of microglia proliferation or peripheral macrophage recruitment in response to CSR, the CSR-induced increases in Iba1 may reflect the initial stages of microglia immunological activation resulting in the production of cytokines and upregulation of inflammatory molecular markers.

In the present study, we investigated microglia inflammatory responses to 4 days of the 3/1 CSR protocol in the PrL and PeF/LH, two brain regions which showed increased Iba1 immunoreactivity in response to CSR (see Section 2.3.1). We performed assays for inflammatory cytokine mRNA expression (**Experiment 1**) and used immunohistochemistry for several pro- and anti-inflammatory molecular markers of microglia activation (Franco & Fernandez-Suarez, 2015) (**Experiment 2**) as well as the purinergic P2Y12 receptor marker of physiological or "homeostatic" microglia (Haynes et al., 2006; Mildner, Huang, Radke, Stenzel, & Priller, 2017) (**Experiment 3**).

3.2 Methods

3.2.1 Animals

All animals were handled in accordance with the guidelines of the Canadian Council on Animal Care, and the animal handling protocols were approved by the Dalhousie University Committee on Laboratory Animals. The rats' suppliers, rats' body weight at arrival, housing conditions, and experimental protocols were the same as those described in Chapter 2 (see Section 2.2.1). Briefly, adult male Wistar rats (n = 66) were initially housed in pairs in a colony

room under a 12h:12h light/dark cycle (lights on at 07:00 am), with food and water available *ad libitum*. Rats were randomly assigned to four or five experimental groups and run in multiple cohorts of five or six rats at a time (Experiments 1–3).

Rats were sleep restricted according to the 3/1 CSR protocol as described in Section 2.2.2. Briefly, rats underwent CSR individually in programmable, motorized activity wheels (Deurveilher et al., 2012). The protocol began at the onset of the light phase, i.e. 07:00 am, and continued for up to 4 days. Time-matched control rats were housed in the same wheel-chambers and the activity wheels was either always locked to allow undisturbed sleep (locked wheel or LW condition), or kept unlocked to provide unlimited opportunity for voluntary wheel rotation (exercise control or EC condition).

Prior to their respective experimental protocol, all rats underwent 4 or 5 days of habituation in LWs. The rats in the CSR condition were additionally habituated to the rotation of the wheels as described in Section 2.2.2; the wheels were otherwise locked. The rats in the EC condition could freely rotate their unlocked wheel throughout habituation.

Rats had *ad libitum* access to food and water throughout the experiment. As described in Chapter 2, their body weights were recorded on the last day of habituation and immediately after their respective protocols (Experiments 1–3).

3.2.1 Experiment 1: Cytokine mRNA expression

3.2.1.1 Treatment groups

Rats were assigned to 4 groups: 2 sleep restriction (SR) groups underwent the 3/1 CSR protocol for either 27 h (SR2; $n = 4$) or 99 h (SR5; $n = 7$), 2 locked-wheel control groups (LW2,

n = 2; LW5, *n* = 5) that were housed, undisturbed, in locked activity wheels for a time period matched to those in the SR2 and SR5 groups, respectively.

At the end of their respective experimental protocols (i.e. 10:00 am), rats were deeply anesthetized with 5% isoflurane (in oxygen) and decapitated. Brains were immediately removed, and frontal cortex blocks were collected from both hemispheres by isolating the most anterior 5 mm portion of the frontal cortex, as described previously (Wallingford et al., 2014), and immediately frozen on dry ice and stored at −80°C.

3.2.1.2 RNA extraction and quantitative reverse transcriptase-polymerase chain reaction

Frontal cortex tissues were homogenized in TRIzol reagent (Ambion by Life Technologies, Carlsbad, CA). Total RNA was extracted using an Aurum Total RNA Fatty and Fibrous Tissue Pack (Bio-Rad, Catalog #732-6870, Hercules, CA) using the spin protocol according to the manufacturer's instructions. RNA quality and quantity were assessed using an Experion Bioanalyzer (Bio-Rad) and an Epoch microplate spectrophotometer (BioTek Instruments, Winooski, VT), respectively. Rats with poor RNA quality (Experion values below 6.5) were excluded from the experiment (*n* = 5 out of 18 rats). Total RNA samples were stored at −20°C prior to analysis.

Rat primers (Thermo Fisher Scientific, Waltham, MA) were used to detect the gene products for Iba1 (see Section 2.3.1.2 for results) as well as the inflammatory cytokines IL1β,TNFα, IL6, and IL10, and the three reference genes beta- 2-microglobulin (β*2M*), glyceraldehyde-3-phosphate dehydrogenase (*GAPDH*), and hypoxanthine phosphoribosyltransferase (*HPRT*) (for primer sequences, see Appendix I, Table I.1). The expression stability of the three reference genes has previously been shown to be unaffected in rat brains by either 6 h of total sleep deprivation or 4 days of REM sleep deprivation (Hassani et

al., 2009). Reverse transcriptase reactions were conducted using the iScript cDNA synthesis kit (Bio-Rad) using 1 µg of total RNA from each sample. qPCR was performed using SsoFast EvaGreen Supermix kit (Bio- Rad) with the CFX 96 Real-Time System C1000 Touch thermal cycler (Bio-Rad): 1 cycle of 30 s at 95°C followed by 40 cycles of 5 s at 95°C, 5 s at 55°C plus plate reading (Nichols et al., 2015). The melting curve consisted of 2 s stops at intervals of 0.5°C between 65°C and 95°C. All quantitative reverse transcriptase-polymerase chain reaction (qRT-PCR) analysis was performed according to MIQE guidelines (Bustin et al., 2009). Each sample was tested in triplicate and values were normalized to the three reference genes. Data analysis was performed with CFX Manager 3.1 software (Bio-Rad) using the ΔΔCq method.

3.2.1.3 IL10 immunohistochemistry and image capture

To determine the cellular localization of IL10 in the frontal cortex, which showed significant changes in IL10 mRNA levels following CSR (see Section 3.3.1), rats were assigned to SR2 (n = 2), SR5 (n = 2), LW2 (n = 1) and LW5 (n = 1) groups. Double-label immunofluorescence was performed using a polyclonal rabbit anti-IL10 antibody (1:100) with a polyclonal guinea pig anti-Iba1 antibody (1:1000), monoclonal mouse anti-NeuN (1:500), or monoclonal mouse anti-glial fibrillary acidic protein (GFAP; 1:500) antibody (see Appendix B, Table B.1 for antibody information). Cy3-conjugated donkey anti-rabbit IgG (1:200; Jackson), Cy2-conjugated donkey anti-guinea pig IgG (1:200; Jackson), and Cy2-conjugated donkey anti-mouse IgG (1:100; Jackson) secondary antibodies were used to visualize the primary antibody labeling. The specificity of the IL10 antibody was confirmed by the manufacturer using Western blot analysis (see Appendix B, Table B.1). In addition, I conducted preadsorption of the anti-IL10 antibody with a 5X excess of the antigen recombinant rat IL10 protein (Abcam, Catalogue # AB9970), which completely abolished immunofluorescence staining (data not shown). A

single fluorescent image of the prelimbic cortex was captured per animal using a 40X objective lens on a laser scanning confocal microscope (Zeiss LSM510).

3.2.2 Experiment 2: Immunohistochemical characterization of microglia molecular phenotype with inflammatory markers

3.2.2.1 Treatment groups, perfusion, and collection of brain sections

Rats were assigned to SR2 (n = 3), SR5 (n = 3), LW2 (n = 1), and LW5 (n = 2) groups. At the end of their respective experimental protocols (i.e., 10:00 AM), rats were anaesthetized and perfused as previously described (see Section 2.2.3.2). Brains were cut into 5 series of 40 µm thick coronal sections that were collected in 0.05M TBS.

3.2.2.2 Immunohistochemistry

To characterize the molecular phenotype of microglia following CSR, sections through the frontal cortex were double labeled with a guinea pig anti-Iba1 antibody (1:1,000) and one of the following antibodies (see Appendix B, Table B.1): monoclonal mouse anti-CD68 (1:100) and anti-OX6/MHCII (1:500) antibodies for pro-inflammatory (often referred to as "M1") markers; and polyclonal rabbit anti-Arginase-1 (1:100), anti-cyclooxygenase-2 (1:200), or anti-mannose receptor/CD206 (1:100) antibodies for anti-inflammatory (often referred to as "M2") markers (Franco & Fernandez-Suarez, 2015). Cy2-conjugated donkey anti-guinea pig IgG (1:100; Jackson), Cy3-conjugated donkey anti-rabbit IgG (1:200; Jackson), and Cy3- conjugated donkey anti-mouse IgG (1:400; Jackson) were used as secondary antibodies. Double-label immunofluorescence using the guinea pig anti-Iba1 antibody (1:1,000; used in this Chapter) with the rabbit anti-Iba1 antibody (1:2,000; used in Chapter 2) showed a virtually complete overlap of

microglia staining for both cell bodies and processes in the cortex (data not shown). A z-stack of 0.5 µm optical sections was collected through the prelimbic cortex for each animal using a 40× objective lens on a laser scanning confocal microscope (Zeiss LSM510).

3.2.3 Experiment 3: Immunohistochemical characterization of microglia molecular phenotype with the homeostatic marker P2Y12 receptor

3.2.3.1 Treatment groups, perfusion, and collection of brain sections

Rats were assigned to 5 groups: SR2 (n = 9), SR5 (n = 9), LW2 (n = 4), LW5 (n = 4), and exercise control (EC; n = 9) groups. The EC group was housed in unlocked wheels that rats could freely rotate for voluntary wheel running for 10 days (including 5 days of habituation). The EC group was included to control for the wheel rotations experienced by rats in the SR groups.

At the end of their respective experimental protocols (i.e., 10:00 AM), rats were anaesthetized and perfused as previously described (Section 2.2.3.2). Brains were cut into 5 series of 30 µm thick coronal sections through the frontal cortex (3.0 mm to 2.8 mm anterior to bregma) and lateral hypothalamus (2.5 mm to 3.5 mm posterior to bregma) using a freezing microtome and were stored in cryoprotectant at -20 °C until used for immunohistochemistry.

3.2.3.2 Immunohistochemistry

One series of sections through the frontal cortex and lateral hypothalamus were incubated with a guinea pig anti-Iba1 antibody (1:1,000) and a polyclonal rabbit anti-P2Y12 receptor antibody (1:500, see Appendix B, Table B.1 for antibody information). The P2Y12 receptor is a specific microglia marker expressed only under physiological (i.e., homeostatic) conditions

(Haynes et al., 2006). Cy2-conjugated donkey anti-guinea pig IgG (1:100; Jackson) and Cy3-conjugated donkey anti-rabbit IgG (1:200; Jackson) were used as secondary antibodies.

3.2.3.3 Image acquisition

Fluorescent images of the PrL and PeFLH (single optical plane; 1024 x 1024 pixels) were captured using a laser scanning confocal microscope (Zeiss LSM 710) using a 10X or 20X objective lens, respectively. Images within the PrL measured 850 x 850 μm^2 (pixel size = 0.83 μm) and within the PeF/LH measured 607 x 607 μm^2 (pixel size = 0.59 μm). Unilateral images were captured on three adjacent sections (150 μm apart) per animal for each brain region.

3.2.3.4 Image analysis (density and intensity)

For analysis, PrL images were cropped for a final analysis box size of 725 x 850 μm^2, while the entire PeF/LH image (607 x 607 μm^2) was used (See Appendix D, Table D.1 for details on the placement of analysis boxes). Each image was split into two separate colour channels for each label (i.e., Iba1, green; P2Y12, red) and converted to grayscale such that pixel values ranged from 0 (black) to 255 (white).

Image analysis was conducted through the multiple steps illustrated in Appendix H, Figure H.1 using individual, merged, and subtracted images in Photoshop. To create the *merged* image, the Iba1 channel was superimposed onto the P2Y12 channel using the 'add' blending mode, so that the value of each pixel in the Iba1 channel was added to the value of the underlying pixel in the P2Y12 channel (Appendix J, Figure J.1, C). Conversely, to create the *subtracted* image, the Iba1 image was superimposed onto the P2Y12 image using the 'subtract' blending mode, so that Iba1 pixel values were subtracted from the P2Y12 pixel values; any negative values were changed to zero (Appendix J, Figure J.1, D). Next, ImageJ was used to apply a threshold

(Triangle Auto Threshold; (Zack, Rogers, & Latt, 1977)) to each image (individual, merged, and subtracted) in order to measure the density and intensity of Iba1 and/or P2Y12 immunoreactivity.

For density, 4 measures were taken: 1) the density of total Iba1 immunoreactivity was measured using the individual Iba1 channel, 2) the density of total P2Y12 immunoreactivity was measured using the individual P2Y12 channel, 3) the density of merged Iba1 and P2Y12 immunoreactivity (including areas single-labeled for Iba1 or P2Y12 plus areas doubled-labeled for both Iba1 and P2Y12) was measured using the merged image, and 4) the density of single P2Y12 immunoreactivity without Iba1 co-localization was measured using the subtracted image. The density was calculated as the percentage of immunoreactive area for each measure by dividing the number of pixels that were below the threshold value by the total number of pixels within the analysis box for each brain region. Pixels that corresponded to a blood vessel within the analysis box were excluded from the total pixel count.

For intensity, the fluorescence intensity (mean gray level) of Iba1 and P2Y12 labelling was measured on respective individual colour channels.

3.2.4 Statistics

Statistical analyses were conducted using GraphPad Prism 6. One- or two-way analyses of variance (ANOVA) were performed to compare treatment groups, followed, when applicable, by Fisher's LSD post hoc tests. When the data did not meet the assumptions of the ANOVA, Kruskal–Wallis tests were used, followed, when applicable, by Dunn's multiple comparison tests. Probability values of <0.05 were considered statistically significant. Data values are expressed as means ± standard error of the mean (SEM).

3.3 Results

3.3.1 Experiment 1: Cytokine mRNA expression and IL10 immunoreactivity

3.3.1.1 Cytokine mRNA expression in the frontal cortex

To determine whether the increase in Iba1 immunoreactivity following CSR is accompanied by changes in the expression of inflammatory cytokines, we examined the mRNA levels of TNFα, IL1β, IL6, and IL10 in the frontal cortex (including the prelimbic cortex) following CSR. The frontal cortex was selected because it is known to be sensitive to sleep loss (Muzur et al., 2002) and has been shown to respond to the 3/1 CSR protocol with increased BDNF protein levels (Wallingford et al., 2014) and to a different CSR protocol with increased IL1β and TNFα mRNA levels (Zielinski et al., 2014). After the exclusion of five rats due to poor RNA quality (see Section 3.2.1.2), the final animal numbers in each group for qRT-PCR analysis were SR2 (n = 4), SR5 (n = 5), LW2 (n = 2), and LW5 (n = 2). There was no obvious group difference between the LW2 and LW5 groups for any cytokine mRNA levels, and thus these two control groups were combined into a single LW group.

The LW, SR2, and SR5 groups did not significantly differ in the normalized mRNA levels of TNFα (H = 1.53, p = 0.49; Figure 3.1, A), IL1β (H = 0.74, p = 0.72; Figure 3.1, B), and IL6 (H = 0.17, p = 0.92; Figure 3.1, C). In contrast, normalized IL10 mRNA levels were significantly different between the three treatment groups (H = 7.14, p = 0.017; Figure 3.1, D): IL10 mRNA levels were higher in the SR2 group than the LW group (p = 0.041) and were at the control levels in the SR5 group (p > 0.99 vs LW).

3.3.1.2 IL10 immunoreactivity in the frontal cortex

As IL10 mRNA levels in the frontal cortex were increased by CSR (see above, Section 3.3.1.1), the cellular localization of IL10 was assessed in the frontal cortex of an additional

cohort of SR2 (n = 2), SR5 (n = 2), LW2 (n = 1), and LW5 (n = 1), animals using immunohistochemistry. Immunohistochemical processing was conducted concurrently on all brain sections as a single cohort. IL10 staining was abolished by preadsorption of the primary antibody with an excess of the antigen recombinant rat IL10 protein (see Section 3.2.1.3), providing additional specificity information for the anti-IL10 antibody used in this study (see also Appendix B, Table B.1). Qualitatively, the intensity of IL10 immunostaining did not appear to differ between the treatment groups.

IL10 immunoreactivity did not co-localize with either the microglia marker Iba1 (Figure 3.1, E) or the astrocytic marker GFAP (data not shown) in the frontal cortex. However, IL10 immunoreactivity was almost exclusively co-localized with NeuN throughout the frontal cortex in all treatment groups. An example of a section double-immunostained for IL10 and the neuronal marker NeuN in an SR2 rat is shown in Figure 3.1, E. NeuN-positive, IL10-negative cells were observed occasionally (Figure 3.1, E).

3.3.1.3 Body weights

In the first cohort of rats used for cytokine expression (Section 3.3.1.1), as observed in Chapter 1, the LW2 and LW5 groups gained body weight from pre-protocol levels (+5.5% and +12.5%, respectively; Appendix H, Table H.4), while the SR2 group lost weight (−4.3%). The SR5 group, however, did not lose weight as in the previous experiments but maintained pre-protocol levels (+0.7%). Nonetheless, this was in contrast to the significant body weight gain observed in the LW5 group (p = 0.0062 vs SR5; Appendix H, Table H.4).

In the second cohort of rats used for IL10 immunohistochemistry (Section 3.3.1.2), the LW2 and LW5 groups gained body weight from pre-protocol levels (+3.6% and +13.0%, respectively), while the SR2 and SR5 groups lost weight (-3.0 and -14.7%, respectively).

3.3.2 Experiment 2: Immunohistochemical characterization of microglia molecular phenotype with inflammatory markers

Finally, we examined the molecular phenotype of microglia in the prelimbic cortex, where microglia morphology was quantified (see Section 2.2.4), in additional SR2 (n = 3), SR5 (n = 3), LW2 (n = 1), and LW5 (n = 2) animals.

Iba1-ir microglia in the prelimbic cortex were not immunoreactive for any of the pro- (CD68 and OX6) or anti- (arginase-1, cyclooxygenase-2, and mannose receptor) inflammatory markers examined in all treatment groups (Figure 3.2). Iba1-ir meningeal macrophages, however, were co-labeled with all these inflammatory markers (Figure 3.2), as has been previously reported (Chinnery, Ruitenberg, & McMenamin, 2010; Faraco, Park, Anrather, & Iadecola, 2017; Hellström Erkenstam et al., 2016), except arginase-1. Additionally, as reported previously (Burudi & Regnier-Vigouroux, 2001; Kaufmann, Worley, Pegg, Bremer, & Isakson, 1996; Kuric & Ruscher, 2014; Perego et al., 2011; Peters et al., 2013), immunolabeling of arginase-1, cyclooxygenase-2, and mannose receptor, but not CD68 and OX6, was found in frontal cortex neurons (Figure 3.2).

Compared to pre-protocol levels, the LW2 and LW5 groups gained body weight (+3.7% and +7.3%, respectively), the SR2 group did not gain weight (+0.1%), and the SR5 group lost weight (−10.4%; Appendix H, Table H.5).

3.3.3 Experiment 3: Immunohistochemical characterization of microglia molecular phenotype with the homeostatic marker P2Y12 receptor

3.3.3.1 Density of Iba1 and P2Y12 immunoreactivity

Given the absence of inflammatory markers in microglia following CSR, I then examined the presence of the homeostatic marker P2Y12 receptor in microglia in the EC (n = 9), LW2 (n = 4), LW5 (n = 4), SR2 (n = 9), and SR5 (n = 9) groups. Iba1 and P2Y12 immunofluorescence densities were analyzed in the PrL and PeF/LH, two brain regions which showed increased Iba1 immunoreactivity in response to CSR (see Section 2.3.1 in Chapter 2).

Virtually all Iba1-ir microglia were strongly co-immunolabeled with P2Y12 receptors, and vice versa, in the PrL (Figure 3.3, C) and PeF/LH (Figure 3.3, D) of all treatment groups. However, within each microglial cell, Iba1 and P2Y12 staining did not completely overlap, consistent with the cytoplasmic and cell membrane localization, respectively, of Iba1 and P2Y12 receptors (Cserep et al., 2020; Haynes et al., 2006). Thus, P2Y12 did not stain microglial cell bodies as distinctly as Iba1 did, while it revealed more complex secondary and tertiary branches than did Iba1. Exclusive presence of P2Y12 receptor immunoreactivity in Iba1-ir microglia and absence of P2Y12 labeling in Iba1-ir meningeal macrophages are consistent with previous reports (Haynes et al., 2006; Mildner et al., 2017).

Quantitatively, the four treatment groups did not significantly differ in the density of total Iba1- or P2Y12-immunoreactivity in either the PrL ($F_{3,58} = 1.46$, $p = 0.24$; Figure 3.3, A) or PeF/LH ($F_{3,58} = 0.85$, $p = 0.47$; Figure 3.3, B). However, irrespective of treatment groups, the total density of P2Y12 immunoreactivity was greater than that of Iba1 in both the PrL ($F_{3,58} = 64.1$, $p < 0.0001$) and PeF/LH ($F_{3,58} = 21.1$, $p < 0.0001$). Consistent with the colocalization between Iba1 and P2Y12 receptor immunolabelling, positive correlations were found between the percent P2Y12-ir area and the percent Iba1-ir area in both the PrL ($r = 0.67$, $p < 0.0001$; Figure 3.4, A) and PeF/LH ($r = 0.76$, $p < 0.0001$; Figure 3.4, B) across all treatment groups.

Given the differences in the cellular localization of Iba1 and P2Y12 receptors within microglia (see above), the density of merged P2Y12 and Iba1 immunoreactivity (which presumably labelled the entire microglia) and of P2Y12 immunoreactivity without Iba1 colocalization (which mainly labelled the most distal microglia processes) were also calculated (see Section 3.2.3.4 for the methods). In both the PrL and PeF/LH, there was no significant difference between treatment groups for either the density of merged P2Y12 and Iba1 immunoreactivity ($F_{3,29}$ = 1.5–2.0, p = 0.14–0.25; Appendix J, Figure J.2, A and C) or the density of P2Y12 without Iba1 colocalization ($F_{3,29}$ = 1.8–2.0, p = 0.14–0.17; Appendix J, Figure J.2, B and D).

3.3.3.2 Intensity of Iba1 and P2Y12 immunoreactivity

In the PrL and PeF/LH, no significant difference was found between treatment groups in the mean fluorescence intensity of Iba1 immunoreactivity ($F_{3,29}$ = 0.56–0.61, p = 0.62–0.65; Appendix J, Figure J.3, A and C) or the mean fluorescence intensity of P2Y12 immunoreactivity ($F_{3,29}$ = 0.42–1.1, p = 0.38–0.74; Appendix J, Figure J.3, B and D).

3.3.3.3 Body weights

The average percent change in body weight at the end of respective protocols from pre-protocol levels varied among the LW2, LW5, EC, SR2, and SR5 groups ($F_{4,30}$ = 15.6, p<0.0001; Table B.4). Specifically, the EC, LW2, and LW5 groups gained weight (+6.5%, +3.4%, and +8.6%, respectively), while the SR2 and SR5 groups lost weight (-1.7% and -5.3%, respectively). Rats in the EC group had a smaller pre-protocol mean body weight (369g) compared to the other groups (393–416g; Appendix H, Table H.6). This was most likely because rats in the EC group were housed in unlocked activity wheels available for voluntary exercise during the preceding habitation period.

3.4 Discussion

Here, we show that frontal cortex mRNA levels of several pro-inflammatory cytokines were not affected by 27 or 99 h of CSR, while mRNA levels of the anti-inflammatory cytokine IL10 were transiently increased after 27 h of CSR. IL10 immunoreactivity, however, was found in cortical neurons and not microglia or astrocytes. Furthermore, while Iba1-ir microglia in the PrL were not immunoreactive for several pro- and anti-inflammatory markers examined, Iba1-ir microglia in the PrL and PeF/LH are immunoreactive for P2Y12 receptors, suggesting a physiological or homeostatic microglia phenotype. The densities of Iba1 and P2Y12 immunoreactivity were not affected by CSR. As previously reported (see Chapter 2), body weight was gradually lost during CSR compared to pre-protocol levels.

3.4.1 Methodological considerations

A non-sleep deprived wheel rotation control group was not included in the assessment of cytokine mRNA levels in this study. However, as discussed for Iba1 immunoreactivity in Chapter 2 (see Section 2.4.1), there is little evidence to support that increased locomotion associated with wheel rotations contributed to the results of the current study, i.e., the lack of changes in pro-inflammatory cytokine expression in the frontal cortex following CSR. Specifically, a previous study (Chennaoui et al., 2015) reported that 7 weeks of forced treadmill running for 1–2 h/day reduced sleep deprivation-induced IL1β mRNA levels in the hippocampus but not in the frontal cortex in rats; neither treadmill running nor sleep deprivation affected TNFα and IL6 mRNA levels in either region (Chennaoui et al., 2015).

3.4.2 Cytokine expression during CSR

In the frontal cortex, in parallel with the initial increase in Iba1 immunoreactivity, the mRNA level of the anti-inflammatory cytokine IL10 was transiently increased after 27 h of CSR, while mRNA levels of the pro-inflammatory cytokines TNFα, IL1β, and IL6 remained unchanged at 27 and 99 h of CSR. The latter finding may be explained by previous reports that IL10 can inhibit microglial production of TNFα, IL1β, and IL6 (Lodge & Sriram, 1996; Sawada, Suzumura, Hosoya, Marunouchi, & Nagatsu, 1999). Our findings, however, are in contrast to previously reported increases in TNFα and IL1β mRNA levels in the frontal cortex and hippocampus after 5 days of CSR (Zielinski et al., 2014), and in the piriform cortex and hippocampus after 21 days of CSR (Manchanda et al., 2018) in adult rats, as well as increases in TNFα and IL6 mRNA levels in the hippocampus after 72 h of REM sleep deprivation in adult mice (Tuan & Lee, 2019; Xue et al., 2019). Nonetheless, mRNA levels do not necessarily predict protein levels, and several cytokine mRNAs are known to be post-transcriptionally modified (Vlasova-St Louis & Bohjanen, 2017). Another study in adolescent mice found a decrease in TNFα protein levels, no change in IL1β protein levels, and undetectable IL6 and IL10 protein levels in the cerebrospinal fluid after 4.5 days of CSR (Bellesi et al., 2017). The discrepancies among these studies are likely due to differences in species, duration of CSR, and/or protocol used, as well as samples (brain regions or cerebrospinal fluid), or mRNA or protein, that were analyzed.

The finding of IL10 immunoreactivity localized in neurons and not in microglia (or astrocytes) in the frontal cortex of control and sleep-restricted animals was unexpected, as microglia are the most studied cellular sources of IL10 (Lobo-Silva, Carriche, Castro, Roque, & Saraiva, 2016). However, the expression of IL10 mRNA and protein has been observed in mouse

cortical neurons under both normal and inflammatory conditions (Schluter, Kaefer, Hof, Wiestler, & Deckert-Schluter, 1997). Nonetheless, this unexpected finding raised questions regarding the specificity of the IL10 antibody used in this thesis. The manufacturer's technical information indicated that a band corresponding to IL10 was recognized by this antibody in Western blot analysis (Appendix B, Table B.1). In addition, we confirmed that preadsorption of the anti-IL10 antibody with an excess of rat IL10 successfully abolished all immunostaining (see Section 3.2.1.3), although this does not exclude the possibility that the antibody binds to a protein in the tissue that is similar to, but different from, IL10. Neuronal levels of IL10 immunostaining did not appear to increase in response to 27 h CSR, as assessed qualitatively in the frontal cortex, while IL10 mRNA did increase; therefore it remains possible that IL10 regulation only occurred at the mRNA, and not protein, level. Additionally, IL10 immunohistochemistry detects IL10 protein and thus does not confirm the cellular location of the increased IL10 mRNA in the frontal cortex in response to CSR. *In situ* hybridization techniques will be necessary to validate the expression of IL10 mRNA in neurons, rather than microglia. Techniques that measure cytokine protein levels specifically in microglia, such as sell sorting procedures paired with Western blot analysis or ELISA, will be important for determining the impact of increased levels of cortical IL10 mRNA in response to CSR.

The significance of increased IL10 mRNA levels in the frontal cortex is unclear and requires further investigation. We previously found that BDNF protein levels were increased in the frontal cortex following 27 h, with a slight decline in this increase after 99 h, of the 3/1 CSR protocol (Wallingford et al., 2014). BDNF has been shown to increase the expression of IL10 in a rat model of ischemia (Jiang et al., 2011). Binding of IL10 at its receptor, present on both glial (including microglia) and neuronal cell types, promotes the survival of glia and neurons (Lobo-

Silva et al., 2016). Therefore, neuroprotective molecules such as IL10 and BDNF may interact to initiate processes that help animals adapt to CSR. In the present study, IL10 expression in the frontal cortex was at control levels after 99 h of CSR; therefore, a sustained increase in IL10 mRNA may not be necessary once these neuroprotective mechanisms have been initiated.

3.4.3 Density of Iba1 immunoreactivity during CSR

In sharp contrast to our previous findings (Section 2.3.1), the density of Iba1 immunoreactivity was not found to increase in the PrL or PeFLH following CSR in the present study, despite the use of the same CSR protocol in both studies. This discrepancy may be due to several factors, the most prominent contributor being differences in the detection method used for Iba1 visualization between the two studies, i.e. diaminobenzidine/nickel (DAB/Ni; Chapter 2) versus immunofluorescence (present study). DAB/Ni immunohistochemistry uses a multi-level signal amplification that is considered more sensitive than the two-step detection method used for immunofluorescence (Shojaeian, Lay, & Zarnani, 2018). Thus, DAB/Ni immunohistochemistry likely more greatly amplifies Iba1 protein signal levels, and in a more finely graded manner, compared to immunofluorescence. This possibility is supported by a generally higher densities of Iba1 immunoreactivity in the PrL and PeFLH observed in Chapter 2 with the DAB/Ni method (22–33% in the PrL and 13–19% in the PeF/LH, across all treatment groups) compared to the densities of Iba1 immunofluorescence in the current study (3.0–3.7% in the PrL and 2.7–3.3% in the PeF/LH, across all treatment groups). Furthermore, in a previous preliminary study by another group, a quantitative comparison of Iba1 staining density using immunofluorescence and DAB/Ni protocols on adjacent brain sections showed a significantly greater Iba1 density using DAB/Ni, suggesting an enhanced amplification of Iba1 antibody

signal using the DAB/Ni method (Baun, Zurhellen, York, Tipton, & Sqitzer III, 2016). Thus, in the present thesis, DAB/Ni immunohistochemistry likely visualized quantities of Iba1 protein in microglia that were not only at high levels, but also at levels below the detection threshold for immunofluorescence.

The use of two different primary antibodies directed at different immunogens were used to visualize Iba1 in Chapter 2 versus the current study (see Appendix B, Table B.1) and may also be considered a possible explanation for the differences in the density of Iba1 immunoreactivity between the two studies. This possibility, however, is unlikely as antibody testing in a pilot study showed virtually complete colocalization of the two immunolabels in microglia (see Section 3.2.2.2).

As discussed in Chapter 2 (see Section 2.4.1), validating the observed changes in Iba1 immunoreactivity with the DAB/Ni method using Western blot will be useful to confirm the changes in Iba1 protein levels in response to CSR.

3.4.4 Density of P2Y12 receptor immunoreactivity during CSR

The P2Y12 receptor is a $G_{i/o}$ protein-coupled receptor expressed in microglia under physiological conditions and is down-regulated during inflammatory responses (Amadio et al., 2014; Haynes et al., 2006). Although the density of P2Y12 receptor immunoreactivity did not change during CSR in either the PrL or PeF/LH, the presence of P2Y12 receptors in Iba1-ir microglia under control and CSR conditions suggests microglia retain a 'homeostatic' phenotype.

Increasing evidence suggests that the P2Y12 receptor in microglia is involved in detecting extracellular signals such as nucleotides (ATP and ADP) to induce chemotaxis, and P2Y12

receptor expression is thought to indicate the physiological or homeostatic state of microglia (Calovi, Mut-Arbona, & Sperlagh, 2019; Cserep et al., 2020; Haynes et al., 2006). In the present study, the density of P2Y12 *without* Iba1 colocalization, which mainly measured the areas occupied by microglia distal process branches, also remained unchanged following CSR, suggesting P2Y12-ir microglia branches did not extend (or shrink) in response to CSR. This finding is consistent with Iba1-based microglia morphological measures in the PrL (and PeF/LH, see Chapter 4, Section 4.3.2) which showed no evidence of process extension during CSR (see Chapter 2, Section 2.3.2). However, given the discrepant results with DAB/Ni immunohistochemistry versus immunofluorescence (Section 3.4.2, above), further assessment of P2Y12 receptor protein levels (e.g., using quantitative DAB/Ni immunohistochemistry or Western blot analyses), and the morphology of P2Y12-ir microglia, is needed to validate these findings.

3.4.5 Homeostatic state of CSR-responsive microglia

We originally hypothesized that the increased Iba1 immunoreactivity observed in response to CSR (see Chapter 2) would represent an inflammatory response. However, several aspects of the microglia response to the 3/1 CSR protocol are not congruent with inflammatory activation (Perry, Nicoll, & Holmes, 2010). In Chapter 2, we found that microglia morphology was not affected by CSR; microglia showed a relatively small cell body and remained ramified, as confirmed quantitatively in the prefrontal cortex (see Section 2.3.2). Additionally, CSR induced neither microglia proliferation nor peripheral macrophage recruitment (see Sections 2.3.3 and 2.3.4). In the present study, frontal cortex mRNA levels of several pro-inflammatory cytokines were not affected, while mRNA levels of the anti-inflammatory cytokine IL10 were transiently

increased. Unexpectedly, however, IL10 immunoreactivity was exclusively found in neurons. Furthermore, microglia in the frontal cortex did not contain pro-inflammatory (CD68 and OX6) or anti-inflammatory (arginase-1, cyclooxygenase-2, and mannose receptor) markers. Rather, microglia in the frontal cortex and lateral hypothalamus expressed the purinergic receptor P2Y12 under both control and CSR conditions.

Homeostatic microglia can initiate synaptic plasticity by contacting spines (Akiyoshi et al., 2018) and phagocytosing pre-synaptic elements (Schafer et al., 2012) through P2Y12 receptor activation (Sipe et al., 2016). Microglia phagocytosis of presynaptic terminals was reported in the adolescent mouse cortex after 4.5 h of CSR (Bellesi et al., 2017) (but see Ref. (Choudhury et al., 2020)), while impaired microglia phagocytosis of post-synaptic elements was associated with a reduction of P2Y12 receptor mRNA levels in the adolescent mouse hippocampus after 72 h of selective REM sleep deprivation (Tuan & Lee, 2019). These forms of synaptic plasticity, if they occur in the PrL and PeF/LH in response to CSR, might be involved in the adaptive changes in sleep/wake patterns and sustained attention observed during the 3/1 CSR protocol (Deurveilher et al., 2015; Deurveilher et al., 2012).

3.5 Conclusions

These results show that microglia remained in a homeostatic state without inflammatory activation in the frontal cortex and lateral hypothalamus in response to 1–4 days of the 3/1 CSR protocol. Responses of these homeostatic microglia, possibly mediated by P2Y12 receptor signaling, may contribute to the adaptive responses produced by CSR through alterations in microglia–neuron interactions in sleep/wake-regulatory brain regions during CSR. I explored this possibility in Chapter 4.

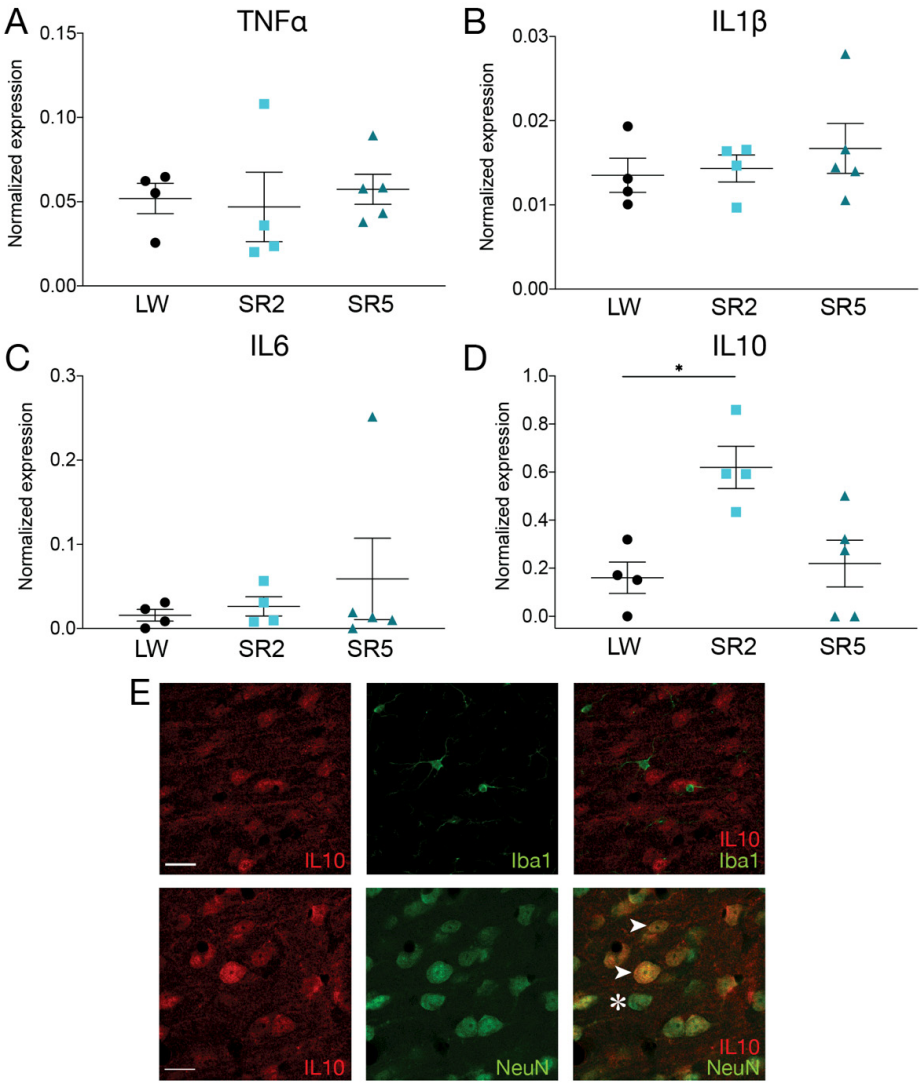

Figure 3.1. Cytokine expression in the frontal cortex under CSR and control conditions. A–D, Mean (± SEM) normalized mRNA levels of tumor necrosis factor-α (TNFα; A), interleukin-1β (IL1β; B), IL6 (C), and IL10 (D) are shown for the LW (n = 4), SR1 (n = 4) and SR5 (n = 5) groups. Each symbol represents a rat. The two time-matched LW groups (LW2 and LW5) were combined into a single LW control group. While TNFα, IL1β, and IL6 mRNA levels were not affected by CSR, IL10 mRNA levels were significantly increased in the SR2 group compared to

the LW group and were at control levels in the SR5 group. *p<0.05 (Dunn's multiple comparison test). E, Representative double immunofluorescence staining of IL10 (red) and Iba1 or NeuN (green) in the frontal cortex of a SR2 rat. White arrowheads indicate examples of double-labeled cells for IL10 and NeuN, whereas the asterisk indicates an example of a cell that is positive for NeuN but negative for IL10. Scale bar=20μm. A–D reprinted from Hall, S., Deurveilher, S., Robertson, G.S., Semba, K. Homeostatic state of microglia in a rat model of chronic sleep restriction, SLEEP, 2020, 1–16 by permission of Oxford University Press.

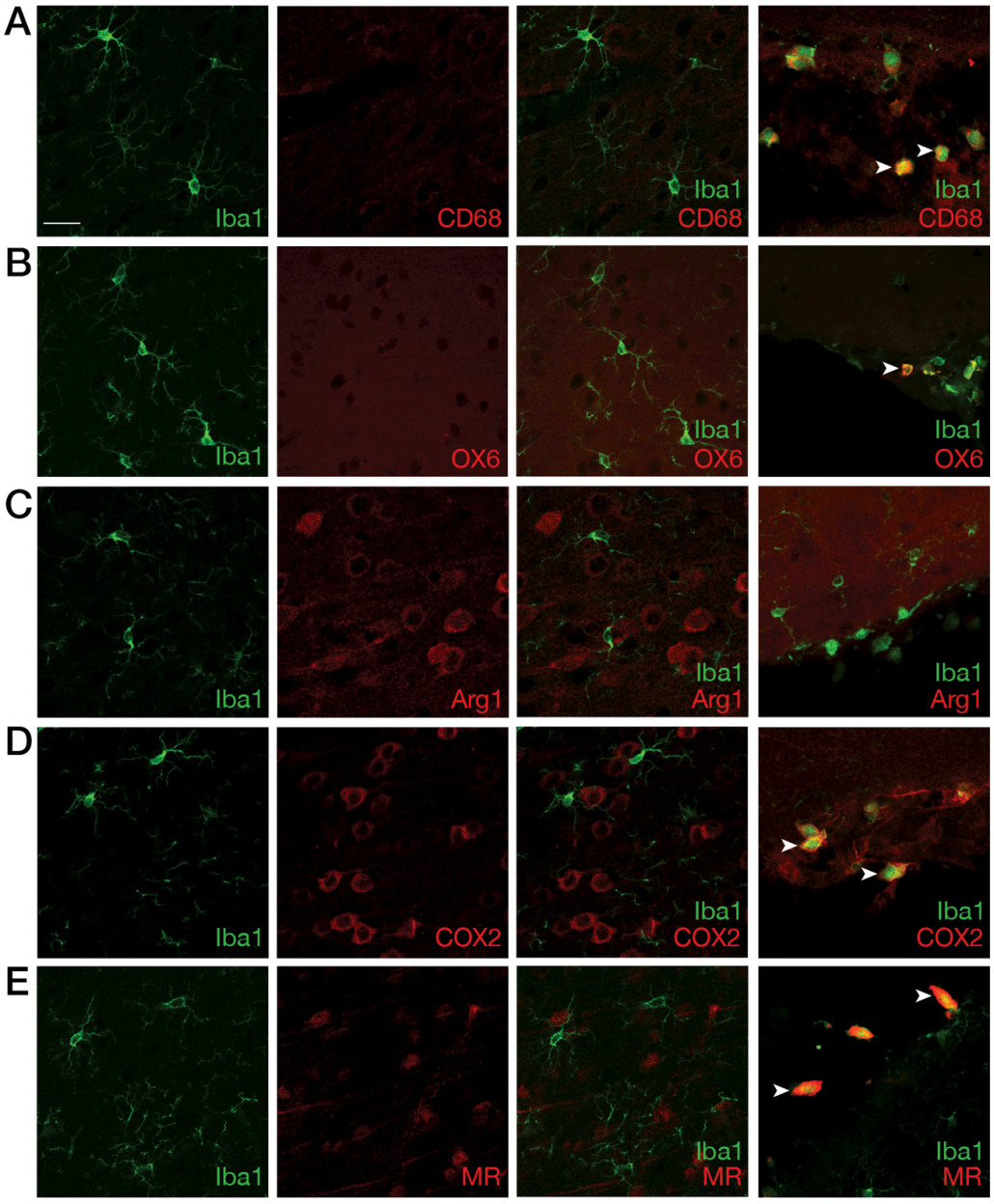

Figure 3.2. Representative confocal images of double-label immunofluorescence for Iba1 (green) and inflammatory markers (red) in the frontal (prelimbic) cortex in a SR5 rat, including the pro-inflammatory ('M1') markers CD68 (A) and OX6 (B) and the anti-inflammatory ('M2') markers Arg1 (C), COX2 (D), and MR (E) (see Table A.1 for further details). There was no

colocalization of Iba1 and any inflammatory markers tested in microglia. However, there was co-labeling of Iba1-ir macrophages in the meninges with CD68, OX6, COX, and MR2 (far-right panels; examples indicated by white arrowheads); Iba1-ir meningeal macrophages did not co-label with Arg1 (C, far right). Scale bar = 20 μm. Abbreviations: Arg1, arginase-1; COX2, cyclooxygenase-2; MR, mannose receptor. Reprinted from Hall, S., Deurveilher, S., Robertson, G.S., Semba, K. Homeostatic state of microglia in a rat model of chronic sleep restriction, SLEEP, 2020, 1–16 by permission of Oxford University Press.

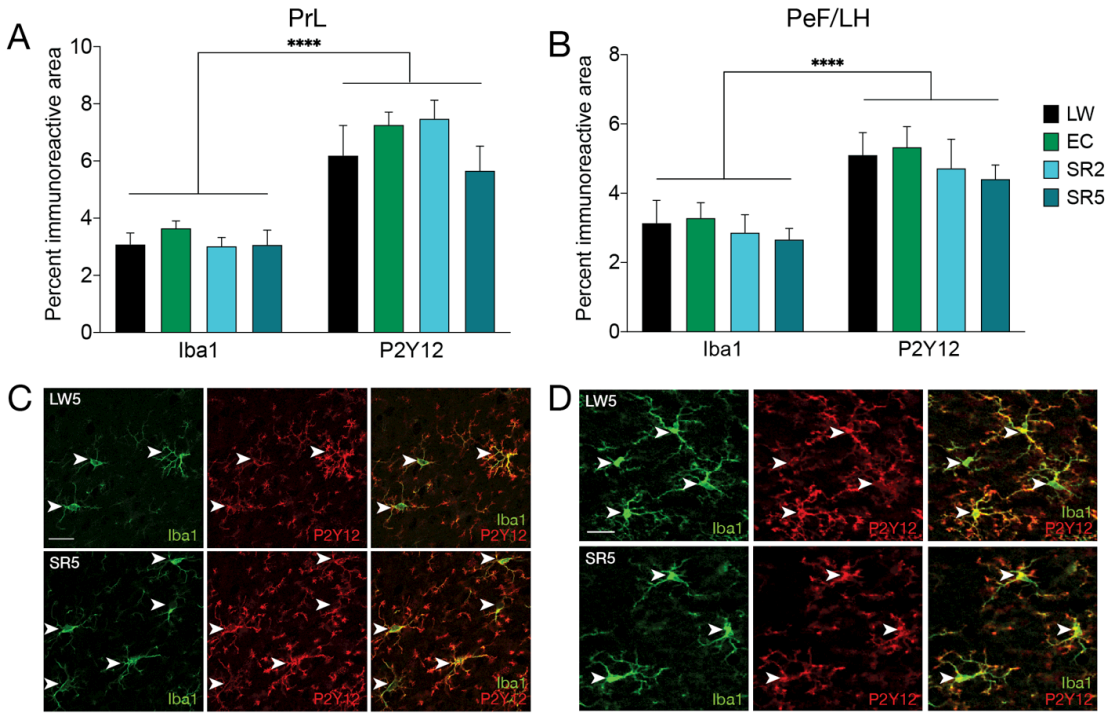

Figure 3.3. The density (percent area) of Iba1 and P2Y12 receptor immunoreactivity in the PrL (A) and PeF/LH (B) following CSR. The LW2 and LW5 control groups were combined into a single LW control group. Data are shown as means + SEM for the LW (n = 7), EC (n = 8), SR2 (n = 9), and SR5 (n = 9) groups. There was no significant effect of CSR on the percent Iba1-ir area (*left*) or P2Y12-ir area (*right*) in either brain region. However, the percent P2Y12-ir area was significantly greater than the percent Iba1-ir area across all treatment groups in both the PrL and Pe/FLH. ****$p < 0.0001$ (main effect of labeling, two-way repeated ANOVA). Representative double-label immunofluorescence images of Iba1 (green) and P2Y12 receptors (red) of a LW5 (*top*) and SR5 (*bottom*) rat are shown for both the PrL (C) and PeF/LH (D). White arrowheads indicate individual microglia cells. Note that virtually all Iba1-ir microglia are also immunoreactive for P2Y12 receptors, and vice versa. Data are shown as means + SEM. Scale bar=20 µm.

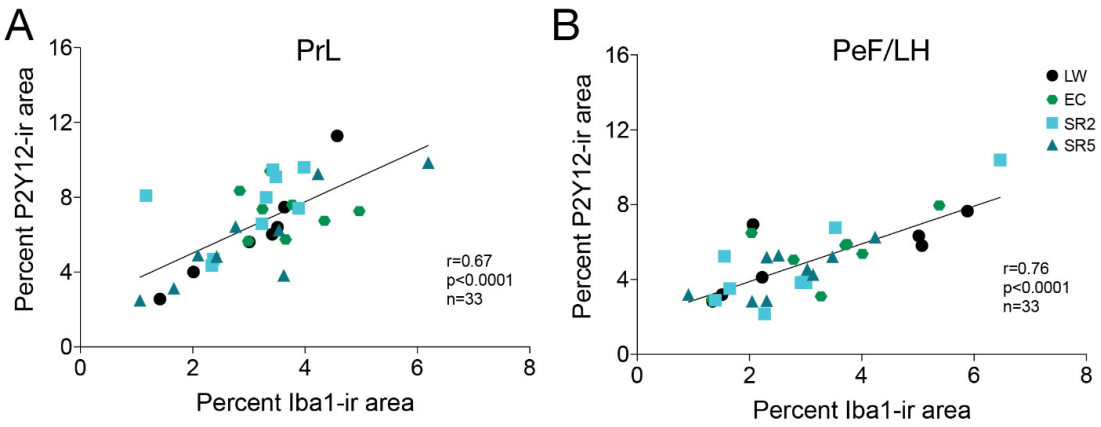

Figure 3.4. Scatterplots of the percent area of P2Y12- versus Iba1-ir in the PrL (A) and PeF/LH (B) during CSR for the LW2 (*n* = 4), LW5 (*n* = 3), SR2 (*n* = 9), SR5 (*n* = 9), and EC (*n* = 8) groups. The LW2 and LW5 control groups were combined into a single LW group (*n* = 7). Each symbol represents a rat. The percent P2Y12-ir area was significantly correlated with the percent Iba1-ir area when all treatment groups were combined in both the PrL and PeF/LH. Regression lines are shown as solid lines.

CHAPTER 4

MICROGLIA APPOSITION ON SLEEP/WAKE-REGULATORY NEURONS IN THE LATERAL HYPOTHALAMUS

4.1 Introduction

In addition to their major role as regulators of innate immunity in the brain, microglia are now recognized as active participants in brain homeostasis (Prinz et al., 2019). Microglia dynamically extend and retract their processes to continuously survey the local brain environment (Nimmerjahn et al., 2005; Wake et al., 2009), making frequent contacts with synaptic elements in a synaptic activity-dependent manner (Tremblay, Lowery, & Majewska, 2010; Wake et al., 2009). Microglia express receptors for virtually all known neurotransmitters (Pocock & Kettenmann, 2007) and can remodel neuronal circuit structure by responding to neuronal activity and phagocytosing synaptic elements (Kettenmann, Kirchhoff, & Verkhratsky, 2013). Additionally, recent studies have identified a subpopulation of microglia, referred to as 'satellite microglia', in the cortex and hippocampus that are in close soma-to-soma contact with neurons (Baalman et al., 2015; Wogram et al., 2016). These satellite microglia are suggested to provide neurons with neurotrophic and metabolic support (Baalman et al., 2015; Wogram et al., 2016). While it is clear that microglia can play a key role in supporting and modulating neuronal connections in the adult brain, it is not fully understood how microglia contribute to essential brain processes, such as sleep/wake regulation.

There is evidence that microglial surveillance, which modulates synaptic functions, is affected by behavioural state and is regulated by neuronal activity. In mice, cortical microglia show diurnal changes in the extension and retraction of their processes, with longer processes during the dark (active) phase when mice are mostly awake (Hayashi et al., 2013). Surprisingly, however, surveillance activities of cortical microglia in mice are *reduced* during wake compared to anesthesia and this reduction is mainly mediated by noradrenergic signaling, which is high during wake (Liu et al., 2019; Stowell et al., 2019). In addition, microglia phagocytosis of

synapses was found to occur more frequently at the onset of the light (inactive) phase, compared to the onset of the dark (active) phase, in the rat prefrontal cortex (Choudhury et al., 2020). Importantly, sleep loss has been shown to alter microglia phagocytosis, but results are inconsistent. For example, 4.5 days of SR resulted in increased elimination of presynaptic elements via microglia phagocytosis in the adolescent mouse cortex (Bellesi et al., 2017). In contrast, 72 h of selective REM sleep deprivation reduced the phagocytosis of presynaptic elements by microglia in the adolescent mouse hippocampus (Tuan & Lee, 2019). Whether these forms of synaptic plasticity occur in other key sleep/wake-regulatory brain regions, such as the lateral hypothalamus, is unknown.

The lateral hypothalamus houses several intermingled populations of sleep/wake-regulatory neurons, including two predominant and mutually inhibitory neuronal populations, namely orexin (ORX)-containing neurons and melanin-concentrating hormone (MCH)-containing neurons (Scammell et al., 2017). ORX neurons are active during wakefulness and promote wake, while MCH neurons are mostly active during REM sleep and promote sleep (Konadhode, Pelluru, & Shiromani, 2014; Modirrousta et al., 2005). A recent study from our lab found that 6 h of sleep deprivation induced astrocyte-mediated bidirectional changes in synaptic plasticity in ORX and MCH neurons (Briggs, Hirasawa, & Semba, 2018), identifying a role for glia in sleep loss-induced changes in synaptic transmission to these two neuronal populations. We previously found increased levels of the neuronal activation marker FosB/ΔFosB in the lateral hypothalamus and other brain regions in response to 4 days of the 3/1 CSR protocol (Hall et al., 2017). Given that microglia can modulate neuronal circuit structure and function, and that microglial surveillance activities are sensitive to sleep loss, we sought to determine whether

microglia physical relationships with ORX and MCH neurons within the lateral hypothalamus are altered by CSR.

In this study, we aimed to: 1) examine microglia contact on ORX and MCH neurons in the lateral hypothalamus, using immunoconfocal microscopy analyses, 2) determine whether microglia contact is dependent on neuronal activation state, using FosB/ΔFosB immunoreactivity as a marker of neuronal activation, and 3) to investigate whether microglia-neuron contact in the lateral hypothalamus is affected by CSR.

4.2 Methods

4.2.1 Animals.

The rats' supplier, body weights at arrival, housing conditions, and experimental protocols were the same as those described in Chapter 2 (see Section 2.2.1). Briefly, adult male Wistar rats (n = 35) were initially housed in pairs in a colony room under a 12 h:12 h light:dark cycle (lights on at 07:00 AM), with food and water available *ad libitum*. The same rats were used in this study and in Experiment 3 of Chapter 3 (Section 3.2.3.1).

4.2.2 Treatment groups.

As described in Section 3.2.3.1, rats were randomly assigned to SR2 (n = 9), SR5 (n = 9), LW2 (n = 4), LW5 (n = 4), and EC (n = 9) groups. Rats in the EC group were housed in unlocked wheels that rats could freely rotate to act as a control for the wheel rotations experienced by rats in the SR groups. Rats were run in multiple cohorts of five or six rats at a time. Prior to their respective experimental protocols, rats were habituated to the activity wheels as described in Section 3.2.1. The 3/1 CSR protocol was used to sleep restrict rats as described in Section 2.2.2.

4.2.3 Immunohistochemistry.

Quadruple fluorescence labelling including triple immunofluorescence was performed on two sets of sections through the lateral hypothalamus (see Section 3.2.3.1). Both sets of sections were incubated overnight at room temperature with a polyclonal guinea pig anti-Iba1 antibody (1:1,000), a monoclonal mouse anti-FosB/ΔFosB antibody (1:1,000), and either a polyclonal goat anti-proMCH antibody (1:50) or a polyclonal rabbit anti-orexin A antibody (1:2,000). The information on these primary antibodies is summarized in Appendix B, Table B.1. Sections were subsequently incubated for 90 min at room temperature with either an alexa488-conjugated donkey anti-guinea pig IgG antibody (1:200; Jackson), a Cy3-conjugated donkey anti-mouse IgG antibody (1:400; Jackson), a dylight405-conjugated donkey anti-goat IgG antibody (1:100; Jackson), or a dylight405-conjugaged donkey anti-rabbit IgG (1:200; Jackson), as appropriate.

A previous study from the lab found that ORX and MCH immunofluorescence did not fill the entire cell body (Briggs et al., 2018). Therefore, in the present study, all sections were additionally incubated in Neurotrace 640/660 Deep-Red Fluorescent Nissl stain (1:75; Cat# N21483, Thermofisher Scientific, Waltham, MA, USA) for 20 min to stain the entire cell body. The Nissl stain facilitated the visualization of the contours of neuronal somata for microglial apposition analysis. Sections were mounted on gelatin-coated glass slides, air dried overnight, and coverslipped using Cytoseal 60 mounting medium (Richard-Allan Scientific, Kalamazoo, MI).

Sections that were judged to be suboptimal for imaging (i.e., poor labelling for any of the four labels, or tissue torn through the lateral hypothalamus due to the multi-label process) were

not imaged and the corresponding rat was excluded from further analysis (n = 6 for MCH staining, n = 10 for ORX staining).

As another technical note, the FosB/ΔFosB antibody used to identify activated neurons in the present study recognizes both the full-length form of FosB, as well as the truncated splice-variant ΔFosB (information provided by the manufacturer), as was the case in our previous study (Hall et al., 2017). In the latter study, we considered that the increased levels of FosB/ΔFosB in several brain regions following CSR likely reflect increases in FosB rather than ΔFosB expression, and that a longer period of CSR might have been necessary to induce ΔFosB expression. On this basis, in the present study we referred to the staining with this antibody as FosB immunoreactivity.

4.2.4 Image acquisition.

Image capture and analysis were conducted by an examiner (S.H.) who was blind to the treatment conditions. A laser scanning confocal microscope (Zeiss LSM 710) was used to acquire immunofluorescent images within the perifornical lateral hypothalamic area (PeF/LH) using a 40X objective lens. Each image consisted of 3 mediolaterally contiguous tiles (each measuring 193 x 193 μm^2, pixel size = 0.189 x 0.189 μm^2), with the middle tile centered directly dorsal to the fornix. The tiles were automatically stitched together using a 70% threshold setting and 10% overlap to get a montage image with a final size of 541 µm wide x 193 µm tall (ZEN software; Carl Zeiss Meditec, Oberkochen, Germany). Optical slices were captured at an interval of 0.85 µm along the z-axis to obtain a ~12 µm thick z-stack. Two adjacent sections (150 µm apart) per animal were imaged.

4.2.5 Microglia morphology analysis

Morphology analyses were performed using the Iba1 images from each acquired z-stack. Image processing involved multiple steps using ImageJ and followed the methods described in Young & Morrison, 2018. Specifically, a maximum projection image was created for each Iba1 image and converted to grayscale. The brightness and contrast of each max projection image were adjusted for optimal visualization of microglia processes. An 'Upsharp Mask' filter was then applied to sharpen and enhance the edge features within each image, followed by noise removal using the Despeckle function. Next, each image was binarized using the Threshold function ('Default Threshold'), followed by Despeckle to remove additional noise and Binary > Close to fill-in any single-pixel gaps in microglial processes.

Microglia morphology parameters were measured on skeleton images using skeleton analysis in ImageJ (Young & Morrison, 2018) (see Figure 4.1). Each Iba1 binary image was skeletonized, and both the length of each branch fragment and the number of branch endpoints were measured for all microglia in each image using 'AnalyzeSkeleton(2D/3D)'. Branch fragments shorter than 0.65 μm were removed. The total branch length and total number of endpoints within each image was computed and subsequently divided by the number of microglia in the image to obtain the mean summed branch length per cell and the mean number of endpoints per cell. The number of microglia was manually counted as the number of microglia cell bodies in each image using the 'Cell Counter' plug-in in ImageJ.

4.2.6 Microglia apposition analysis.

Using ImageJ, each image from each z-stack was corrected for uneven background illumination using the 'Rolling Ball Background Subtraction' function (50-pixel radius) and for black and white pixel noise ('salt and pepper' noise) using the Despeckle function.

Each image was split into 4 separate colour channels for each label (i.e., MCH or ORX, blue; Iba1, green; FosB, red; and Nissl, white). The montage image centered dorsal to the fornix was halved vertically to produce two boxes (270.5 x 193.0 μm^2) so that apposition analyses were done separately for the medial and lateral regions of the PeF/LH.

Microglia apposition analysis was conducted through the multiple steps illustrated in Figure 4.2. Each image was first processed to generate a binary image using Image J. Specifically, 2D maximum intensity z-projection images were created for each colour channel. This process displays the pixels across the optical sections of a 3D image stack that had the highest pixel intensity value (i.e., brightest) within that 3D image stack to create a final 2D 'max projection image'. A threshold (Triangle Auto Threshold; (Zack et al., 1977)) was then applied to each max projection image to produce a binary image for each colour channel.

Next, the binary images for Nissl and Iba1 were processed to generate a differential image using Photoshop (Adobe). First, the 'trace contour' filter was applied to the Nissl binary image to generate a one-pixel-wide somatic contour, as described previously (Briggs et al., 2018). Then, using the 'difference' blending mode in Photoshop, the Iba1 binary image was superimposed onto the Nissl somatic contour to create a differential image. As a result, the portions of the neuron somatic contour directly apposed by Iba1 appeared in red, while those that were not apposed by Iba1 appeared in blue, in each differential image. Next, each differential image was converted to grayscale, resulting in a gray-scale value of 105 for the portions of the somatic

contour directly apposed by Iba1, and a gray-scale value of 250 for portions not apposed by Iba1. Differential images were created for Iba1 and one of the following: 1) Nissl+ cells, 2) MCH- and ORX-ir neurons, and 3) MCH/FosB- and ORX/FosB-ir neurons.

To quantify Iba1 apposition using ImageJ, a threshold was set at 105 to measure the area of pixels occupied by Iba1-apposed somatic contour, and then at 250 to measure the area of pixels occupied by the entire somatic contour (i.e., apposed plus non-apposed), for each differential image. The percentage of Iba1-apposed somatic contour ('percent Iba1 apposition') was calculated by dividing the area of apposed somatic contour by the area of total somatic contour. The portions of microglia cell bodies not in apposition with a Nissl+ cell were excluded from apposition analyses.

4.2.7 Microglia satellite analysis.

The number of satellite microglia [i.e., microglia that make soma-to-soma contact with a neuron (Baalman et al., 2015)] were manually counted using Cell Counter in ImageJ using max projection images of combined Iba1, ORX or MCH, and Nissl channels. For a microglia cell to be counted as a satellite microglia, the Iba1-ir cell body had to be discernible and in contact with another Nissl+ cell body, as confirmed by colocalization between Iba1 and Nissl. In instances where colocalization was questionable, satellite microglia contact was examined using the z-stack composite image of the Iba1, ORX or MCH, and Nissl channels. The percentage of satellite microglia was determined by dividing the number of satellite microglia by the total number of microglia in the image. To calculate the percentage of ORX and MCH neurons in contact with a satellite microglia, the number of ORX or MCH neurons contacted by a satellite microglia was divided by the total number of ORX or MCH neurons, respectively.

4.2.8 Statistics.

Statistical analyses were conducted using GraphPad Prism 7. One-way ANOVAs or mixed effects model analyses were performed to compare treatment groups followed, when applicable, by Fisher's LSD post-hoc tests. A mixed effects model analysis was used instead of a two-way ANOVA in order to perform comparisons between cell type (i.e., ORX and MCH neurons) with unequal rat numbers within treatment groups. Probability values of <0.05 were considered statistically significant. Data values are expressed as means ± standard error of the mean (SEM).

4.3 Results

The LW2 and LW5 control groups did not significantly differ between each other for any of the parameters measured (p=0.09–0.92); therefore, they were combined into a single control group (LW).

The EC group was housed in unlocked wheels for voluntary wheel running for the same time period as the SR5 group. The average daily number of wheel rotations (2,132 ± 589 rotations; Appendix L, Figure L.1) in the EC group was similar to the average daily number of rotations imposed on the SR2 and SR5 groups (2,545 rotations).

Microglia morphology and appositions were analysed separately in the medial and lateral regions of the PeF/LH. However, none of the parameters examined significantly differed between the two regions (p = 0.09–0.62); therefore, the results are reported for the entire PeF/LH.

4.3.1 Microglia cell counts.

Neither 27 h (SR2) nor 99 h (SR5) of CSR significantly changed the total number of Iba1-ir microglia in the PeF/LH (Table 4.1; $F_{3,30} = 0.227$, $p = 0.877$).

4.3.2 Microglia morphology.

Across all treatment groups, microglia had small cell bodies and appeared ramified with long, highly branched processes (Figure 4.1A). Skeleton analysis was used to determine microglia process (branch) length and branching complexity (endpoints) in the PeF/LH. No significant difference was found between the LW, EC, SR2, and SR5 groups for the total summed branch length ($F_{3,25} = 0.88$, $p = 0.47$; Figure 4.3A), total number of endpoints ($F_{3,25} = 0.89$, $p = 0.46$; Figure 4.3B), average summed branch length per microglia ($F_{3,27} = 1.99$, $p = 0.14$; Figure 4.3D), or average number of endpoints per microglia ($F_{3,27} = 1.83$, $p = 0.17$; Figure 4.3E).

The total summed microglia process length was positively correlated with the total number of microglia process endpoints across all treatment groups ($r = 0.94$, $p<0.0001$, Figure 4.3, C). Similarly, the summed microglia process length per cell and the number of microglia process endpoints per cell were positively correlated ($r = 0.74$, $p<0.0001$; Figure 4.3, F) across all treatment groups.

4.3.3 ORX and MCH immunoreactive neurons in the PeF/LH

The total number of either MCH or ORX neurons was unchanged in response to CSR (Table 4.1; $F_{3,46} = 0.84$, $p = 0.48$). Similarly, CSR had no significant effect on the somatic contour length of these neurons (Appendix K, Figure K.1; $F_{3,30} = 0.19$, $p = 0.90$). Note that the

somatic contour length is measured as the summed area of pixels occupied by the one-pixel wide somatic contour.

Irrespective of treatments groups, no significant differences were observed between ORX and MCH neurons for either the total cell numbers ($F_{1,46} = 2.3$, $p = 0.14$; Table 4.1) or the somatic contour length ($F_{1,16} = 0.074$, $p = 0.79$; Appendix K, Figure K.1).

4.3.4 FosB immunoreactivity in the PeF/LH

Using FosB/ΔFosB as a marker for chronic neuronal activation (J. Chen, Kelz, Hope, Nakabeppu, & Nestler, 1997; McClung et al., 2004), we previously observed an increase in the number of FosB/ΔFosB-ir cells in the PeF/LH and other brain regions in response to 99 h of CSR (Hall et al., 2017); 27 h of CSR were not examined in that study. Thus, we first asked whether the total number of FosB-ir cells in the PeF/LH increased in response to both 27 and 99 h of CSR. The total number of FosB-ir cells was, indeed, significantly greater in the SR2 than the EC group (+57%, $p = 0.010$), and remained significantly elevated in the SR5 group (+46% vs. LW, $p = 0.015$; +71% vs. EC, $p = 0.0013$; Figure 4.4, A).

We next assessed the percentages of MCH and ORX neurons that were double-labelled for FosB. Irrespective of treatment groups, the percent of ORX/FosB-ir neurons (7.6% on average) was significantly greater than the percent of MCH/FosB-ir neurons (2.5% on average; $F_{1,16} = 8.70$, $p = 0.0094$; Figure 4.4, B). However, CSR had no significant effect on either of these percentages ($F_{3,30} = 0.83$, $p = 0.49$).

4.3.5 Microglia apposition on ORX and MCH neurons.

We examined microglia apposition on cells within the PeF/LH across all treatment groups, and whether microglia apposition was altered in response to CSR. The percentage of the total somatic contour in apposition with Iba1 ('percent Iba1 apposition') in all Nissl+ cell bodies was approximately 5% across all treatment groups (Figure 4.5) and was not significantly affected by CSR ($F_{3,25} = 0.52$, $p = 0.67$). When microglia apposition was assessed specifically on MCH and ORX neurons, the percent Iba1 apposition was generally low, although it was significantly greater on MCH (4.6% on average) compared to ORX (3.6% on average) neurons across all treatment groups ($F_{1,16} = 5.94$, $p = 0.027$; Figure 4.7). However, no significant difference was found following CSR in either neuronal population ($F_{3,30} = 0.066$, $p = 0.98$), as was the case for Nissl+ cells.

To assess whether microglial apposition with MCH and ORX neurons is dependent on neuronal activity, Iba1 apposition was assessed on MCH and ORX neurons that were co-immunoreactive for FosB. Irrespective of treatment groups, the percent Iba1 apposition on MCH/FosB-ir and ORX/FosB-ir neurons was very low (1.9% and 2.4%, respectively; Figure 4.8), with no significant difference between neuronal phenotypes ($F_{1,46} = 0.18$, $p = 0.67$). CSR did not significantly change the percent Iba1 apposition on either MCH/FosB-ir or ORX/FosB-ir neurons ($F_{3,46} = 0.73$, $p = 0.54$; Figure 4.8).

4.3.6 Microglia cell body contact on ORX and MCH neurons.

We next asked whether microglia contact MCH and/or ORX neurons, or any other neurons, with their cell bodies (i.e., satellite microglia) and, if so, whether the number of satellite microglia contacting these neurons is altered following CSR. Satellite microglia were frequently

observed to contact various Nissl+ cells in the PeF/LH. These included MCH and ORX neurons, other fairly large neuron-like cells, as well as smaller glia-like cells with sizes comparable to microglia (Figure 4.6 A,B).

Irrespective of treatment groups, a large proportion (approximately 67%; range 63–69%) of microglia contacted a Nissl+ cell body with their respective cell body (Figure 4.9, A). A sizeable proportion (approximately 9% and 10%, respectively) of MCH and ORX neurons were contacted by satellite microglia across the treatment groups, with no significant difference between the two neuronal phenotypes ($F_{3,30}$ = 1.31, p = 0.29; Figure 4.9, B). However, CSR had no significant effect on either the percentage of satellite microglia contacting Nissl+ cells ($F_{3,30}$ = 0.53, p = 0.67) or the percentage of ORX or MCH neurons contacted by a satellite microglia ($F_{1,16}$ = 0.45, p = 0.51).

No significant correlation was found between the percentage of satellite microglia on Nissl+ cells and the total number of FosB-ir cells (Figure 4.10), suggesting that the proportion of satellite microglia was not associated with the levels of neuronal activity.

4.3.7 Body weights.

The comparisons of rat body weights between treatment groups is reported in Section 3.3.3 (Appendix H, H.6).

4.4 Discussion

Here, we demonstrate that microglia closely appose small subpopulations of both MCH and ORX neurons in the PeF/LH with their processes and/or cell bodies. Overall, MCH neurons had a greater proportion of their somatic contour in apposition with microglia compared to ORX

neurons (4.6% vs. 3.6%, respectively). ORX neurons were more active, as evidenced by FosB immunoreactivity, than MCH neurons across all treatment groups. However, microglia appositions on these neurons were not dependent on neuronal activation state. Additionally, a sizeable (approximately 10%) proportion of both MCH and ORX neurons were in contact with a microglia cell body. Similar to process appositions, microglia cell body appositions on these neurons were not dependent on neuronal activation state. Microglia process and cell body appositions on ORX and MCH neurons remained unaltered following 27 and 99 h of the 3/1 CSR protocol.

As reported earlier in this thesis (Chapters 2 and 3), CSR resulted in a gradual loss of body weight compared to pre-protocol levels. The weight loss during CSR is unlikely to be due to the physical activity associated with wheel rotations during the 3 h sleep deprivation periods in the 3/1 protocol, as animals in the EC group, which freely rotated the wheels to reach a daily number of rotations similar to the daily number of forced rotations in the SR animals, gained weight.

4.4.1 Methodological considerations and limitations

A number of methodological issues should be considered. First, 2D analysis is a preferred method of image analysis for efficiency and simplicity, and in the present study, microglia apposition (both processes and cell bodies) was analyzed on z-projected 2D images. This results in a margin of error created by the thickness of each image z-stack (~12μm) as well as the pixel size (0.188 μm) used for image acquisition. This may result in some instances of microglia apposition that may not actually be in direct contact with an adjacent cell despite close proximity. Furthermore, a 2D cross-sectional view is limited to the surface of the neuron covered

within the z-stack image and therefore information on microglia process apposition over the entire surface of apposed neurons is unavailable.

Another issue relates to the fact that microglia apposition was examined on fixed tissue at a single time point (i.e., at the end of the respective experimental protocols). Microglia processes are known to be highly dynamic, cycling through periods of extension and retraction on a time scale of minutes in live tissue (Nimmerjahn et al., 2005). Therefore, studies on fixed tissue provide only a "snapshot" of microglia–neuron interactions. Future analysis of 3D reconstructed images and/or *in vivo* live imaging studies would strengthen the current results and improve our understanding of the spatial relationship between microglia and neurons.

Finally, the Nissl stain used in the present study visualizes the cell bodies of not only neurons but also other cell types including glia. Microglia somas (which were identified by Iba1/Nissl co-labelling) were removed prior to apposition analysis in the present study, but the Nissl+ cell bodies of other glial cells, such as astrocytes, were included in the somatic contour outlines. Additionally, the phenotype(s) of most Nissl+ cells contacted by microglia were not identified in the present study.

Despite these limitations, however, the methods used in the present study detected a difference in the degree of microglia apposition between ORX and MCH neurons, and revealed that as high as two-thirds of microglia form soma-to-soma contact with other cells in the lateral hypothalamus.

4.4.2 FosB immunoreactivity in response to CSR

We were able to replicate the previously observed increase in the total number of FosB-ir cells in the PeF/LH after 99 h of CSR (Hall et al., 2017). The present study extends these

previous results by showing an increase in the number of FosB-ir cells after 27 h of CSR, and by identifying the neuronal phenotype of a fraction of the FosB+ cells. Based on FosB immunoreactivity, more ORX neurons were activated across all treatment groups compared to MCH neurons. ORX neurons are active during wakefulness with exploration, while MCH neurons are active during REM sleep (Konadhode et al., 2014; Modirrousta et al., 2005). Therefore, the present finding aligns with the wake-associated behaviours of animals in the EC, SR2, and SR5 groups, including voluntary wheel rotations for the EC group, and sleep deprivation via forced wheel rotations for the SR2 and SR5 groups. The LW group, which experienced the lowest level of motor activity and was not expected to show a high number of activated ORX neurons, tended to have a lower number of FosB+ ORX neurons compared to the EC, SR2, and SR5 groups.

Despite this cell type-specific difference in FosB immunoreactivity, the percentage of activated ORX neurons remained low (~8%) and was statistically unchanged in response to CSR. ORX neurons fire more action potentials during wake, especially during active wake, and promote wakefulness (Lee et al., 2005). Additionally, ORX neurons express increased levels of c-Fos, a marker of acute neuronal activation, in response to 3 h of sleep deprivation in rats (Modirrousta et al., 2005). Thus, the absence of further ORX neuron activation following CSR relative to the control (LW) condition was somewhat surprising. This lack of FosB expression in ORX neurons could be related to a low arousal level during the 3 h sleep deprivation periods of CSR, especially as CSR progresses. Both REM sleep and NREM sleep amounts are increased above baseline levels during the 1-h sleep opportunity periods across the 4 days of CSR (Deurveilher et al., 2012), suggesting a build-up of sleep pressure during the sleep deprivation

periods. Thus, sleep-restricted animals may be in a lowered state of arousal during the 3 h sleep deprivation periods of CSR, resulting in low FosB expression in ORX neurons.

The maintenance of wake during the sleep deprivation periods may be mediated by neurons in other sleep/wake-regulatory brain regions, including GABA-ergic neurons in the lateral hypothalamus. Whether microglia interact with sleep/wake-regulatory neurons within and outside the PeFLH (see Chapter 2), and whether microglia contact with these neurons is altered by CSR, are interesting questions for future study.

4.4.3 Microglia cell numbers following CSR

In the current study, Iba1-ir microglia cell counts based on immunofluorescence were not found to increase in the PeF/LH following the 3/1 CSR protocol in the present study, similar to our findings on the density of Iba1 immunoreactivity using immunofluorescence in Chapter 3 (see Section 3.3.3). This is in marked contrast to our earlier findings of increased numbers of Iba1-ir microglia following CSR using DAB/Ni immunohistochemistry in Chapter 2 (see Section 2.3.1). As discussed in Section 3.2.4, several factors may contribute to this inconsistency, including differences in the detection method (immunofluorescence versus DAB/Ni) and the antibodies used to visualize Iba1. Another possible factor is the difference in counting methods between the two studies (semi-automated cell counts in Chapter 2 vs manual cell counts in the current study). Despite these issues, it was necessary to use immunofluoresence to visualize multiple antigens simultaneously.

Despite the discrepancy between microglia numbers in the two studies, the observed lack of change in microglia cell numbers following CSR using immunofluorescence is consistent with the results of Chapter 2, which suggest that increased microglia numbers following CSR are due

to the up-regulation of Iba1 levels in pre-existing microglia, as opposed to an actual increase in microglia cell numbers (i.e., via proliferation or recruitment of peripheral macrophages).

4.4.4 Microglia morphology following CSR

Similar to the prelimbic cortex (see Section 2.3.2), microglia morphology in the PeF/LH was not affected by CSR. This is interesting because the two studies used different morphological analysis methods (Sholl analysis in Chapter 2 vs Skeleton analysis in the present study) and visualization methods (DAB/Ni vs immunofluorescence). In both the PrL and PeF/LH, microglia appeared to have a ramified phenotype with many long, highly branched processes and small cell bodies. Iba1-ir microglia in the PrL and PeF/LH also expressed the P2Y12 receptor (see Section 3.3.3), which is specifically expressed by non-immunologically activated microglia (Butovsky et al., 2014). Collectively, the current study expands on the Chapter 2 study by demonstrating that microglia in the PeF/LH retain a ramified morphology, in addition to the expression of P2Y12 receptors, and therefore are not immunologically activated in response to CSR, as was found in the prelimbic cortex. These 'homeostatic' microglia could participate in homeostatic functions such as neuronal surveillance and/or synaptic remodeling (Wake et al., 2013).

4.4.5 Microglia apposition in the PeF/LH

Only 5% of the total somatic contour of Nissl+ cells in the PeF/LH was in apposition with microglia processes and/or cell bodies and it remained unaltered following CSR. This level of microglia apposition may reflect a 'standard' level of microglia–neuron contact that occurs during routine microglia surveillance in the lateral hypothalamus and could serve a

'housekeeping' function, such as clearing up metabolic by-products, deteriorated tissue, or damaged neuronal elements (Wake et al., 2013). A recent study observed specialized junctions characterized by P2Y12 receptor signalling at sites of microglia process contact on neuron somas and suggested these contacts may occur in order for microglia to sense the 'well-being' of the contacted neuron (Cserep et al., 2020). In response to brain injury, microglia process coverage of neuronal somas characterized by these specialized somatic junctions increased on damaged, but still viable, neurons (Cserep et al., 2020), suggesting a neuroprotective role. Microglia apposition in the lateral hypothalamus may have a similar neuroprotective function.

We observed a greater proportion of microglial apposition on the cell body contour of MCH compared to ORX neurons across all treatment groups (4.6% vs 3.6%, on average), despite the similar numbers and cell body sizes of MCH and ORX neurons in the analysis box used. Interestingly, these proportions were not affected by neuronal activity as evidenced by FosB immunoreactivity, which was higher in ORX than MCH neurons as expected. Given that microglia contribute to synaptic plasticity (Wake et al., 2013), it is possible that greater microglia apposition on MCH neurons may reflect an increased role of microglia in synaptic remodeling and/or synapse removal on these neurons. In contrast to MCH neurons, which receive primarily inhibitory synaptic inputs on their cell bodies (van den Pol, Acuna-Goycolea, Clark, & Ghosh, 2004), ORX neuron cell bodies predominantly receive excitatory inputs (Horvath & Gao, 2005). The reduced microglia apposition on ORX versus MCH neurons observed in the present study might possibly suggest a lesser role of microglia in modulating excitatory as opposed to inhibitory synaptic transmission.

Additionally, a greater proportion of microglia apposition on MCH compared to ORX neurons may indicate a greater need for 'housekeeping' functions on MCH neurons. This is

somewhat unexpected, because sleep deprivation for 7 days (12 h/day) in mice resulted in the degeneration of ORX neurons in the lateral hypothalamus (Obukuro et al., 2013). Similarly, a reduction in lateral hypothalamic ORX neuron numbers has been observed following 14 weeks of sleep fragmentation in mice; the remaining ORX neurons were found to be metabolically compromised and showed increased expression of TNFα (Y. Zhu, Fenik, Zhan, Xin, & Veasey, 2015). Interestingly, MCH neurons did not show similar reductions in cell number or metabolic impairment (Obukuro et al., 2013; Y. Zhu et al., 2015). It is possible that a slightly higher level of microglia apposition with MCH compared to ORX neurons confers a greater level of neuroprotection in response to subsequent CNS pathological challenges.

4.4.6 Satellite microglia in the PeF/LH

Intriguingly, a large proportion of microglia (67%) in the PeF/LH were observed to contact other cells with their respective cell bodies, regardless of treatment group. Target cells appear to include neurons, including both ORX and MCH neurons, and glia. This subpopulation of microglia is referred to as perineuronal "satellite" microglia (Baalman et al., 2015; Wogram et al., 2016). The specific function of satellite microglia remains to be fully elucidated, but this subpopulation is thought to provide neurotrophic support or be involved in synaptic remodeling (Z. Chen et al., 2014; Kettenmann et al., 2013).

A sizeable proportion (~10%) of both MCH and ORX neurons were observed to be in contact with a microglia cell body. How these MCH and ORX neurons are selectively contacted by satellite microglia contact is unknown. A lack of correlation between the percentage of satellite microglia and the number of FosB-ir cells suggests that neuron activity may not regulate satellite microglia occurrences. The proportion (67%) of satellite microglia (on any Nissl+ cell)

observed in the PeF/LH was much larger than what has previously been reported in other brain regions, e.g., 15% of microglia were found to make soma-to-soma contact with neurons in the adult mouse cortex (Baalman et al., 2015). Since Nissl is not selective for neurons (as discussed in Section 4.4.1), satellite microglia contact with other glial cells, in addition to neurons, likely contributes to the high proportion of satellite microglia observed in the present study.

In the current study, satellite microglia were seen in contact with cell somas of a comparable size to that of microglia, possibly reflecting microglia contact with non-neuronal cells. As astrocytes are the most abundant glial cells in the CNS (Farhy-Tselnicker & Allen, 2018), these contacts may indicate microglia-astrocyte association. In support of this possibility, a preliminary electron microscopy study in the lab reported direct soma-to-soma contact between astrocytes and microglia in the rat PeF/LH (Semba, Briggs, Hatada, Deurveilher, & Kubota, 2019). If microglia preferentially contact nearby astrocytes via their cell body in the PeF/LH, microglia may function to support astrocytes in responding to the activity of sleep/wake neurons and/or with synaptic remodeling functions.

4.5 Conclusions

This study demonstrates that microglial processes and cell bodies closely associate with the cell somas of sleep/wake-regulatory ORX and MCH neurons, as well as unidentified neurons and presumably non-neuronal cells including astrocytes, in the PeF/LH. These associations were not altered by 4 days of CSR and likely represent routine surveillance activities. CSR resulted in an increase in the numbers of FosB-ir cells in the PeF/LH. However, most FosB-ir cells were neither ORX nor MCH positive and may represent other sleep/wake-regulatory neurons, such as GABAergic neurons. The close structural relationship between microglia and other cells within

the lateral hypothalamus suggests that microglia could modulate the activity of sleep/wake-regulatory and other neurons, possibly in conjunction with astrocytes, to regulate sleep behaviour and sleep homeostasis.

Table 4.1. The total numbers of ORX-, MCH-, and Iba1-immunoreactive (ir) cells in the PeF/LH in the LW, EC, SR2, and SR5 groups.

Cell Type	Treatment Group							
	LW	n	**EC**	n	**SR2**	n	**SR5**	n
ORX	20.5 ± 2.9	6	15.0 ± 1.3	5	18.2 ± 3.4	6	19.2 ± 1.6	8
MCH	19.5 ± 2.6	8	19.6 ± 4.7	7	21.2 ± 7.9	6	23.3 ± 2.3	8
Iba1	24.8 ± 2.9	8	25.7 ± 2.2	9	24.9 ± 1.5	8	27.4 ± 3.0	9

Values represent means ± SEM of unilateral counts obtained from 2-4 adjacent sections (150 µm apart) in confocal images of the PeF/LH (counting box: 541 µm x 193 µm). Rats in the two time-matched, locked-wheel control groups (LW2 and LW5) were combined into a single control group (LW) as there was no significant group difference for any cell type examined ($p = 0.09–0.92$). The total numbers of ORX- and MCH-ir neurons include both single (peptide)- and double (peptide and FosB)-labelled cells. The number of Iba1-ir microglia was calculated from sections labelled for both MCH and ORX and averaged across all sections. CSR had no effect on the total numbers of ORX- and MCH-ir neurons, nor was there any effect on the number of Iba1-ir microglia. MCH, melanin-concentrating hormone, ORX, orexin.

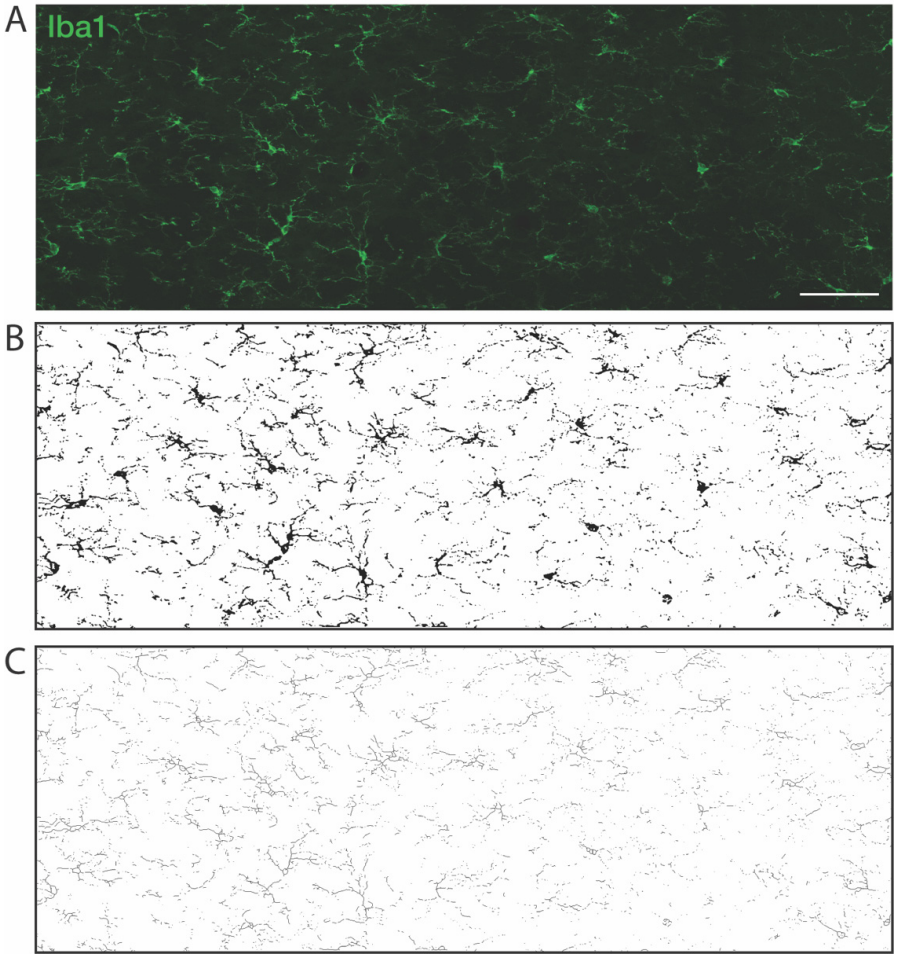

Figure 4.1. Image processing for microglia morphology analysis in the PeF/LH. Iba1 (green) maximum intensity projection images (A) were converted to binary images (B) and then skeletonized (C) in ImageJ. Skeleton images were used to measure microglia branch length and branching complexity (see Section 4.2.5 in Chapter 4). Scale bar = 50 µm.

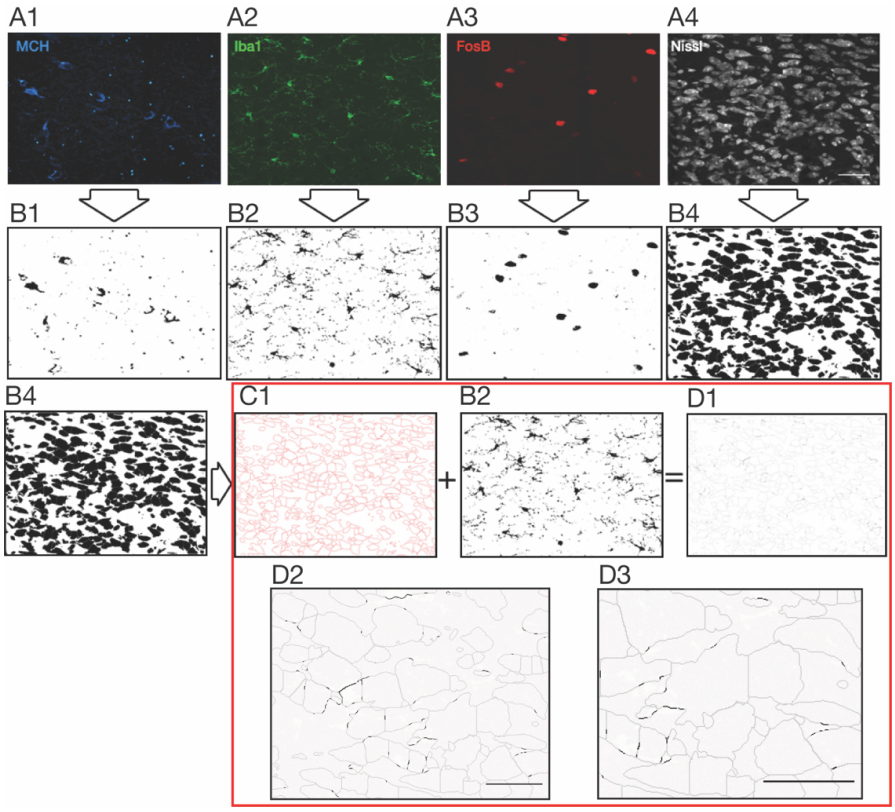

Figure 4.2. Image processing for analyses of microglia apposition with MCH neurons. The same procedure was used for apposition analyses with ORX neurons. Maximum projection images (A1−4) for each label (MCH, Iba1, FosB, and Nissl) were converted to binary images (B1−4) in ImageJ. A one-pixel-wide outline of all Nissl-stained cell bodies was generated in Photoshop (C1) and was then superimposed onto the Iba1 binary image (B2) to reveal the portions of the somatic outline in direct apposition with Iba1-ir processes or cell bodies (D1). Enlarged, high-contrast images of D1 (D2 and D3) show the portions of the somatic contour in direct apposition with Iba1 (black) and those that are not (grey). The percentage of Iba1 apposition was calculated by dividing the area of apposed somatic contour by the area of total somatic contour (i.e., apposed plus non-apposed pixels). See section 4.2.6 in the Methods for further details. Scale bars = 25 µm, A1–B4; 20 µm, D2 and D3.

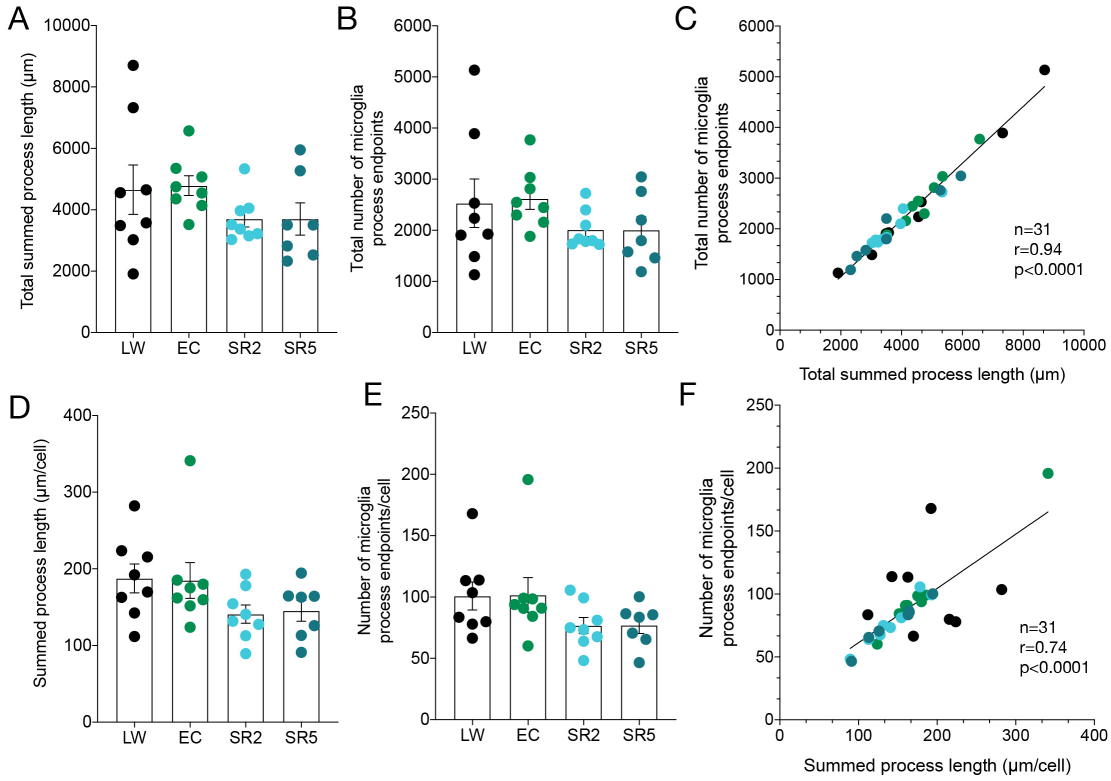

Figure 4.3. Microglia branch length (*left*), branching complexity (number of endpoints; *middle*), and scatterplots of branch length versus branching complexity (*right*) in the PeF/LH following CSR. The LW2 and LW5 control groups were combined into a single LW control group. The total summed microglia branch length (A) and total number of microglia process endpoints (B) were measured using Skeleton Analysis (see Section 4.2.5 for details). These values were subsequently divided by the number of microglia cells in each image to obtain the mean summed process length per microglia (C) and the mean number of process endpoints per microglia (D). Data are shown as means ± SEM for the LW (n = 8), EC (n = 8), SR2 (n = 8), and SR5 (n = 7) groups. Each symbol represents a rat. CSR did not significantly change either the branch length or the number of process endpoints of microglia (p = 0.86 and 0.46, respectively) nor did it change the branch length per microglia or number of process endpoints per microglia (p = 0.14

and 0.17, respectively; one-way ANOVA). Microglia branch length was positively correlated with branching complexity for total (C) and single (F) microglia. Regression lines are shown as solid lines.

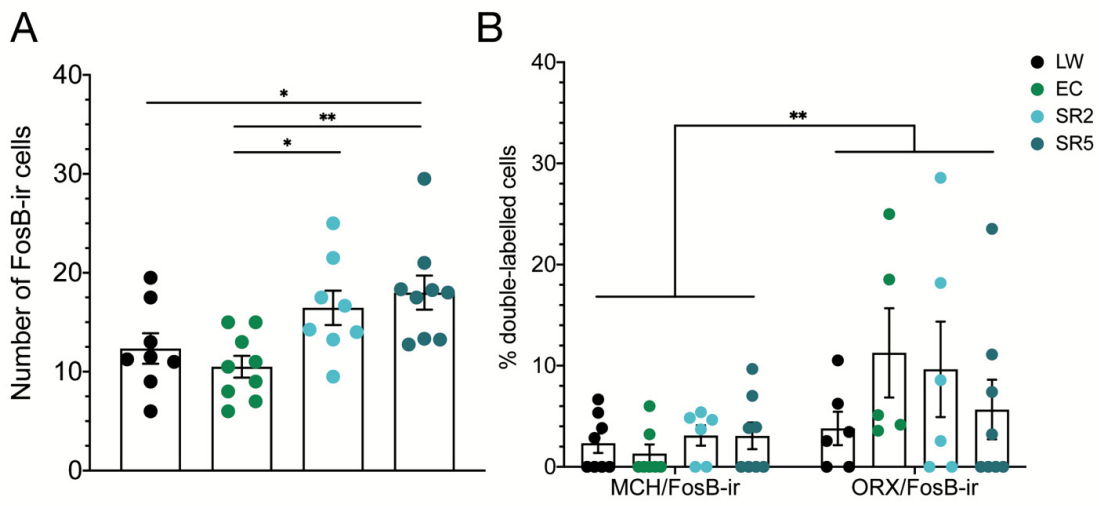

Figure 4.4. The total number of FosB-ir cells (A) and the percentage of MCH/FosB-ir (B, *left*) and ORX/FosB-ir (B, *right*) neurons in the PeF/LH following CSR. The LW2 and LW5 control groups were combined into a single LW control group. Each symbol represents a rat. Data are shown as means ± SEM for the LW (n = 6–8), EC (n = 5–9), SR2 (n = 6), and SR5 (n = 8) groups. The number of FosB-ir cells (A) includes both single- (FosB only) and double-labelled (MCH or ORX/FosB) cells. The percent double-labelled cells (B) were calculated by dividing the number of double-labelled MCH/FosB-ir and ORX/FosB-ir cells by the total number of MCH and ORX cells, respectively (see Table 4.1). A, The total number of FosB-ir cells was significantly increased in the SR2 (vs EC) and SR5 (vs LW and EC) groups. B, The percentage of neither MCH/FosB-ir nor ORX/FosB-ir neurons was significantly changed following CSR. However, the percentage of ORX/FosB-ir neurons was significantly greater than the percentage of MCH/FosB-ir neurons across all treatment groups. A, *$p<0.05$, ** $p<0.01$ (Fischer's LSD post hoc tests); B, ** $p<0.01$ (main effect of Neuron Phenotype, Mixed Effects Model).

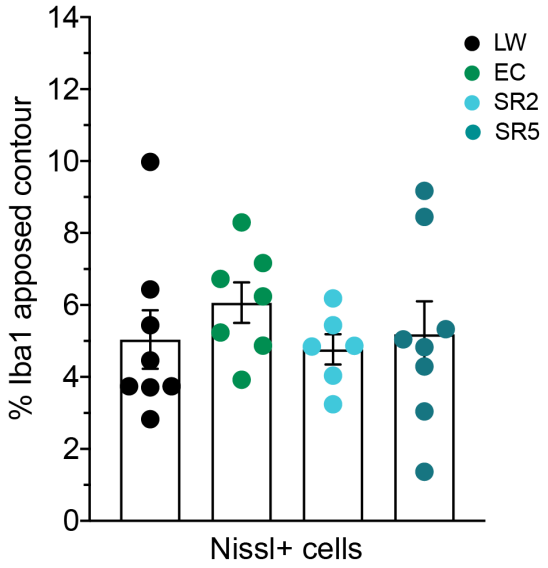

Figure 4.5. The percent Iba1 apposition on all Nissl+ cells in the PeF/LH following CSR. The LW2 and LW5 control groups were combined into a single LW control group. Each symbol represents a rat. Data are shown as means ± SEM for the LW (n = 8), EC (n = 7), SR2 (n = 6), and SR5 (n = 8) groups. Nissl+ cells include cells that were immunoreactive for MCH, ORX and/or FosB and those that were not. The percent Iba1 apposition was calculated by dividing the area of apposed somatic contour by the area of total somatic contour (i.e., apposed plus not apposed pixels) of Nissl+ cells (see Section 4.2.6 for further details). CSR did not significantly affect the percent Iba1 apposition on Nissl+ cells (p = 0.67, one-way ANOVA).

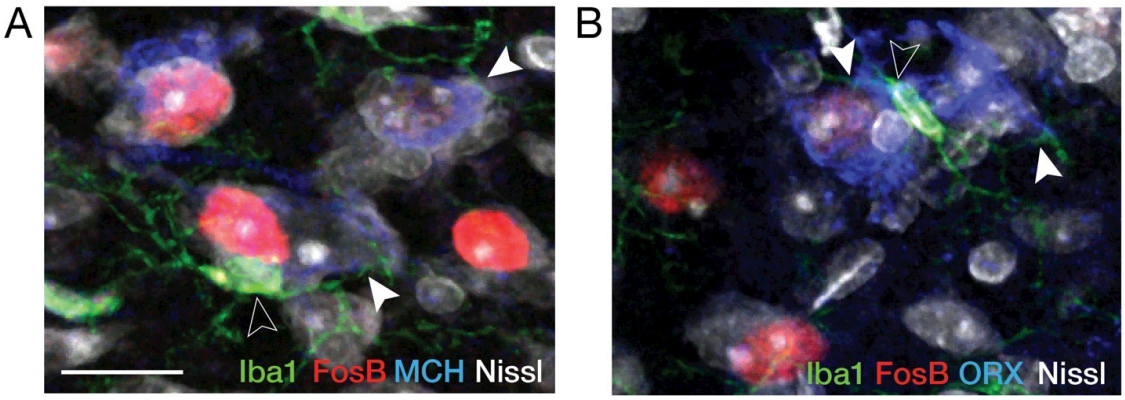

Figure 4.6. Examples of microglia contact on MCH (A) and ORX (B) neurons in the PeF/LH of a SR5 rat. Microglia (green) contact both MCH (A, blue) and ORX (B, blue) neurons with their cell bodies (open arrowheads; 'satellite microglia') and/or processes (white arrowheads); some of the MCH and ORX neurons contacted by microglia were double-labelled with FosB (red). The sections were counter-stained with fluorescent Nissl (white). Scale bars = 15µm.

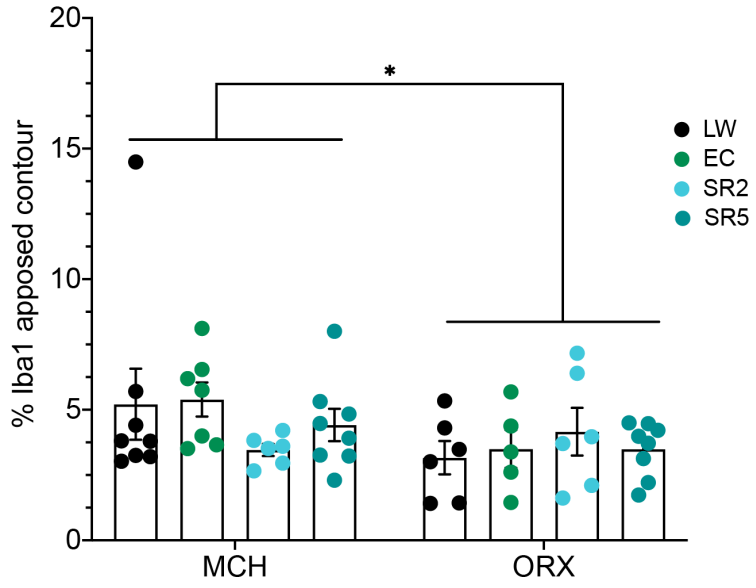

Figure 4.7. The percent Iba1 apposition on MCH (*left*) and ORX (*right*) neurons in the PeF/LH following CSR. The LW2 and LW5 control groups were combined into a single LW control group. Each symbol represents a rat. Data are shown as means ± SEM for the LW (n = 6–8), EC (n = 5–7), SR2 (n = 6), and SR5 (n = 8) groups. MCH and ORX neurons include neurons co-labelled with FosB and those that were not. The percent Iba1 apposition was calculated by dividing the area of apposed somatic contour by the area of total somatic. CSR did not significantly affect the percent Iba1 apposition on either MCH or ORX neurons. However, the percent Iba1 apposition was significantly greater on MCH neurons than on ORX neurons across all treatment groups. *$p<0.05$ (main effect of Neuron Phenotype, Mixed Effects Model).

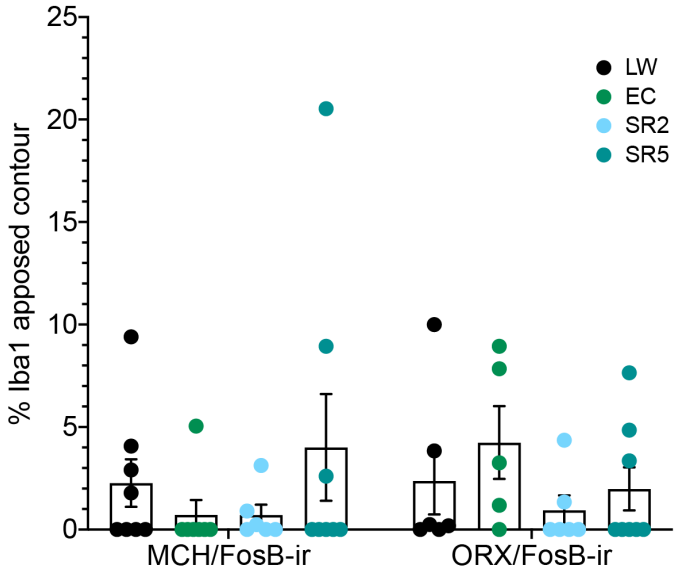

Figure 4.8. The percent Iba1 apposition on MCH/FosB-ir (*left*) and ORX/FosB-ir (*right*) neurons in the PeF/LH following CSR. The LW2 and LW5 control groups were combined into a single LW control group. Each symbol represents a rat. Data are shown as means ± SEM for the LW (n = 6–8), EC (n = 5–7), SR2 (n = 6), and SR5 (n = 8) groups. The percent Iba1 apposition was calculated by dividing the area of apposed somatic contour by the area of total somatic. CSR did not significantly change the percent Iba1 apposition on either MCH/FosB-ir or ORX/FosB-ir neurons, nor was there a significant difference between neuronal phenotypes (Mixed Effects Model).

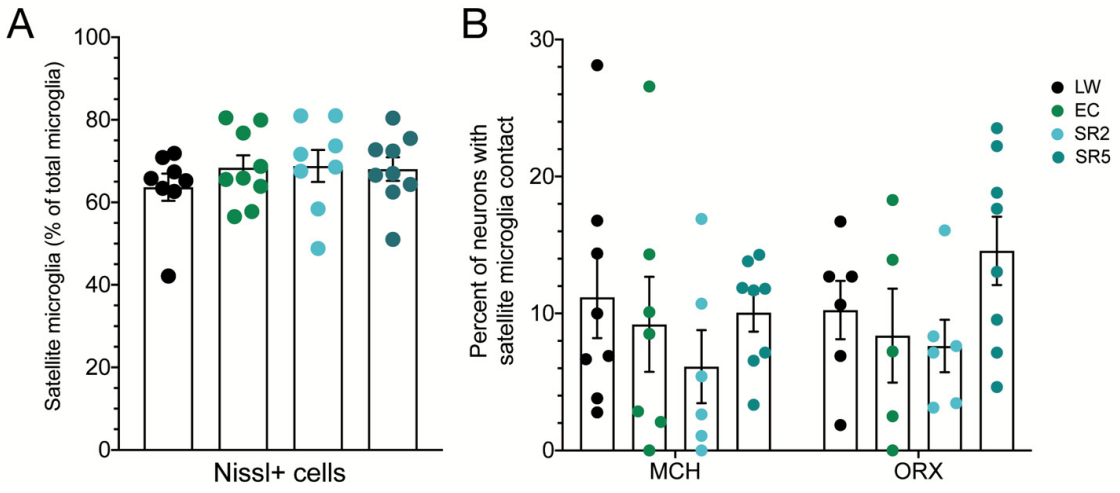

Figure 4.9. The percentage of microglia whose cell bodies contact a Nissl+ cell body (i.e., satellite microglia) (A) and the percentage of MCH and ORX neurons whose somata are in contact with a satellite microglia (B) in the PeF/LH following CSR. The LW2 and LW5 control groups were combined into a single LW control group. Each symbol represents a rat. Data are shown as means ± SEM for the LW (*n* = 6–8), EC (*n* = 5–9), SR2 (*n* = 6–8), and SR5 (*n* = 8–9) groups. The percentage of satellite microglia (A) was calculated by dividing the number of satellite microglia by the total number of microglia in each image. The percentage of MCH and ORX neurons in contact with a satellite microglia (B) was determined by dividing the number of MCH or ORX neurons contacted by a satellite microglia by the total number of MCH or ORX neurons, respectively. CSR did not significantly affect the percent of satellite microglia contacting Nissl+ cells (p = 0.67, one-way ANOVA). Similarly, the percent of MCH or ORX neurons in contact with a satellite microglia was not affected by CSR (p = 0.51), and no difference was found between neuronal phenotypes (p = 0.29, Mixed Effects Model).

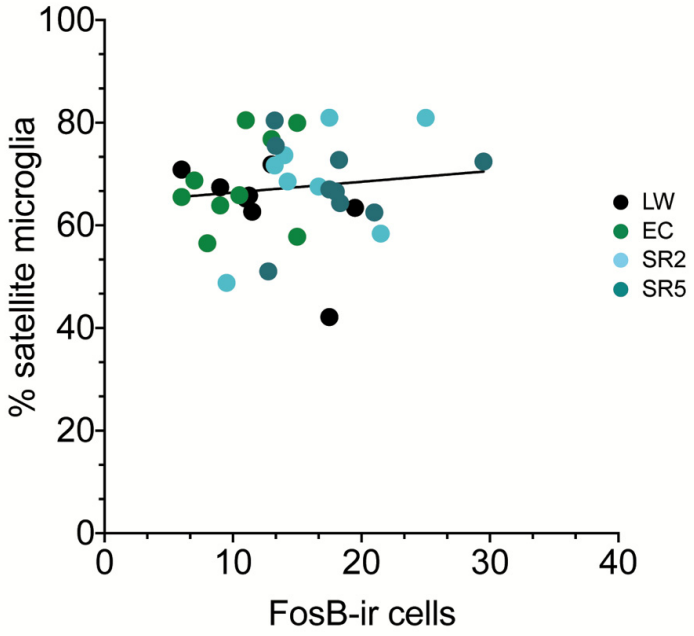

Figure 4.10. Scatterplot of the percent of satellite microglia versus the total number of FosB-ir cells in the PeF/LH for the LW (n = 8), EC (n = 9), SR2 (n = 8), and SR5 (n = 9) groups. Each symbol represents a rat. The number of FosB-ir cells includes both single- (FosB only) and double-labelled (FosB and MCH or ORX) cells. The percentage of satellite microglia was not found to be significantly correlated with the total number of FosB-ir cells in the PeF/LH across all treatment groups (r = 0.12, p = 0.50). Regression line is shown as a solid line.

CHAPTER 5

GENERAL DISCUSSION

5.1 Major Findings

The goal of this thesis was to characterize the microglia response to CSR in important sleep/wake- and cognitive-related brain regions in order to gain insights into their roles in the altered, long-lasting sleep responses to CSR as well as other physiological and cognitive consequences of CSR, using a well-established rat CSR model.

First, using DAB/Ni immunohistochemistry, I demonstrated that 27 and 99 h of the 3/1 CSR protocol induced brain region-specific and duration-dependent increases in Iba1 immunoreactivity in microglia. The Iba1 immunoreactivity remained elevated in most CSR-responsive brain regions after 6 days of recovery following CSR. Neither microglia proliferation nor peripheral macrophage recruitment were found to contribute to the CSR-induced increases in Iba1 immunoreactivity, suggesting that this increase is due to an upregulation of Iba1 protein levels in resident microglia. Second, Iba1-ir microglia in the frontal cortex and lateral hypothalamus, two representative areas that showed increased Iba1 immunoreactivity in response to CSR, did not change their morphology in response to CSR and remained ramified with small cell bodies. In addition, these microglia did not contain pro- and anti-inflammatory markers but contained the purinergic P2Y12 receptor. These results suggest that microglia maintain a physiological or homeostatic phenotype in their response to CSR. Third, consistent with the homeostatic phenotype, the mRNA levels of several pro-inflammatory cytokines in the frontal cortex that are typically expressed in immunologically activated microglia remained unaltered during CSR. Although the mRNA levels of the anti-inflammatory cytokine IL10 in the frontal cortex were transiently increased after 27 h of CSR, IL10 immunoreactivity appeared to be exclusively located in neurons rather than in microglia. Fourth, multi-label confocal microscopy analyses indicated that microglia were often in contact with other cells in the lateral

hypothalamus through their processes and cell bodies. Microglia were also observed in close apposition with small subpopulations of both MCH and ORX neurons in the lateral hypothalamus. However, the proportion of microglia–neuron contact on these neuronal populations remained unaltered following CSR.

Collectively, these findings indicate that microglia respond to CSR conducted using the '3/1' protocol by upregulating their expression of Iba1. Microglia are not immunologically activated in response to the 3/1 CSR protocol but rather retain a homeostatic phenotype. In addition, this research provides novel insight into the structural relationship between microglia and ORX and MCH neurons, two key sleep/wake-regulatory neuron populations in the lateral hypothalamus. The findings of this thesis aid in characterizing the microglia response to CSR in key sleep/wake regulatory brain regions. Based on this data, studies that further investigate whether microglia contribute to the adaptive responses in sleep and sustained attention observed in response to CSR should focus on microglia functions specific to the homeostatic, rather than immunologically-activated, state.

5.2 Homeostatic microglia phenotype following CSR

In this thesis, in addition to Iba1 as a canonical marker for microglia, various phenotypic markers of microglia were tested to examine the microglia response to CSR. The P2Y12 receptor, in particular, was useful for positively identifying a homeostatic microglia phenotype during CSR. However, microglia are known to show a remarkable diversity in their functional phenotypes, and their spatial, temporal, and disease state-specific heterogeneity within the mammalian brain has become increasingly recognized in recent studies (Tan et al., 2020).

In this thesis, I provide evidence of a homeostatic microglia phenotype, as opposed to immunological microglia activation, in response to CSR. Given that homeostatic microglia participate in a wide variety of biologically important roles, ranging from neuronal surveillance to synaptic remodeling to supporting neurogenesis, specialized subsets of homeostatic microglia likely exist and could be differently altered during CSR. Thus, additional techniques are warranted that can molecularly identify region-specific microglia functional phenotypes during CSR, particularly at the single-cell level.

Microglia can be examined at the single-cell level using flow cytometry, immunohistochemistry, or *in situ* hybridization (Masuda et al., 2020). Although useful, these techniques can introduce bias given the limited number of markers available and thus are unable to capture the full diversity of microglia. Recent technological advances, such as the arrival of single-cell RNA sequencing (scRNA-seq), have enabled high-throughput, comprehensive, and unbiased analysis of microglia transcriptional signatures in both the healthy and diseased brain (Macosko et al., 2015). A recent study by Hammond et al. (2019) used scRNA-seq to describe microglia transcriptional states in the developing, aged, and injured whole mouse brain. While virtually all microglia were found to express the common microglia markers P2Y12 receptor, fractalkine receptor, and Tmem119 across the lifespan, nine distinct microglia states were identified that showed unique gene expression patterns within the healthy versus the injured brain, as well as across different ages (Hammond et al., 2019). The transcriptional diversity of microglia states showing both spatial and temporal heterogeneity is further supported with additional studies by other groups in both mice and humans (Masuda et al., 2020). Much more work is needed to further classify these recently discovered, unique microglia states and current

work is focusing on identifying the distinct roles of microglia subpopulations in both the healthy and pathological brain.

Future studies that examine microglia transcriptional signatures in key sleep/wake-regulatory and cognitive brain regions during CSR could reveal a more comprehensive and unbiased molecular view of CSR-responsive homeostatic microglia. Additionally, this type of analysis may reveal unique subsets of homeostatic microglia, both within and between brain regions, that may provide critical information on the region-specific responses to CSR. These insights could aid in the development of specific biomarkers and provide new insights for the development of targeted therapeutics to help mitigate the impairments in cognition and health that are associated with CSR.

5.3 Microglia contact on MCH and ORX neurons in the lateral hypothalamus

Microglia contacting MCH and ORX neurons in the lateral hypothalamus was consistently observed, but the prevalence did not change during CSR. As discussed in Section 4.4.5, this level of microglia apposition on MCH and ORX neurons may reflect a 'standard' level of microglia contact during their routine neuronal surveillance activities specific to these neuron types. This is consistent with the observation that, while microglia cell bodies remain mostly immobile under non-pathological conditions, the ramified branches of microglia processes remain in constant motion, and frequently contact neuronal elements (Nimmerjahn et al., 2005; Tremblay et al., 2010; Wake et al., 2009). Given that Iba1 immunohistochemistry does not label the most distal microglia processes, improved visualization of these more distal processes using P2Y12 receptor immunohistochemistry may contribute to a better understanding of how microglia interact with sleep/wake-regulatory neuron populations. Indeed, we performed P2Y12 immunohistochemistry

in the PeF/LH and found no significant change in response to CSR; however, P2Y12 contact on MCH and ORX neurons was not studied. We noted that P2Y12 receptor immunoreactivity in the PeF/LH was rather abundant across all treatment groups and appeared to be expressed by virtually all Iba1-ir microglia (see Section 3.3.3.1). Intriguingly, extensive apposition of MCH and/or ORX neurons by P2Y12-ir microglia distal processes during CSR could imply that very distal microglia process contact could alter synaptic transmission to these neurons, as microglia are shown to actively participate in synaptic plasticity through the displacement of axosomatic synaptic terminals away from neuronal cell bodies in both the developing and adult brain (Z. Chen et al., 2014; Tremblay et al., 2010; Wake et al., 2009). *In vivo* live imaging studies that examine the interaction of microglia distal processes, e.g., using transgenic animals that express fluorescent P2Y12 receptors, with neuronal elements in sleep/wake-regulatory brain areas during CSR could provide interesting insights on microglia dynamics in response to CSR.

This thesis provided new insights on how microglia interact with other cells in the lateral hypothalamus, in particular with MCH and ORX neurons, two important populations of sleep/wake-regulatory neurons. However further studies are warranted in order to understand the roles of microglia within the lateral hypothalamus as well as other sleep/wake regulatory-brain regions, in mediating both the homeostatic and allostatic sleep responses to CSR. Future studies that inhibit homeostatic microglia functions, such as antagonizing the P2Y12 receptor or through the pharmacological depletion of microglia, will be essential for understanding of the role of homeostatic microglia in the altered sleep responses during CSR.

5.4 Microglia priming: Vulnerability to subsequent stressors or immune challenge following CSR?

In the present study, we observed increases in Iba1 immunoreactivity in select brain regions in response to CSR that remained elevated in most of the brain areas after 6 days of recovery sleep following CSR (section 2.3.1). These long-lasting increases in Iba1 immunoreactivity may result in altered microglia responses to future stressors (e.g., acute sleep loss) and/or immunological challenges.

It is possible that microglia responses to CSR may be involved in the mechanisms underlying the previously reported alterations in the homeostatic sleep responses to a subsequent period of sleep loss. Notably, in mice, 3 days of CSR significantly attenuated homeostatic increases in sleep time and intensity in response to 6 h of sleep deprivation for two weeks following CSR (Clasadonte et al., 2014). Additionally, mice treated with minocycline, a drug that attenuates microglia pro-inflammatory responses, showed significantly reduced homeostatic increases in NREM EEG slow wave activity in response to sleep deprivation for 3 h (Wisor et al., 2011). Future studies could examine homeostatic sleep responses following a subsequent period of acute sleep deprivation after CSR under conditions of microglia inhibition or depletion.

CSR may 'prime' microglia to alter neuroinflammatory responses to subsequent immune challenges. As mentioned above, LPS is a bacterial endotoxin and it is commonly used to induce immunological activation of microglia in both rats (W. G. Kim et al., 2000) and humans (Sandiego et al., 2015). Studies suggest that under conditions of chronic stress (Frank, Hershman, Weber, Watkins, & Maier, 2014; Wohleb et al., 2012), circadian disruption (Castanon-Cervantes et al., 2010), and aging (Niraula, Sheridan, & Godbout, 2017), microglia become "primed", altering subsequent neuroinflammatory responses to an immune challenge.

For example, rats that were exposed to the stress hormone corticosterone for 10 days, and were subsequently challenged with LPS, showed increased hippocampal mRNA levels of several pro-inflammatory cytokines compared to vehicle-treated control animals (Frank et al., 2014). In mice, 4 weeks of circadian disruption (weekly 6-h phase advances of the light/dark cycle) resulted in increased serum levels of pro-inflammatory cytokines in response to an injection of LPS (Castanon-Cervantes et al., 2010). Conversely, a few studies suggest that 24 or 48 h of sleep deprivation *reduces* microglia pro-inflammatory responses to peripheral LPS administration. Sleep deprivation for 48 h was found to attenuate LPS-induced increases in TNFα and while increasing IL10 levels in the mouse forebrain (Weil et al., 2009) and in Siberian hamsters 24 h of sleep deprivation reduced increases in IL-1 mRNA in the hypothalamus following LPS (Ingiosi et al., 2013). It is possible that neuroinflammatory responses to immune insults following sleep loss are attenuated following a shorter period of sleep deprivation (24–48h), while longer periods of sleep loss (> 48 h) exacerbate responses to subsequent immune challenges.

Future studies that examine microglia responses (e.g., microglia molecular phenotype, morphology, and cytokine expression) to immune challenge following a period of CSR will provide novel insight into the long-term consequences of CSR on health, as well as aid in our understanding of the functional significance of microglia responses during CSR.

5.5 Conclusions

The research described in this thesis provides evidence for a homeostatic microglia phenotype in response to CSR in specific sleep/wake-regulatory and cognitive brain regions in rats. Follow-up studies are necessary to elucidate the functional significance of increased Iba1 immunoreactivity and to validate a homeostatic microglia phenotype in each of the CSR-

responsive brain regions. CSR may alter microglia functions, such as neuronal surveillance and synaptic remodeling activities, which may have important implications for the role of microglia in the regulation of sleep behaviour and sleep homeostasis. Together, these results contribute to our understanding of the role microglia play in brain homeostasis during CSR and will hopefully aid in the development of procedures to reduce the negative impact of CSR on cognition and health. Future studies that inhibit homeostatic microglia functions, such as antagonizing the P2Y12 receptor or through the pharmacological depletion of microglia, will be important for a better understanding of the role of microglia in the altered sleep responses to CSR.

REFERENCES

Akiyoshi, R., Wake, H., Kato, D., Horiuchi, H., Ono, R., Ikegami, A., . . . Nabekura, J. (2018). Microglia Enhance Synapse Activity to Promote Local Network Synchronization. *eNeuro, 5*(5). doi:10.1523/ENEURO.0088-18.2018

Aldabal, L., & Bahammam, A. S. (2011). Metabolic, endocrine, and immune consequences of sleep deprivation. *Open Respiratory Medicine Journal, 5*, 31-43. doi:10.2174/1874306401105010031

Amadio, S., Parisi, C., Montilli, C., Carrubba, A. S., Apolloni, S., & Volonte, C. (2014). P2Y(12) receptor on the verge of a neuroinflammatory breakdown. *Mediators of Inflammation, 2014*, 975849. doi:10.1155/2014/975849

Apergis-Schoute, J., Iordanidou, P., Faure, C., Jego, S., Schone, C., Aitta-Aho, T., . . . Burdakov, D. (2015). Optogenetic evidence for inhibitory signaling from orexin to MCH neurons via local microcircuits. *Journal of Neuroscience, 35*(14), 5435-5441. doi:10.1523/JNEUROSCI.5269-14.2015

Baalman, K., Marin, M. A., Ho, T. S., Godoy, M., Cherian, L., Robertson, C., & Rasband, M. N. (2015). Axon initial segment-associated microglia. *Journal of Neuroscience, 35*(5), 2283-2292. doi:10.1523/JNEUROSCI.3751-14.2015

Bah, T. M., Deurveilher, S., Egom, E. E., Rusak, B., Rose, R. A., & Semba, K. (2014). *Effects of chronic sleep restriction on cardiac and thermoregulatory functions in rats.* Paper presented at the Society for Neuroscience Abstract, Presentation No 258.18.

Banasr, M., Valentine, G. W., Li, X. Y., Gourley, S. L., Taylor, J. R., & Duman, R. S. (2007). Chronic unpredictable stress decreases cell proliferation in the cerebral cortex of the adult rat. *Biological Psychiatry, 62*(5), 496-504. doi:10.1016/j.biopsych.2007.02.006

Banks, S., & Dinges, D. F. (2007). Behavioral and physiological consequences of sleep restriction. *Journal of Clinical Sleep Medicine, 3*(5), 519-528. Retrieved from http://www.ncbi.nlm.nih.gov/pubmed/17803017

Barf, R. P., Van Dijk, G., Scheurink, A. J., Hoffmann, K., Novati, A., Hulshof, H. J., . . . Meerlo, P. (2012). Metabolic consequences of chronic sleep restriction in rats: changes in body weight regulation and energy expenditure. *Physiol Behav, 107*(3), 322-328. doi:10.1016/j.physbeh.2012.09.005

Basner, M., Rao, H., Goel, N., & Dinges, D. F. (2013). Sleep deprivation and neurobehavioral dynamics. *Current Opinion in Neurobiology, 23*(5), 854-863. doi:10.1016/j.conb.2013.02.008

Baun, J., Zurhellen, C., York, T., Tipton, B., & Sqitzer III, R. C. (2016). *Quantification of immunhistochemistry on adjacent sections comparing fluorescent and DAB markers.* Paper presented at the Society for Neuroscience Abstract, Presentation No 272.13.

Belenky, G., Wesensten, N. J., Thorne, D. R., Thomas, M. L., Sing, H. C., Redmond, D. P., . . . Balkin, T. J. (2003). Patterns of performance degradation and restoration during sleep restriction and subsequent recovery: a sleep dose-response study. *Journal of Sleep Research, 12*(1), 1-12. doi:10.1046/j.1365-2869.2003.00337.x

Bellesi, M., de Vivo, L., Chini, M., Gilli, F., Tononi, G., & Cirelli, C. (2017). Sleep Loss Promotes Astrocytic Phagocytosis and Microglial Activation in Mouse Cerebral Cortex. *Journal of Neuroscience, 37*(21), 5263-5273. doi:10.1523/JNEUROSCI.3981-16.2017

Bennett, M. L., Bennett, F. C., Liddelow, S. A., Ajami, B., Zamanian, J. L., Fernhoff, N. B., . . . Barres, B. A. (2016). New tools for studying microglia in the mouse and human CNS. *Proceedings of the National Academy of Sciences of the United States of America, 113*(12), E1738-1746. doi:10.1073/pnas.1525528113

Berridge, C. W., Schmeichel, B. E., & Espana, R. A. (2012). Noradrenergic modulation of wakefulness/arousal. *Sleep Medicine Reviews, 16*(2), 187-197. doi:10.1016/j.smrv.2011.12.003

Bioulac, S., Micoulaud-Franchi, J. A., Arnaud, M., Sagaspe, P., Moore, N., Salvo, F., & Philip, P. (2017). Risk of Motor Vehicle Accidents Related to Sleepiness at the Wheel: A Systematic Review and Meta-Analysis. *Sleep, 40*(10). doi:10.1093/sleep/zsx134

Bjorness, T. E., Kelly, C. L., Gao, T., Poffenberger, V., & Greene, R. W. (2009). Control and function of the homeostatic sleep response by adenosine A1 receptors. *Journal of Neuroscience, 29*(5), 1267-1276. doi:10.1523/JNEUROSCI.2942-08.2009

Bonde, S., Ekdahl, C. T., & Lindvall, O. (2006). Long-term neuronal replacement in adult rat hippocampus after status epilepticus despite chronic inflammation. *European Journal of Neuroscience, 23*(4), 965-974. doi:10.1111/j.1460-9568.2006.04635.x

Borbely, A. A. (1982). A two process model of sleep regulation. *Human Neurobiology, 1*(3), 195-204. Retrieved from https://www.ncbi.nlm.nih.gov/pubmed/7185792

Borbely, A. A., & Achermann, P. (1999). Sleep homeostasis and models of sleep regulation. *Journal of Biological Rhythms, 14*(6), 557-568. Retrieved from http://www.ncbi.nlm.nih.gov/pubmed/10643753

Borbely, A. A., Daan, S., Wirz-Justice, A., & Deboer, T. (2016). The two-process model of sleep regulation: a reappraisal. *Journal of Sleep Research, 25*(2), 131-143. doi:10.1111/jsr.12371

Borbély, A. A., & Neuhaus, H. U. (1979). Sleep-deprivation: Effects on sleep and EEG in the rat. *Journal of comparative physiology, 133*, 71-87.

Breder, C. D., Dinarello, C. A., & Saper, C. B. (1988). Interleukin-1 immunoreactive innervation of the human hypothalamus. *Science, 240*(4850), 321-324. doi:10.1126/science.3258444

Breder, C. D., Tsujimoto, M., Terano, Y., Scott, D. W., & Saper, C. B. (1993). Distribution and characterization of tumor necrosis factor-alpha-like immunoreactivity in the murine central nervous system. *Journal of Comparative Neurology, 337*(4), 543-567. doi:10.1002/cne.903370403

Briggs, C., Hirasawa, M., & Semba, K. (2018). Sleep deprivation distinctly alters glutamate transporter 1 apposition and excitatory transmission to orexin and MCH neurons. *Journal of Neuroscience*. doi:10.1523/JNEUROSCI.2179-17.2018

Broberger, C., De Lecea, L., Sutcliffe, J. G., & Hokfelt, T. (1998). Hypocretin/orexin- and melanin-concentrating hormone-expressing cells form distinct populations in the rodent lateral hypothalamus: relationship to the neuropeptide Y and agouti gene-related protein systems. *Journal of Comparative Neurology, 402*(4), 460-474. Retrieved from http://www.ncbi.nlm.nih.gov/pubmed/9862321

Bruttger, J., Karram, K., Wortge, S., Regen, T., Marini, F., Hoppmann, N., . . . Waisman, A. (2015). Genetic Cell Ablation Reveals Clusters of Local Self-Renewing Microglia in the Mammalian Central Nervous System. *Immunity, 43*(1), 92-106. doi:10.1016/j.immuni.2015.06.012

Burudi, E. M., & Regnier-Vigouroux, A. (2001). Regional and cellular expression of the mannose receptor in the post-natal developing mouse brain. *Cell Tissue Res, 303*(3), 307-317. doi:10.1007/s004410000311

Bustin, S. A., Benes, V., Garson, J. A., Hellemans, J., Huggett, J., Kubista, M., . . . Wittwer, C. T. (2009). The MIQE guidelines: minimum information for publication of quantitative real-time PCR experiments. *Clinical Chemistry, 55*(4), 611-622. doi:10.1373/clinchem.2008.112797

Butovsky, O., Jedrychowski, M. P., Moore, C. S., Cialic, R., Lanser, A. J., Gabriely, G., . . . Weiner, H. L. (2014). Identification of a unique TGF-beta-dependent molecular and functional signature in microglia. *Nature Neuroscience, 17*(1), 131-143. doi:10.1038/nn.3599

Butovsky, O., & Weiner, H. L. (2018). Microglial signatures and their role in health and disease. *Nature Reviews: Neuroscience, 19*(10), 622-635. doi:10.1038/s41583-018-0057-5

Calovi, S., Mut-Arbona, P., & Sperlagh, B. (2019). Microglia and the Purinergic Signaling System. *Neuroscience, 405*, 137-147. doi:10.1016/j.neuroscience.2018.12.021

Castanon-Cervantes, O., Wu, M., Ehlen, J. C., Paul, K., Gamble, K. L., Johnson, R. L., . . . Davidson, A. J. (2010). Dysregulation of inflammatory responses by chronic circadian disruption. *Journal of Immunology, 185*(10), 5796-5805. doi:10.4049/jimmunol.1001026

Chaput, J., Wong, S. L., & Michaud, I. (2017). *Duration and quality of sleep among Canadians aged 18 to 79*. Retrieved from

Chen, J., Kelz, M. B., Hope, B. T., Nakabeppu, Y., & Nestler, E. J. (1997). Chronic Fos-related antigens: stable variants of deltaFosB induced in brain by chronic treatments. *Journal of Neuroscience, 17*(13), 4933-4941. Retrieved from http://www.ncbi.nlm.nih.gov/pubmed/9185531

Chen, Z., Jalabi, W., Hu, W., Park, H. J., Gale, J. T., Kidd, G. J., . . . Trapp, B. D. (2014). Microglial displacement of inhibitory synapses provides neuroprotection in the adult brain. *Nat Commun, 5*, 4486. doi:10.1038/ncomms5486

Chennaoui, M., Gomez-Merino, D., Drogou, C., Geoffroy, H., Dispersyn, G., Langrume, C., . . . Sauvet, F. (2015). Effects of exercise on brain and peripheral inflammatory biomarkers induced by total sleep deprivation in rats. *J Inflamm (Lond), 12*, 56. doi:10.1186/s12950-015-0102-3

Chinnery, H. R., Ruitenberg, M. J., & McMenamin, P. G. (2010). Novel characterization of monocyte-derived cell populations in the meninges and choroid plexus and their rates of replenishment in bone marrow chimeric mice. *J Neuropathol Exp Neurol, 69*(9), 896-909. doi:10.1097/NEN.0b013e3181edbc1a

Choi, Y. S., Cho, H. Y., Hoyt, K. R., Naegele, J. R., & Obrietan, K. (2008). IGF-1 receptor-mediated ERK/MAPK signaling couples status epilepticus to progenitor cell proliferation in the subgranular layer of the dentate gyrus. *Glia, 56*(7), 791-800. doi:10.1002/glia.20653

Choudhury, M. E., Miyanishi, K., Takeda, H., Islam, A., Matsuoka, N., Kubo, M., . . . Tanaka, J. (2020). Phagocytic elimination of synapses by microglia during sleep. *Glia, 68*(1), 44-59. doi:10.1002/glia.23698

Clasadonte, J., McIver, S. R., Schmitt, L. I., Halassa, M. M., & Haydon, P. G. (2014). Chronic sleep restriction disrupts sleep homeostasis and behavioral sensitivity to alcohol by

reducing the extracellular accumulation of adenosine. *Journal of Neuroscience, 34*(5), 1879-1891. doi:10.1523/JNEUROSCI.2870-12.2014

Colwell, C. S., & Matveyenko, A. V. (2014). Timing is everything: implications for metabolic consequences of sleep restriction. *Diabetes, 63*(6), 1826-1828. doi:10.2337/db14-0283

Connor, J., Norton, R., Ameratunga, S., Robinson, E., Civil, I., Dunn, R., . . . Jackson, R. (2002). Driver sleepiness and risk of serious injury to car occupants: population based case control study. *BMJ, 324*(7346), 1125. doi:10.1136/bmj.324.7346.1125

Cserep, C., Posfai, B., Lenart, N., Fekete, R., Laszlo, Z. I., Lele, Z., . . . Denes, A. (2020). Microglia monitor and protect neuronal function through specialized somatic purinergic junctions. *Science, 367*(6477), 528-537. doi:10.1126/science.aax6752

Daley, M., Morin, C. M., LeBlanc, M., Gregoire, J. P., & Savard, J. (2009). The economic burden of insomnia: direct and indirect costs for individuals with insomnia syndrome, insomnia symptoms, and good sleepers. *Sleep, 32*(1), 55-64. Retrieved from http://www.ncbi.nlm.nih.gov/pubmed/19189779

Davalos, D., Grutzendler, J., Yang, G., Kim, J. V., Zuo, Y., Jung, S., . . . Gan, W. B. (2005). ATP mediates rapid microglial response to local brain injury in vivo. *Nature Neuroscience, 8*(6), 752-758. doi:10.1038/nn1472

de Lecea, L. (2012). Hypocretins and the neurobiology of sleep-wake mechanisms. *Progress in Brain Research, 198*, 15-24. doi:10.1016/B978-0-444-59489-1.00003-3

Del Rio-Hortega Bereciartu, J. (2020). Pio del Rio-Hortega: The Revolution of Glia. *Anat Rec (Hoboken), 303*(5), 1232-1241. doi:10.1002/ar.24266

del Valle, J., Camins, A., Pallas, M., Vilaplana, J., & Pelegri, C. (2008). A new method for determining blood-brain barrier integrity based on intracardiac perfusion of an Evans Blue-Hoechst cocktail. *Journal of Neuroscience Methods, 174*(1), 42-49. doi:10.1016/j.jneumeth.2008.06.025

Delpech, J. C., Madore, C., Nadjar, A., Joffre, C., Wohleb, E. S., & Laye, S. (2015). Microglia in neuronal plasticity: Influence of stress. *Neuropharmacology, 96*(Pt A), 19-28. doi:10.1016/j.neuropharm.2014.12.034

Deurveilher, S., Bush, J. E., Rusak, B., Eskes, G. A., & Semba, K. (2015). Psychomotor vigilance task performance during and following chronic sleep restriction in rats. *Sleep, 38*(4), 515-528. doi:10.5665/sleep.4562

Deurveilher, S., Rusak, B., & Semba, K. (2012). Time-of-day modulation of homeostatic and allostatic sleep responses to chronic sleep restriction in rats. *Am J Physiol Regul Integr Comp Physiol, 302*(12), R1411-1425. doi:10.1152/ajpregu.00678.2011

Deurveilher, S., Ryan, N., Burns, J., & Semba, K. (2013). Social and environmental contexts modulate sleep deprivation-induced c-Fos activation in rats. *Behavioural Brain Research, 256*, 238-249. doi:10.1016/j.bbr.2013.08.029

Deurveilher, S., & Semba, K. (2019). Physiological and Neurobehavioral Consequences of Chronic Sleep Restriction in Rodent Models. In H. C. Dringenberg (Ed.), *Handbook of Behavioral Neuroscience* (Vol. 30, pp. 557-567). Amsterdam: Academic Press.

Dijk, D. J., & Duffy, J. F. (1999). Circadian regulation of human sleep and age-related changes in its timing, consolidation and EEG characteristics. *Annals of Medicine, 31*(2), 130-140. doi:10.3109/07853899908998789

Donat, C. K., Scott, G., Gentleman, S. M., & Sastre, M. (2017). Microglial Activation in Traumatic Brain Injury. *Frontiers in Aging Neuroscience, 9*, 208. doi:10.3389/fnagi.2017.00208

Dorrian, J., Rogers, N. L., & Dinges, D. F. (2005). *Psychomotor vigilance performance: Neurocognitive assay sensitive to sleep loss.* Marcel Dekker New York, NY,

Everson, C. A., & Szabo, A. (2009). Recurrent restriction of sleep and inadequate recuperation induce both adaptive changes and pathological outcomes. *Am J Physiol Regul Integr Comp Physiol, 297*(5), R1430-1440. doi:10.1152/ajpregu.00230.2009

Everson, C. A., & Szabo, A. (2011). Repeated exposure to severely limited sleep results in distinctive and persistent physiological imbalances in rats. *PloS One, 6*(8), e22987. doi:10.1371/journal.pone.0022987

Faraco, G., Park, L., Anrather, J., & Iadecola, C. (2017). Brain perivascular macrophages: characterization and functional roles in health and disease. *Journal of Molecular Medicine, 95*(11), 1143-1152.

Faraut, B., Boudjeltia, K. Z., Vanhamme, L., & Kerkhofs, M. (2012). Immune, inflammatory and cardiovascular consequences of sleep restriction and recovery. *Sleep Medicine Reviews, 16*(2), 137-149. doi:10.1016/j.smrv.2011.05.001

Farhy-Tselnicker, I., & Allen, N. J. (2018). Astrocytes, neurons, synapses: a tripartite view on cortical circuit development. *Neural Dev, 13*(1), 7. doi:10.1186/s13064-018-0104-y

Floyd, R. A., & Krueger, J. M. (1997). Diurnal variation of TNF alpha in the rat brain. *Neuroreport, 8*(4), 915-918. doi:10.1097/00001756-199703030-00020

Franco, R., & Fernandez-Suarez, D. (2015). Alternatively activated microglia and macrophages in the central nervous system. *Progress in Neurobiology, 131*, 65-86. doi:10.1016/j.pneurobio.2015.05.003

Frank, M. G., Hershman, S. A., Weber, M. D., Watkins, L. R., & Maier, S. F. (2014). Chronic exposure to exogenous glucocorticoids primes microglia to pro-inflammatory stimuli and induces NLRP3 mRNA in the hippocampus. *Psychoneuroendocrinology, 40*, 191-200. doi:10.1016/j.psyneuen.2013.11.006

Fuller, P. M., Gooley, J. J., & Saper, C. B. (2006). Neurobiology of the sleep-wake cycle: sleep architecture, circadian regulation, and regulatory feedback. *Journal of Biological Rhythms, 21*(6), 482-493. doi:10.1177/0748730406294627

Ginhoux, F., Greter, M., Leboeuf, M., Nandi, S., See, P., Gokhan, S., . . . Merad, M. (2010). Fate mapping analysis reveals that adult microglia derive from primitive macrophages. *Science, 330*(6005), 841-845. doi:10.1126/science.1194637

Goldstein, D. S., & McEwen, B. (2002). Allostasis, homeostats, and the nature of stress. *Stress, 5*(1), 55-58. doi:10.1080/102538902900012345

Gomez-Gonzalez, B., Hurtado-Alvarado, G., Esqueda-Leon, E., Santana-Miranda, R., Rojas-Zamorano, J. A., & Velazquez-Moctezuma, J. (2013). REM sleep loss and recovery regulates blood-brain barrier function. *Current Neurovascular Research, 10*(3), 197-207. Retrieved from http://www.ncbi.nlm.nih.gov/pubmed/23713739

Granon, S., & Poucet, B. (2000). Involvement of the rat prefrontal cortex in cognitive functions: A central role for the prelimbic area. *Psychobiology, 28*(2), 229-237.

Greene, R. W., Bjorness, T. E., & Suzuki, A. (2017). The adenosine-mediated, neuronal-glial, homeostatic sleep response. *Current Opinion in Neurobiology, 44*, 236-242. doi:10.1016/j.conb.2017.05.015

Haack, M., & Mullington, J. M. (2005). Sustained sleep restriction reduces emotional and physical well-being. *Pain, 119*(1-3), 56-64. doi:10.1016/j.pain.2005.09.011

Hafner, M., Stepanek, M., Taylor, J., Troxel, W. M., & van Stolk, C. (2016). *Why sleep matters – the economic costs of insufficient sleep*. Santa Monica, CA, USA: RAND Corporation.

Hall, S., Deurveilher, S., Ko, K. R., Burns, J., & Semba, K. (2017). Region-specific increases in FosB/DeltaFosB immunoreactivity in the rat brain in response to chronic sleep restriction. *Behavioural Brain Research, 322*(Pt A), 9-17. doi:10.1016/j.bbr.2017.01.024

Hammond, T. R., Dufort, C., Dissing-Olesen, L., Giera, S., Young, A., Wysoker, A., . . . Stevens, B. (2019). Single-Cell RNA Sequencing of Microglia throughout the Mouse Lifespan and in the Injured Brain Reveals Complex Cell-State Changes. *Immunity, 50*(1), 253-271 e256. doi:10.1016/j.immuni.2018.11.004

Hanisch, U. K., & Kettenmann, H. (2007). Microglia: active sensor and versatile effector cells in the normal and pathologic brain. *Nature Neuroscience, 10*(11), 1387-1394. doi:10.1038/nn1997

Haruwaka, K., Ikegami, A., Tachibana, Y., Ohno, N., Konishi, H., Hashimoto, A., . . . Wake, H. (2019). Dual microglia effects on blood brain barrier permeability induced by systemic inflammation. *Nat Commun, 10*(1), 5816. doi:10.1038/s41467-019-13812-z

Hassani, O. K., Lee, M. G., & Jones, B. E. (2009). Melanin-concentrating hormone neurons discharge in a reciprocal manner to orexin neurons across the sleep-wake cycle. *Proceedings of the National Academy of Sciences of the United States of America, 106*(7), 2418-2422. doi:10.1073/pnas.0811400106

Hayashi, Y., Koyanagi, S., Kusunose, N., Takayama, F., Okada, R., Wu, Z., . . . Nakanishi, H. (2013). Diurnal Spatial Rearrangement of Microglial Processes through the Rhythmic Expression of P2Y12 Receptors. *Neurological Disorders, 1*(2), 120.

Haynes, S. E., Hollopeter, G., Yang, G., Kurpius, D., Dailey, M. E., Gan, W. B., & Julius, D. (2006). The P2Y12 receptor regulates microglial activation by extracellular nucleotides. *Nature Neuroscience, 9*(12), 1512-1519. doi:10.1038/nn1805

He, J., Hsuchou, H., He, Y., Kastin, A. J., Wang, Y., & Pan, W. (2014). Sleep restriction impairs blood-brain barrier function. *Journal of Neuroscience, 34*(44), 14697-14706. doi:10.1523/JNEUROSCI.2111-14.2014

Hellström Erkenstam, N., Smith, P. L., Fleiss, B., Nair, S., Svedin, P., Wang, W., . . . Brown, K. L. (2016). Temporal characterization of microglia/macrophage phenotypes in a mouse model of neonatal hypoxic-ischemic brain injury. *Frontiers in Cellular Neuroscience, 10*, 286.

Hinwood, M., Morandini, J., Day, T. A., & Walker, F. R. (2012). Evidence that microglia mediate the neurobiological effects of chronic psychological stress on the medial prefrontal cortex. *Cerebral Cortex, 22*(6), 1442-1454. doi:10.1093/cercor/bhr229

Hinwood, M., Tynan, R. J., Charnley, J. L., Beynon, S. B., Day, T. A., & Walker, F. R. (2013). Chronic stress induced remodeling of the prefrontal cortex: structural re-organization of microglia and the inhibitory effect of minocycline. *Cerebral Cortex, 23*(8), 1784-1797. doi:10.1093/cercor/bhs151

Ho, J. M., Ducich, N. H., Nguyen, N. K., & Opp, M. R. (2018). Acute sleep disruption- and high-fat diet-induced hypothalamic inflammation are not related to glucose tolerance in mice. *Neurobiol Sleep Circadian Rhythms, 4*, 1-9. doi:10.1016/j.nbscr.2017.09.003

Horvath, T. L., & Gao, X. B. (2005). Input organization and plasticity of hypocretin neurons: possible clues to obesity's association with insomnia. *Cell Metabolism, 1*(4), 279-286. doi:10.1016/j.cmet.2005.03.003

Hsu, J. C., Lee, Y. S., Chang, C. N., Chuang, H. L., Ling, E. A., & Lan, C. T. (2003). Sleep deprivation inhibits expression of NADPH-d and NOS while activating microglia and astroglia in the rat hippocampus. *Cells Tissues Organs, 173*(4), 242-254. doi:70380

Huang, Y., Xu, Z., Xiong, S., Sun, F., Qin, G., Hu, G., . . . Peng, B. (2018). Repopulated microglia are solely derived from the proliferation of residual microglia after acute depletion. *Nature Neuroscience, 21*(4), 530-540. doi:10.1038/s41593-018-0090-8

Huber, R., Tononi, G., & Cirelli, C. (2007). Exploratory behavior, cortical BDNF expression, and sleep homeostasis. *Sleep, 30*(2), 129-139. doi:10.1093/sleep/30.2.129

Hurtado-Alvarado, G., Velazquez-Moctezuma, J., & Gomez-Gonzalez, B. (2017). Chronic sleep restriction disrupts interendothelial junctions in the hippocampus and increases blood-brain barrier permeability. *J Microsc, 268*(1), 28-38. doi:10.1111/jmi.12583

Imeri, L., Bianchi, S., & Opp, M. R. (2006). Inhibition of caspase-1 in rat brain reduces spontaneous nonrapid eye movement sleep and nonrapid eye movement sleep enhancement induced by lipopolysaccharide. *Am J Physiol Regul Integr Comp Physiol, 291*(1), R197-204. doi:10.1152/ajpregu.00828.2005

Imeri, L., & Opp, M. R. (2009). How (and why) the immune system makes us sleep. *Nature Reviews: Neuroscience, 10*(3), 199-210. doi:10.1038/nrn2576

Ingiosi, A. M., Opp, M. R., & Krueger, J. M. (2013). Sleep and immune function: glial contributions and consequences of aging. *Current Opinion in Neurobiology, 23*(5), 806-811. doi:10.1016/j.conb.2013.02.003

Ito, D., Tanaka, K., Suzuki, S., Dembo, T., & Fukuuchi, Y. (2001). Enhanced expression of Iba1, ionized calcium-binding adapter molecule 1, after transient focal cerebral ischemia in rat brain. *Stroke, 32*(5), 1208-1215. doi:10.1161/01.str.32.5.1208

Jiang, Y., Wei, N., Lu, T., Zhu, J., Xu, G., & Liu, X. (2011). Intranasal brain-derived neurotrophic factor protects brain from ischemic insult via modulating local inflammation in rats. *Neuroscience, 172*, 398-405. doi:10.1016/j.neuroscience.2010.10.054

Jones, B. E. (2020). Arousal and sleep circuits. *Neuropsychopharmacology, 45*(1), 6-20. doi:10.1038/s41386-019-0444-2

Junek, A., Rusak, B., & Semba, K. (2010). Short-term sleep deprivation may alter the dynamics of hippocampal cell proliferation in adult rats. *Neuroscience, 170*(4), 1140-1152. doi:10.1016/j.neuroscience.2010.08.018

Karperien, A., Ahammer, H., & Jelinek, H. F. (2013). Quantitating the subtleties of microglial morphology with fractal analysis. *Frontiers in Cellular Neuroscience, 7*, 3. doi:10.3389/fncel.2013.00003

Kaufmann, W. E., Worley, P. F., Pegg, J., Bremer, M., & Isakson, P. (1996). COX-2, a synaptically induced enzyme, is expressed by excitatory neurons at postsynaptic sites in rat cerebral cortex. *Proceedings of the National Academy of Sciences of the United States of America, 93*(6), 2317-2321. doi:10.1073/pnas.93.6.2317

Kettenmann, H., Hanisch, U. K., Noda, M., & Verkhratsky, A. (2011). Physiology of microglia. *Physiological Reviews, 91*(2), 461-553. doi:10.1152/physrev.00011.2010

Kettenmann, H., Kirchhoff, F., & Verkhratsky, A. (2013). Microglia: new roles for the synaptic stripper. *Neuron, 77*(1), 10-18. doi:10.1016/j.neuron.2012.12.023

Kierdorf, K., & Prinz, M. (2017). Microglia in steady state. *Journal of Clinical Investigation, 127*(9), 3201-3209. doi:10.1172/JCI90602

Kim, S. U., & de Vellis, J. (2005). Microglia in health and disease. *Journal of Neuroscience Research, 81*(3), 302-313. doi:10.1002/jnr.20562

Kim, W. G., Mohney, R. P., Wilson, B., Jeohn, G. H., Liu, B., & Hong, J. S. (2000). Regional difference in susceptibility to lipopolysaccharide-induced neurotoxicity in the rat brain: role of microglia. *Journal of Neuroscience, 20*(16), 6309-6316. Retrieved from http://www.ncbi.nlm.nih.gov/pubmed/10934283

Kim, Y., Laposky, A. D., Bergmann, B. M., & Turek, F. W. (2007). Repeated sleep restriction in rats leads to homeostatic and allostatic responses during recovery sleep. *Proceedings of the National Academy of Sciences of the United States of America, 104*(25), 10697-10702. doi:10.1073/pnas.0610351104

Konadhode, R. R., Pelluru, D., & Shiromani, P. J. (2014). Neurons containing orexin or melanin concentrating hormone reciprocally regulate wake and sleep. *Frontiers in Systems Neuroscience, 8*, 244. doi:10.3389/fnsys.2014.00244

Kondo, S., Kohsaka, S., & Okabe, S. (2011). Long-term changes of spine dynamics and microglia after transient peripheral immune response triggered by LPS in vivo. *Molecular Brain, 4*, 27. doi:10.1186/1756-6606-4-27

Krueger, J. M., Majde, J. A., & Rector, D. M. (2011). Cytokines in immune function and sleep regulation. *Handbook of Clinical Neurology, 98*, 229-240. doi:10.1016/B978-0-444-52006-7.00015-0

Krueger, J. M., Obal, F. J., Fang, J., Kubota, T., & Taishi, P. (2001). The role of cytokines in physiological sleep regulation. *Annals of the New York Academy of Sciences, 933*, 211-221. Retrieved from http://www.ncbi.nlm.nih.gov/pubmed/12000022

Krueger, J. M., Walter, J., Dinarello, C. A., Wolff, S. M., & Chedid, L. (1984). Sleep-promoting effects of endogenous pyrogen (interleukin-1). *American Journal of Physiology, 246*(6 Pt 2), R994-999. doi:10.1152/ajpregu.1984.246.6.R994

Kuric, E., & Ruscher, K. (2014). Dynamics of major histocompatibility complex class II-positive cells in the postischemic brain--influence of levodopa treatment. *Journal of Neuroinflammation, 11*, 145. doi:10.1186/s12974-014-0145-z

Kushikata, T., Fang, J., & Krueger, J. M. (1999). Interleukin-10 inhibits spontaneous sleep in rabbits. *J Interferon Cytokine Res, 19*(9), 1025-1030. doi:10.1089/107999099313244

Laposky, A. D., Bass, J., Kohsaka, A., & Turek, F. W. (2008). Sleep and circadian rhythms: key components in the regulation of energy metabolism. *FEBS Letters, 582*(1), 142-151. doi:10.1016/j.febslet.2007.06.079

Lee, M. G., Hassani, O. K., & Jones, B. E. (2005). Discharge of identified orexin/hypocretin neurons across the sleep-waking cycle. *Journal of Neuroscience, 25*(28), 6716-6720. doi:10.1523/JNEUROSCI.1887-05.2005

Leemburg, S., Vyazovskiy, V. V., Olcese, U., Bassetti, C. L., Tononi, G., & Cirelli, C. (2010). Sleep homeostasis in the rat is preserved during chronic sleep restriction. *Proceedings of the National Academy of Sciences of the United States of America, 107*(36), 15939-15944. doi:10.1073/pnas.1002570107

Liddelow, S. A., & Barres, B. A. (2017). Reactive Astrocytes: Production, Function, and Therapeutic Potential. *Immunity, 46*(6), 957-967. doi:10.1016/j.immuni.2017.06.006

Liu, Y. U., Ying, Y., Li, Y., Eyo, U. B., Chen, T., Zheng, J., . . . Wu, L. J. (2019). Neuronal network activity controls microglial process surveillance in awake mice via norepinephrine signaling. *Nature Neuroscience, 22*(11), 1771-1781. doi:10.1038/s41593-019-0511-3

Lobo-Silva, D., Carriche, G. M., Castro, A. G., Roque, S., & Saraiva, M. (2016). Balancing the immune response in the brain: IL-10 and its regulation. *Journal of Neuroinflammation, 13*(1), 297. doi:10.1186/s12974-016-0763-8

Lodge, P. A., & Sriram, S. (1996). Regulation of microglial activation by TGF-beta, IL-10, and CSF-1. *Journal of Leukocyte Biology, 60*(4), 502-508. Retrieved from http://www.ncbi.nlm.nih.gov/pubmed/8864135

London, A., Cohen, M., & Schwartz, M. (2013). Microglia and monocyte-derived macrophages: functionally distinct populations that act in concert in CNS plasticity and repair. *Frontiers in Cellular Neuroscience, 7*, 34. doi:10.3389/fncel.2013.00034

Lovatel, G. A., Bertoldi, K., Elsnerb, V. R., Piazza, F. V., Basso, C. G., Moyses Fdos, S., . . . Siqueira, I. R. (2014). Long-term effects of pre and post-ischemic exercise following global cerebral ischemia on astrocyte and microglia functions in hippocampus from Wistar rats. *Brain Research, 1587*, 119-126. doi:10.1016/j.brainres.2014.08.068

Macosko, E. Z., Basu, A., Satija, R., Nemesh, J., Shekhar, K., Goldman, M., . . . McCarroll, S. A. (2015). Highly Parallel Genome-wide Expression Profiling of Individual Cells Using Nanoliter Droplets. *Cell, 161*(5), 1202-1214. doi:10.1016/j.cell.2015.05.002

Manchanda, S., Singh, H., Kaur, T., & Kaur, G. (2018). Low-grade neuroinflammation due to chronic sleep deprivation results in anxiety and learning and memory impairments. *Mol Cell Biochem*. doi:10.1007/s11010-018-3343-7

Masuda, T., Sankowski, R., Staszewski, O., & Prinz, M. (2020). Microglia Heterogeneity in the Single-Cell Era. *Cell Reports, 30*(5), 1271-1281. doi:10.1016/j.celrep.2020.01.010

McClung, C. A., Ulery, P. G., Perrotti, L. I., Zachariou, V., Berton, O., & Nestler, E. J. (2004). DeltaFosB: a molecular switch for long-term adaptation in the brain. *Brain Research: Molecular Brain Research, 132*(2), 146-154. doi:10.1016/j.molbrainres.2004.05.014

McCoy, J. G., & Strecker, R. E. (2011). The cognitive cost of sleep lost. *Neurobiol Learn Mem, 96*(4), 564-582. doi:10.1016/j.nlm.2011.07.004

McEwen, B. S. (2006). Sleep deprivation as a neurobiologic and physiologic stressor: Allostasis and allostatic load. *Metabolism, 55*(10 Suppl 2), S20-23. doi:10.1016/j.metabol.2006.07.008

McEwen, B. S., & Gianaros, P. J. (2011). Stress- and allostasis-induced brain plasticity. *Annual Review of Medicine, 62*, 431-445. doi:10.1146/annurev-med-052209-100430

McEwen, B. S., & Karatsoreos, I. N. (2015). Sleep Deprivation and Circadian Disruption: Stress, Allostasis, and Allostatic Load. *Sleep Medicine Clinics, 10*(1), 1-10. doi:10.1016/j.jsmc.2014.11.007

McEwen, B. S., & Stellar, E. (1993). Stress and the individual. Mechanisms leading to disease. *Archives of Internal Medicine, 153*(18), 2093-2101. Retrieved from https://www.ncbi.nlm.nih.gov/pubmed/8379800

Meerlo, P., Koehl, M., van der Borght, K., & Turek, F. W. (2002). Sleep restriction alters the hypothalamic-pituitary-adrenal response to stress. *Journal of Neuroendocrinology, 14*(5), 397-402. Retrieved from http://www.ncbi.nlm.nih.gov/pubmed/12000545

Mildner, A., Huang, H., Radke, J., Stenzel, W., & Priller, J. (2017). P2Y12 receptor is expressed on human microglia under physiological conditions throughout development and is sensitive to neuroinflammatory diseases. *Glia, 65*(2), 375-387. doi:10.1002/glia.23097

Mistlberger, R. E. (2005). Circadian regulation of sleep in mammals: role of the suprachiasmatic nucleus. *Brain Research: Brain Research Reviews, 49*(3), 429-454. doi:10.1016/j.brainresrev.2005.01.005

Mistlberger, R. E., & Rusak, B. (2005). Biological rhythms and behaviour. *The behaviour of animals: mechanisms, function, and evolution*, 71-96.

Modirrousta, M., Mainville, L., & Jones, B. E. (2005). Orexin and MCH neurons express c-Fos differently after sleep deprivation vs. recovery and bear different adrenergic receptors. *European Journal of Neuroscience, 21*(10), 2807-2816. doi:10.1111/j.1460-9568.2005.04104.x

Moore, R. Y. (2007). Suprachiasmatic nucleus in sleep-wake regulation. *Sleep Medicine, 8 Suppl 3*, 27-33. doi:10.1016/j.sleep.2007.10.003

Morrison, H. W., & Filosa, J. A. (2013). A quantitative spatiotemporal analysis of microglia morphology during ischemic stroke and reperfusion. *Journal of Neuroinflammation, 10*, 4. doi:10.1186/1742-2094-10-4

Muzur, A., Pace-Schott, E. F., & Hobson, J. A. (2002). The prefrontal cortex in sleep. *Trends in Cognitive Sciences, 6*(11), 475-481. doi:10.1016/s1364-6613(02)01992-7

Nichols, M., Zhang, J., Polster, B. M., Elustondo, P. A., Thirumaran, A., Pavlov, E. V., & Robertson, G. S. (2015). Synergistic neuroprotection by epicatechin and quercetin:

Activation of convergent mitochondrial signaling pathways. *Neuroscience, 308*, 75-94. doi:10.1016/j.neuroscience.2015.09.012

Nimmerjahn, A., Kirchhoff, F., & Helmchen, F. (2005). Resting microglial cells are highly dynamic surveillants of brain parenchyma in vivo. *Science, 308*(5726), 1314-1318. doi:10.1126/science.1110647

Niraula, A., Sheridan, J. F., & Godbout, J. P. (2017). Microglia Priming with Aging and Stress. *Neuropsychopharmacology, 42*(1), 318-333. doi:10.1038/npp.2016.185

Obukuro, K., Nobunaga, M., Takigawa, M., Morioka, H., Hisatsune, A., Isohama, Y., . . . Katsuki, H. (2013). Nitric oxide mediates selective degeneration of hypothalamic orexin neurons through dysfunction of protein disulfide isomerase. *Journal of Neuroscience, 33*(31), 12557-12568. doi:10.1523/JNEUROSCI.0595-13.2013

Ohsawa, K., Imai, Y., Kanazawa, H., Sasaki, Y., & Kohsaka, S. (2000). Involvement of Iba1 in membrane ruffling and phagocytosis of macrophages/microglia. *Journal of Cell Science, 113 (Pt 17)*, 3073-3084. Retrieved from https://www.ncbi.nlm.nih.gov/pubmed/10934045

Ohsawa, K., Imai, Y., Sasaki, Y., & Kohsaka, S. (2004). Microglia/macrophage-specific protein Iba1 binds to fimbrin and enhances its actin-bundling activity. *Journal of Neurochemistry, 88*(4), 844-856. Retrieved from http://www.ncbi.nlm.nih.gov/pubmed/14756805

Olah, M., Ping, G., De Haas, A. H., Brouwer, N., Meerlo, P., Van Der Zee, E. A., . . . Boddeke, H. W. (2009). Enhanced hippocampal neurogenesis in the absence of microglia T cell interaction and microglia activation in the murine running wheel model. *Glia, 57*(10), 1046-1061. doi:10.1002/glia.20828

Opp, M. R., & Krueger, J. M. (1994). Interleukin-1 is involved in responses to sleep deprivation in the rabbit. *Brain Research, 639*(1), 57-65. doi:10.1016/0006-8993(94)91764-7

Orihuela, R., McPherson, C. A., & Harry, G. J. (2016). Microglial M1/M2 polarization and metabolic states. *British Journal of Pharmacology, 173*(4), 649-665. doi:10.1111/bph.13139

Paolicelli, R. C., & Gross, C. T. (2011). Microglia in development: linking brain wiring to brain environment. *Neuron Glia Biology, 7*(1), 77-83. doi:10.1017/S1740925X12000105

Perego, C., Fumagalli, S., & De Simoni, M. G. (2011). Temporal pattern of expression and colocalization of microglia/macrophage phenotype markers following brain ischemic injury in mice. *Journal of Neuroinflammation, 8*, 174. doi:10.1186/1742-2094-8-174

Perry, V. H., & Holmes, C. (2014). Microglial priming in neurodegenerative disease. *Nature Reviews: Neurology, 10*(4), 217-224. doi:10.1038/nrneurol.2014.38

Perry, V. H., Nicoll, J. A., & Holmes, C. (2010). Microglia in neurodegenerative disease. *Nature Reviews: Neurology, 6*(4), 193-201. doi:10.1038/nrneurol.2010.17

Peters, D., Berger, J., Langnaese, K., Derst, C., Madai, V. I., Krauss, M., . . . Laube, G. (2013). Arginase and Arginine Decarboxylase - Where Do the Putative Gate Keepers of Polyamine Synthesis Reside in Rat Brain? *PloS One, 8*(6), e66735. doi:10.1371/journal.pone.0066735

Peyron, C., Tighe, D. K., van den Pol, A. N., de Lecea, L., Heller, H. C., Sutcliffe, J. G., & Kilduff, T. S. (1998). Neurons containing hypocretin (orexin) project to multiple neuronal systems. *Journal of Neuroscience, 18*(23), 9996-10015. Retrieved from http://www.ncbi.nlm.nih.gov/pubmed/9822755

Pocock, J. M., & Kettenmann, H. (2007). Neurotransmitter receptors on microglia. *Trends in Neurosciences, 30*(10), 527-535. doi:10.1016/j.tins.2007.07.007

Prinz, M., Jung, S., & Priller, J. (2019). Microglia Biology: One Century of Evolving Concepts. *Cell, 179*(2), 292-311. doi:10.1016/j.cell.2019.08.053

Ransohoff, R. M. (2016). A polarizing question: do M1 and M2 microglia exist? *Nature Neuroscience, 19*(8), 987-991. doi:10.1038/nn.4338

Rao, Y., Lu, M., Ge, F., Marsh, D. J., Qian, S., Wang, A. H., . . . Gao, X. B. (2008). Regulation of synaptic efficacy in hypocretin/orexin-containing neurons by melanin concentrating hormone in the lateral hypothalamus. *Journal of Neuroscience, 28*(37), 9101-9110. doi:10.1523/JNEUROSCI.1766-08.2008

The Rat Nervous System. (2004). Academic Press.

Rechtschaffen, A. (1998). Current perspectives on the function of sleep. *Perspectives in Biology and Medicine, 41*(3), 359-390. doi:10.1353/pbm.1998.0051

Reynolds, A. C., & Banks, S. (2010). Total sleep deprivation, chronic sleep restriction and sleep disruption. *Progress in Brain Research, 185*, 91-103. doi:10.1016/B978-0-444-53702-7.00006-3

Roman, V., Van der Borght, K., Leemburg, S. A., Van der Zee, E. A., & Meerlo, P. (2005). Sleep restriction by forced activity reduces hippocampal cell proliferation. *Brain Research, 1065*(1-2), 53-59. doi:10.1016/j.brainres.2005.10.020

Roy, A., Fung, Y. K., Liu, X., & Pahan, K. (2006). Up-regulation of microglial CD11b expression by nitric oxide. *Journal of Biological Chemistry, 281*(21), 14971-14980. doi:10.1074/jbc.M600236200

Sakurai, T., Mieda, M., & Tsujino, N. (2010). The orexin system: roles in sleep/wake regulation. *Annals of the New York Academy of Sciences, 1200*, 149-161. doi:10.1111/j.1749-6632.2010.05513.x

Sandiego, C. M., Gallezot, J. D., Pittman, B., Nabulsi, N., Lim, K., Lin, S. F., . . . Cosgrove, K. P. (2015). Imaging robust microglial activation after lipopolysaccharide administration in humans with PET. *Proceedings of the National Academy of Sciences of the United States of America, 112*(40), 12468-12473. doi:10.1073/pnas.1511003112

Saper, C. B. (2013). The neurobiology of sleep. *Continuum (Minneap Minn), 19*(1 Sleep Disorders), 19-31. doi:10.1212/01.CON.0000427215.07715.73

Sasaki, Y., Ohsawa, K., Kanazawa, H., Kohsaka, S., & Imai, Y. (2001). Iba1 is an actin-cross-linking protein in macrophages/microglia. *Biochem Biophys Res Commun, 286*(2), 292-297. doi:10.1006/bbrc.2001.5388

Sawada, M., Suzumura, A., Hosoya, H., Marunouchi, T., & Nagatsu, T. (1999). Interleukin-10 inhibits both production of cytokines and expression of cytokine receptors in microglia. *Journal of Neurochemistry, 72*(4), 1466-1471. Retrieved from http://www.ncbi.nlm.nih.gov/pubmed/10098850

Scammell, T. E., Arrigoni, E., & Lipton, J. O. (2017). Neural Circuitry of Wakefulness and Sleep. *Neuron, 93*(4), 747-765. doi:10.1016/j.neuron.2017.01.014

Schafer, D. P., Lehrman, E. K., Kautzman, A. G., Koyama, R., Mardinly, A. R., Yamasaki, R., . . . Stevens, B. (2012). Microglia sculpt postnatal neural circuits in an activity and complement-dependent manner. *Neuron, 74*(4), 691-705. doi:10.1016/j.neuron.2012.03.026

Schluter, D., Kaefer, N., Hof, H., Wiestler, O. D., & Deckert-Schluter, M. (1997). Expression pattern and cellular origin of cytokines in the normal and Toxoplasma gondii-infected murine brain. *American Journal of Pathology, 150*(3), 1021-1035. Retrieved from https://www.ncbi.nlm.nih.gov/pubmed/9060839

Semba, K., Briggs, C., Hatada, S., Deurveilher, S., & Kubota, Y. (2019). *Astrocytic processes associated with synapses to orexin neurons: 3-dimensional analysis using correlative light-electron microscopy.* Paper presented at the Society for Neuroscience Abstract, Presention No 205.02.

Sengupta, P. (2013). The Laboratory Rat: Relating Its Age With Human's. *International Journal of Preventive Medicine, 4*(6), 624-630. Retrieved from https://www.ncbi.nlm.nih.gov/pubmed/23930179

Shoham, S., Davenne, D., Cady, A. B., Dinarello, C. A., & Krueger, J. M. (1987). Recombinant tumor necrosis factor and interleukin 1 enhance slow-wave sleep. *American Journal of Physiology, 253*(1 Pt 2), R142-149. doi:10.1152/ajpregu.1987.253.1.R142

Shojaeian, S., Lay, N. M., & Zarnani, A. (2018). Detection Systems in Immunohistochemistry. *IntechOpen*, 1-25.

Short, M. A., & Banks, S. (2014). The Functional Impact of Sleep Deprivation, Sleep Restriction, and Sleep Fragmentation. In M. T. Bianchi (Ed.), *Sleep Deprivation and Disease: Effects on the Body, Brain and Behavior* (pp. 13-26). New York: Springer Science+Business Media.

Sierra, A., Encinas, J. M., Deudero, J. J., Chancey, J. H., Enikolopov, G., Overstreet-Wadiche, L. S., . . . Maletic-Savatic, M. (2010). Microglia shape adult hippocampal neurogenesis through apoptosis-coupled phagocytosis. *Cell Stem Cell, 7*(4), 483-495. doi:10.1016/j.stem.2010.08.014

Silva, R. H., Kameda, S. R., Carvalho, R. C., Takatsu-Coleman, A. L., Niigaki, S. T., Abilio, V. C., . . . Frussa-Filho, R. (2004). Anxiogenic effect of sleep deprivation in the elevated plus-maze test in mice. *Psychopharmacology, 176*(2), 115-122. doi:10.1007/s00213-004-1873-z

Sipe, G. O., Lowery, R. L., Tremblay, M. E., Kelly, E. A., Lamantia, C. E., & Majewska, A. K. (2016). Microglial P2Y12 is necessary for synaptic plasticity in mouse visual cortex. *Nat Commun, 7*, 10905. doi:10.1038/ncomms10905

Smith, J. A., Das, A., Ray, S. K., & Banik, N. L. (2012). Role of pro-inflammatory cytokines released from microglia in neurodegenerative diseases. *Brain Research Bulletin, 87*(1), 10-20. doi:10.1016/j.brainresbull.2011.10.004

Stephenson, R., Caron, A. M., & Famina, S. (2015). Behavioral sleep-wake homeostasis and EEG delta power are decoupled by chronic sleep restriction in the rat. *Sleep, 38*(5), 685-697. doi:10.5665/sleep.4656

Stowell, R. D., Sipe, G. O., Dawes, R. P., Batchelor, H. N., Lordy, K. A., Whitelaw, B. S., . . . Majewska, A. K. (2019). Noradrenergic signaling in the wakeful state inhibits microglial surveillance and synaptic plasticity in the mouse visual cortex. *Nature Neuroscience, 22*(11), 1782-1792. doi:10.1038/s41593-019-0514-0

Streit, W. J., Mrak, R. E., & Griffin, W. S. (2004). Microglia and neuroinflammation: a pathological perspective. *Journal of Neuroinflammation, 1*(1), 14. doi:10.1186/1742-2094-1-14

Streit, W. J., Walter, S. A., & Pennell, N. A. (1999). Reactive microgliosis. *Progress in Neurobiology, 57*(6), 563-581. Retrieved from http://www.ncbi.nlm.nih.gov/pubmed/10221782

Sun, W., Suzuki, K., Toptunov, D., Stoyanov, S., Yuzaki, M., Khiroug, L., & Dityatev, A. (2019). In vivo Two-Photon Imaging of Anesthesia-Specific Alterations in Microglial Surveillance and Photodamage-Directed Motility in Mouse Cortex. *Frontiers in Neuroscience, 13*, 421. doi:10.3389/fnins.2019.00421

Taishi, P., Bredow, S., Guha-Thakurta, N., Obal, F., Jr., & Krueger, J. M. (1997). Diurnal variations of interleukin-1 beta mRNA and beta-actin mRNA in rat brain. *Journal of Neuroimmunology, 75*(1-2), 69-74. doi:10.1016/s0165-5728(97)00002-7

Takahashi, K., Lin, J. S., & Sakai, K. (2008). Neuronal activity of orexin and non-orexin waking-active neurons during wake-sleep states in the mouse. *Neuroscience, 153*(3), 860-870. doi:10.1016/j.neuroscience.2008.02.058

Tan, Y. L., Yuan, Y., & Tian, L. (2020). Microglial regional heterogeneity and its role in the brain. *Molecular Psychiatry, 25*(2), 351-367. doi:10.1038/s41380-019-0609-8

Tartar, J. L., Ward, C. P., Cordeira, J. W., Legare, S. L., Blanchette, A. J., McCarley, R. W., & Strecker, R. E. (2009). Experimental sleep fragmentation and sleep deprivation in rats increases exploration in an open field test of anxiety while increasing plasma corticosterone levels. *Behavioural Brain Research, 197*(2), 450-453. doi:10.1016/j.bbr.2008.08.035

Trachsel, L., Tobler, I., Achermann, P., & Borbely, A. A. (1991). Sleep continuity and the REM-nonREM cycle in the rat under baseline conditions and after sleep deprivation. *Physiol Behav, 49*(3), 575-580. doi:10.1016/0031-9384(91)90283-t

Tremblay, M. E., Lowery, R. L., & Majewska, A. K. (2010). Microglial interactions with synapses are modulated by visual experience. *PLoS Biology, 8*(11), e1000527. doi:10.1371/journal.pbio.1000527

Tremblay, M. E., Stevens, B., Sierra, A., Wake, H., Bessis, A., & Nimmerjahn, A. (2011). The role of microglia in the healthy brain. *Journal of Neuroscience, 31*(45), 16064-16069. doi:10.1523/JNEUROSCI.4158-11.2011

Tsunematsu, T., Ueno, T., Tabuchi, S., Inutsuka, A., Tanaka, K. F., Hasuwa, H., . . . Yamanaka, A. (2014). Optogenetic manipulation of activity and temporally controlled cell-specific ablation reveal a role for MCH neurons in sleep/wake regulation. *Journal of Neuroscience, 34*(20), 6896-6909. doi:10.1523/JNEUROSCI.5344-13.2014

Tuan, L. H., & Lee, L. J. (2019). Microglia-mediated synaptic pruning is impaired in sleep-deprived adolescent mice. *Neurobiology of Disease, 130*, 104517. doi:10.1016/j.nbd.2019.104517

Tynan, R. J., Naicker, S., Hinwood, M., Nalivaiko, E., Buller, K. M., Pow, D. V., . . . Walker, F. R. (2010). Chronic stress alters the density and morphology of microglia in a subset of stress-responsive brain regions. *Brain, Behavior, and Immunity, 24*(7), 1058-1068. doi:10.1016/j.bbi.2010.02.001

van den Pol, A. N., Acuna-Goycolea, C., Clark, K. R., & Ghosh, P. K. (2004). Physiological properties of hypothalamic MCH neurons identified with selective expression of reporter gene after recombinant virus infection. *Neuron, 42*(4), 635-652. doi:10.1016/s0896-6273(04)00251-x

Van Dongen, H. P., Maislin, G., Mullington, J. M., & Dinges, D. F. (2003). The cumulative cost of additional wakefulness: dose-response effects on neurobehavioral functions and sleep physiology from chronic sleep restriction and total sleep deprivation. *Sleep, 26*(2), 117-126. Retrieved from http://www.ncbi.nlm.nih.gov/pubmed/12683469

Vgontzas, A. N., Bixler, E. O., Lin, H. M., Prolo, P., Trakada, G., & Chrousos, G. P. (2005). IL-6 and its circadian secretion in humans. *Neuroimmunomodulation, 12*(3), 131-140. doi:10.1159/000084844

Vlasova-St Louis, I., & Bohjanen, P. R. (2017). Post-transcriptional regulation of cytokine and growth factor signaling in cancer. *Cytokine Growth Factor Rev, 33*, 83-93. doi:10.1016/j.cytogfr.2016.11.004

Wadhwa, M., Chauhan, G., Roy, K., Sahu, S., Deep, S., Jain, V., . . . Panjwani, U. (2018). Caffeine and Modafinil Ameliorate the Neuroinflammation and Anxious Behavior in Rats during Sleep Deprivation by Inhibiting the Microglia Activation. *Frontiers in Cellular Neuroscience, 12*, 49. doi:10.3389/fncel.2018.00049

Wadhwa, M., Kumari, P., Chauhan, G., Roy, K., Alam, S., Kishore, K., . . . Panjwani, U. (2017). Sleep deprivation induces spatial memory impairment by altered hippocampus neuroinflammatory responses and glial cells activation in rats. *Journal of Neuroimmunology, 312*, 38-48. doi:10.1016/j.jneuroim.2017.09.003

Wake, H., Moorhouse, A. J., Jinno, S., Kohsaka, S., & Nabekura, J. (2009). Resting microglia directly monitor the functional state of synapses in vivo and determine the fate of

ischemic terminals. *Journal of Neuroscience, 29*(13), 3974-3980. doi:10.1523/JNEUROSCI.4363-08.2009

Wake, H., Moorhouse, A. J., Miyamoto, A., & Nabekura, J. (2013). Microglia: actively surveying and shaping neuronal circuit structure and function. *Trends in Neurosciences, 36*(4), 209-217. doi:10.1016/j.tins.2012.11.007

Walker, M. P. (2019). A Societal Sleep Prescription. *Neuron, 103*(4), 559-562. doi:10.1016/j.neuron.2019.06.015

Wallingford, J. K., Deurveilher, S., Currie, R. W., Fawcett, J. P., & Semba, K. (2014). Increases in mature brain-derived neurotrophic factor protein in the frontal cortex and basal forebrain during chronic sleep restriction in rats: possible role in initiating allostatic adaptation. *Neuroscience, 277*, 174-183. doi:10.1016/j.neuroscience.2014.06.067

Weil, Z. M., Norman, G. J., Karelina, K., Morris, J. S., Barker, J. M., Su, A. J., . . . DeVries, A. C. (2009). Sleep deprivation attenuates inflammatory responses and ischemic cell death. *Experimental Neurology, 218*(1), 129-136. doi:10.1016/j.expneurol.2009.04.018

Weinhard, L., di Bartolomei, G., Bolasco, G., Machado, P., Schieber, N. L., Neniskyte, U., . . . Gross, C. T. (2018). Microglia remodel synapses by presynaptic trogocytosis and spine head filopodia induction. *Nat Commun, 9*(1), 1228. doi:10.1038/s41467-018-03566-5

Wisor, J. P., Schmidt, M. A., & Clegern, W. C. (2011). Evidence for neuroinflammatory and microglial changes in the cerebral response to sleep loss. *Sleep, 34*(3), 261-272. Retrieved from http://www.ncbi.nlm.nih.gov/pubmed/21358843

Wogram, E., Wendt, S., Matyash, M., Pivneva, T., Draguhn, A., & Kettenmann, H. (2016). Satellite microglia show spontaneous electrical activity that is uncorrelated with activity of the attached neuron. *European Journal of Neuroscience, 43*(11), 1523-1534. doi:10.1111/ejn.13256

Wohleb, E. S., Fenn, A. M., Pacenta, A. M., Powell, N. D., Sheridan, J. F., & Godbout, J. P. (2012). Peripheral innate immune challenge exaggerated microglia activation, increased the number of inflammatory CNS macrophages, and prolonged social withdrawal in socially defeated mice. *Psychoneuroendocrinology, 37*(9), 1491-1505. doi:10.1016/j.psyneuen.2012.02.003

Xie, Y., Ba, L., Wang, M., Deng, S. Y., Chen, S. M., Huang, L. F., . . . Ding, F. F. (2020). Chronic sleep fragmentation shares similar pathogenesis with neurodegenerative diseases: Endosome-autophagosome-lysosome pathway dysfunction and microglia-mediated neuroinflammation. *CNS Neuroscience & Therapeutics, 26*(2), 215-227. doi:10.1111/cns.13218

Xu, D., Lian, D., Wu, J., Liu, Y., Zhu, M., Sun, J., . . . Li, L. (2017). Brain-derived neurotrophic factor reduces inflammation and hippocampal apoptosis in experimental Streptococcus pneumoniae meningitis. *Journal of Neuroinflammation, 14*(1), 156. doi:10.1186/s12974-017-0930-6

Xue, R., Wan, Y., Sun, X., Zhang, X., Gao, W., & Wu, W. (2019). Nicotinic Mitigation of Neuroinflammation and Oxidative Stress After Chronic Sleep Deprivation. *Frontiers in Immunology, 10*, 2546. doi:10.3389/fimmu.2019.02546

Yen, L. F., Wei, V. C., Kuo, E. Y., & Lai, T. W. (2013). Distinct patterns of cerebral extravasation by Evans blue and sodium fluorescein in rats. *PloS One, 8*(7), e68595. doi:10.1371/journal.pone.0068595

Young, K., & Morrison, H. (2018). Quantifying Microglia Morphology from Photomicrographs of Immunohistochemistry Prepared Tissue Using ImageJ. *J Vis Exp*(136). doi:10.3791/57648

Zack, G. W., Rogers, W. E., & Latt, S. A. (1977). Automatic measurement of sister chromatid exchange frequency. *Journal of Histochemistry and Cytochemistry, 25*(7), 741-753. doi:10.1177/25.7.70454

Zhang, J., Zhu, Y., Zhan, G., Fenik, P., Panossian, L., Wang, M. M., . . . Veasey, S. (2014). Extended wakefulness: compromised metabolics in and degeneration of locus ceruleus neurons. *Journal of Neuroscience, 34*(12), 4418-4431. doi:10.1523/JNEUROSCI.5025-12.2014

Zhao, H. Y., Wu, H. J., He, J. L., Zhuang, J. H., Liu, Z. Y., Huang, L. Q., & Zhao, Z. X. (2017). Chronic Sleep Restriction Induces Cognitive Deficits and Cortical Beta-Amyloid Deposition in Mice via BACE1-Antisense Activation. *CNS Neuroscience & Therapeutics, 23*(3), 233-240. doi:10.1111/cns.12667

Zhu, B., Dong, Y., Xu, Z., Gompf, H. S., Ward, S. A., Xue, Z., . . . Xie, Z. (2012). Sleep disturbance induces neuroinflammation and impairment of learning and memory. *Neurobiology of Disease, 48*(3), 348-355. doi:10.1016/j.nbd.2012.06.022

Zhu, W., Cao, F. S., Feng, J., Chen, H. W., Wan, J. R., Lu, Q., & Wang, J. (2017). NLRP3 inflammasome activation contributes to long-term behavioral alterations in mice injected with lipopolysaccharide. *Neuroscience, 343*, 77-84. doi:10.1016/j.neuroscience.2016.11.037

Zhu, Y., Fenik, P., Zhan, G., Xin, R., & Veasey, S. C. (2015). Degeneration in Arousal Neurons in Chronic Sleep Disruption Modeling Sleep Apnea. *Frontiers in Neurology, 6*, 109. doi:10.3389/fneur.2015.00109

Zielinski, M. R., Kim, Y., Karpova, S. A., McCarley, R. W., Strecker, R. E., & Gerashchenko, D. (2014). Chronic sleep restriction elevates brain interleukin-1 beta and tumor necrosis factor-alpha and attenuates brain-derived neurotrophic factor expression. *Neuroscience Letters, 580*, 27-31. doi:10.1016/j.neulet.2014.07.043

APPENDIX A: MICROGLIA-SPECIFIC MARKERS

Table A.1. Microglia-specific markers used in the present thesis

Name	Type	Description	Reference
Ionized calcium-binding adaptor molecule-1 (Iba1)	Cytoplasmic protein	Calcium-binding protein involved actin-bundling activity and cytoskeletal reorganization that regulates membrane ruffling and phagocytosis	Imai et al., (1996); Sasaki et al., (2001)
P2Y12 receptor	Surface receptor	Gi/o protein-coupled purinergic receptor involved in chemotaxis through the detection of nucleotides (ATP and ADP)	Butovsky et al., (2014); Moore et al., (2015)
CD68[a]	Lysosomal protein/surface receptor	Debris removal and phagocytosis	Perego et al., (2011)
Major histocompatibility complex-II (MCHII/OX6)[a]	Surface receptor	Role in antigen presentation	Harms et al., (2013); David & Kroner, (2011)
Arginase-1 (Arg1)[b]	Enzyme	Involved in converting arginine to ornithine and urea	Corraliza et al., (1995)
Cyclooxygenase-2 (COX2)[b]	Enzyme	Role in prostaglandin synthesis	David & Kroner, (2011)
Mannose receptor (MR)[b]	Surface receptor	Involved in pathogen clearance	Perego et al., (2011)

[a] often referred as 'M1' or pro-inflammatory marker
[b] often referred as 'M2' or anti-inflamamtory marker

APPENDIX B: PRIMARY ANTIBODIES USED FOR IMMUNOHISTOCHEMISTRY

Table B.1. Primary antibodies used for immunohistochemistry

Antigen	Host	Source	Immunogen[a]	Specificity	Thesis Chapter
Arginase-1	Rabbit	Abcam, Cat# ab91279, Cambridge, MA, USA	KLH-conjugated synthetic peptide corresponding to amino acid residue 300 to the C-terminus of mouse liver arginase	Western blot analysis showed a band at ~37 kDa and a second band at ~40 kDa in mouse liver tissue lysate.[a]	3
Bromodeoxyuridine (BrdU)	Sheep	Fitzgerald Industries International, Cat# 20R-BS001, Concord, MA	Raised against highly purified BrdU	No staining in an animal that did not receive BrdU injections (current study). Presence of positive cells in the hippocampal dentate gyrus and the subventricular zone (current study).	2
CD68	Mouse	Bio-Rad, Cat# MCA341R, Hercules, CA, USA, RRID: AB_2291300	ED1 antigen (CD68) from rat spleen cells	Western blot analysis showed a single band at ~110 kDa corresponding to CD68 [1].	3
Cyclooxygenase-2 (COX2)	Rabbit	Abcam, Cat# ab15191	Synthetic peptide the sequence of which is located within amino acid residue 550 and the C-terminus of rat COX2	Western blot analysis showed a single band at ~69 kDa corresponding to COX2.[a]	3
FosB/ΔFosB	Mouse	Abcam, Cat# 11959	Synthetic peptide corresponding to human FosB	Western blot analysis showed two bands at ~46–48 and 35 kDa corresponding to the	4

				full length FosB and ΔFosB isoforms.[a]	
Glial fibrillary acidic protein (GFAP)	Mouse	Millipore/Sigma, Cat#MAB3402	Purified glial filament	Western blot analysis showed a single 51 kDa band corresponding to GFAP.[a]	2
Iba1	Rabbit	Wako Pure Chemical Industries, Cat# 019-19741, Osaka, Japan	Synthetic peptide corresponding to the C-terminus of rat Iba1	Western blot analysis showed a single 17 kDa band corresponding to Iba1.[a]	2
Iba1	Guinea Pig	Synaptic Systems, Cat# 234004, Göttingen, Germany	Synthetic peptide corresponding to amino acid residues 134-147 of rat Iba1	Western blot analysis showed a single band at ~17 kDa corresponding to Iba1.[a]	3,4
Interleukin-10 (IL10)	Rabbit	Abcam, Cat# ab9969	Synthetic peptide corresponding to amino acid residues 19–178 of rat IL-10	Western blot analysis showed two bands at 17–21 kDa corresponding to the IL10 homodimer [2].	3
Mannose receptor (CD206)	Rabbit	Abcam, Cat# ab64693	KLH-conjugated synthetic peptide the sequence of which is located within amino acid residue 1400 to the C-terminus of human mannose receptor	Western blot analysis showed a single band at ~166 kDa corresponding to CD206 [3].	3
NeuN	Mouse	Millipore/Sigma, Cat#MAB377	GST/His-tagged synthetic peptide corresponding	Western blot analysis showed a single band at ~46–48 kDa	3

			to the first 97 amino acid residues from the N-terminus of murine NeuN	corresponding to NeuN.[a]	
Orexin/Hypocretin (ORX)	Rabbit	Millipore/Sigma, Cat#AB3704, Burlington, MA, USA	Synthetic peptide corresponding to the C-terminal portion of the bovine Orexin-A peptide	Antibody has been shown to specifically label ORX neurons and was tested in a preadsorption assay using synthetic human orexin-A [4].	4
OX6 (MHCII)	Mouse	BD Biosciences, Cat# 554926, San Jose, CA, USA	Purified Ia-like glycoproteins from rat thymocytes	Complete co-localization of OX6 and Iba1 immunoreactivities in microglia of Aβ-treated mice [5].	3
P2Y12 receptor	Rabbit	Anaspec, Cat# AS-55043A, San Jose, CA, USA	KLH-conjugated synthetic peptide corresponding to the C-terminus of mouse P2Y12 receptor	Western blot analysis confirmed a single band at ~50 kDa corresponding to P2Y12 receptor [6].	3,4
pro-melanin-concentrating hormone (MCH)	Goat	Santa Cruz Biotechnology, Cat# sc-14509	Epitope mapping near the C-terminus of pro-MCH precursor of human origin	Complete elimination of immunolabelling in a preadsorption assay [7].	4

[a]Manufacturer's technical information

1. Peng JH, Cui T, Sun ZL, et al. Effects of Puerariae Radix Extract on Endotoxin Receptors and Tnf-Alpha Expression Induced by Gut-Derived Endotoxin in Chronic Alcoholic Liver Injury. *Evid Based Complement Alternat Med*. 2012;2012:234987.

2. Wu J, Sun L, Li H, Shen H, et al. Roles of Programmed Death Protein 1/Programmed Death-Ligand 1 in Secondary Brain Injury Intracerebral Hemorrhage in Rats: Selective Modulation of Microglia Polarization to Anti-Inflammatory Phenotype. *J Neuroinflammation.* 2017;14(1):36.

3. Ji J, Wang P, Zhou Q, et al. Ccl8 Enhances Sensitivity of Cutaneous Squamous Cell Carcinoma to Photodynamic Therapy by Recruiting M1 Macrophages. *Photodiagnosis Photodyn Ther.* 2019;26:235-243.

4. Alexandre D, Hautot C, Mehio M, et al. The Orexin Type 1 Receptor is Overexpressed in Advanced Prostate Cancer with a Neuroendocrine Differentiation, and Mediates Apoptosis. *Eur J Cancer*. 2014;50(12):2126-2133.

5. Nell HJ, Whitehead SN, Cechetto DF. Age-Dependent Effect of Beta-Amyloid Toxicity on Basal Forebrain Cholinergic Neurons and Inflammation in the Rat Brain. *Brain Pathol*. 2015;25(5):531-542.

6. Yu T, Zhang X, Shi H, et al. P2y12 Regulates Microglia Activation and Excitatory Synaptic Transmission in Spinal Lamina Ii Neurons During Neuropathic Pain in Rodents. *Cell Death Dis.* 2019;10(3):165.

7. Deurveilher S, Lo H, Murphy J, et al. Differential c-Fos Immunoreactivity in Arousal-Promoting Cell Groups Following Systemic Administration of Caffeine in Rats. *J Comp Neurol*. 2006;498:667-689.

APPENDIX C: GFAP IMMUNOHISTOCHEMISTRY ANALYSIS IN SLEEP/WAKE-REGULATORY AND LIMBIC BRAIN REGIONS FOLLOWING CSR

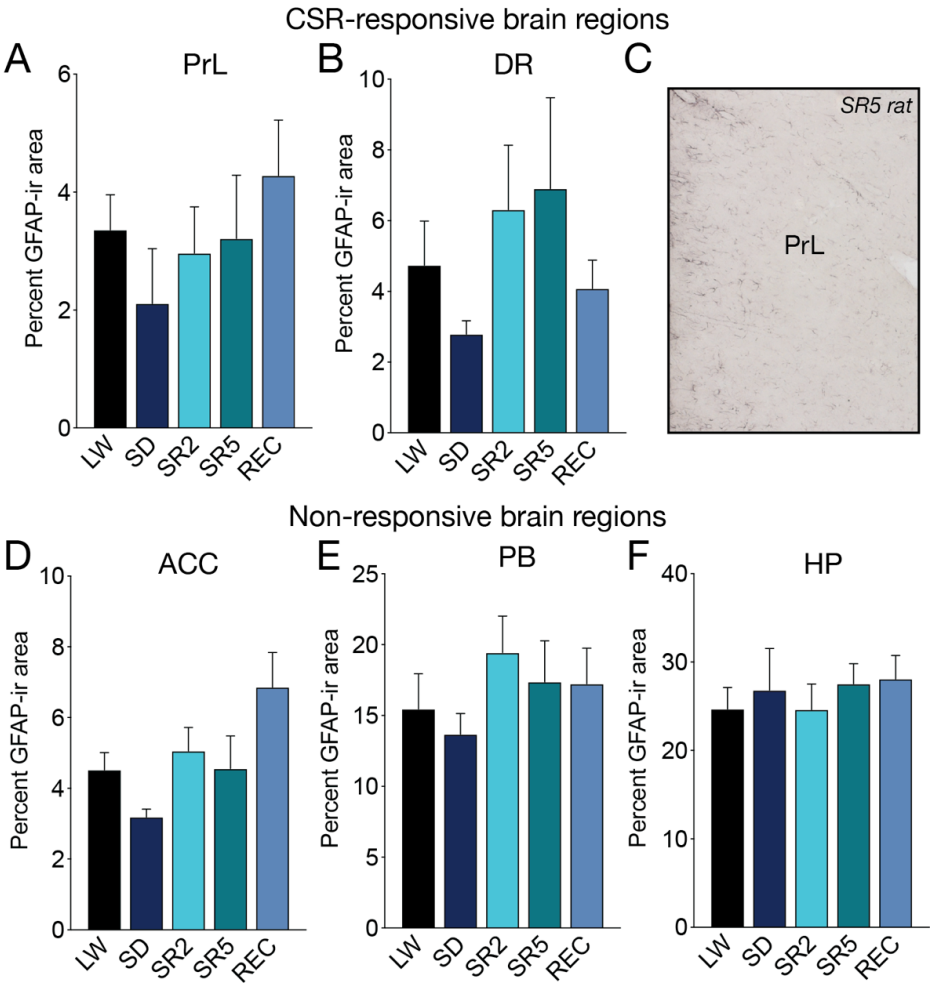

Figure C.1. The density of GFAP immunoreactivity (percent GFAP-ir areas) in select brain regions that were examined for the density of Iba1 immunoreactivity (see Figure 2.2 and Appendix D, Table D.2). The areas examined area: two CSR-responsive brain regions including the prelimbic cortex (PrL; A) and dorsal raphe nucleus (DR; B) and three brain regions that did not show CSR-induced increases in Iba1 including the anterior cingulate cortex

(ACC; D), parabrachial nucleus (PB, E), and the dentate gyus of the hippocampus (HP; F). An example of GFAP immunoreactivity in the PrL of an SR5 rats is shown in C. Data are shown as means + SEM for the LW (n = 14 to 16), SD (n = 3 or 4), SR2 (n = 8 or 9), SR5 (n = 7 or 8) and REC (n = 4 or 5) groups. GFAP density was obtained from the same analysis boxes used to assess Iba1 immunoreactivity (see Appendix D, Table D.1) and are expressed per section per side of the brain (average of 2 sections). CSR did not significantly change the percent GFAP-ir area in any of the brain regions examined (One-way ANOVAs).

APPENDIX D: IMMUNOHISTOCHEMICAL ANALYSES OF IBA1 IMMUNOREACTIVITY

Table D.1. Brain regions selected for analyses of Iba1 immunoreactivity.

Brain Region	AP Distance from Bregma (mm)[a]	n[b]	Analysis Area Size[c] (µm x µm)	Analysis Box/Circle/Oval Placement[c]
Prelimbic cortex (PrL)	A3.0–2.8	2	800 x 1100	Box placed with its dorsal segment 500 µm below the top of the forceps minor of the corpus callosum, and its medial segment at the midline of the brain
Anterior cingulate cortex (ACC)	A1.7–A0.7	2	800 x 1100	Box positioned with its dorsolateral segment touching the corpus callosum, and its medial segment at the midline of brain
Paraventricular hypothalamic nucleus (PVH), parvicellular	P1.6–P1.8	1	420 x 230	Oval positioned below the ventral surface of the dorsal cap of the PVH, and its most medial point lateral to the wall of the third ventricle
Central amygdala (CeA)	P1.9–P2.8	3	700 x 700	P1.9: Circle placed just dorsolateral to the commissural stria terminalis (cst) P2.8: Circle positioned lateral to the cst, with the midline of the circle placed in line with cst
Dentate gyrus (DG) of the dorsal hippocampus	P3.1–P3.3	2	1000 x 800	Box placed 200 µm from the medial tip of the DG to include both superior and inferior granular cell layers
Perifornical lateral hypothalamic area (PeF/LH)	P3.2–P3.4	2	700 x 550	Box centered in the PeF/LH, with the midline of its ventral segment bisecting the fornix
Dorsal raphe nucleus (DR)	P7.7–P7.9	2	1400 x 460	Box positioned in the middle of the DR just below the cerebral aqueduct
Lateral parabrachial nucleus (PB)	P9.1–P9.3	2	1000 x 250	Box centered in the lateral PB just above the superior cerebellar peduncle
Locus coeruleus (LC)	P9.5–P9.7	2	150 x 350	Box positioned in the center of the LC identified by its dense cluster of cells

				located ventrolateral to the fourth ventricle
Nucleus of the solitary tract (NTS)	P13.2–13.4	2	400 x 400	Circle positioned lateral to the fourth ventricle and medial to the solitary tract

Reprinted from Hall, S., Deurveilher, S., Robertson, G.S., Semba, K. Homeostatic state of microglia in a rat model of chronic sleep restriction, SLEEP, 2020, 1–16 and used by permission of Oxford University Press.

[a] Anterior-posterior (AP) levels given relative to bregma in mm [1].

[b] Number of sections analyzed in each brain region.

[c] Area sizes and placements were based on those previously described [2,3]. Each contour for analysis was placed within the brain region of interest using nuclei boundaries and landmarks according to the Paxinos and Watson rat brain atlas [1].

1. Paxinos G, Watson C. *The Rat Brain in Stereotaxic Coordinates: Compact Sixth Edition.* Elsevier; 2009.

2. Hall S, Deurveilher S, Ko KR, Burns J, Semba K. Region-Specific Increases in FosB/DeltaFosB Immunoreactivity in the Rat Brain in Response to Chronic Sleep Restriction. *Behav Brain Res.* 2017;322(Pt A):9-17.

3. Deurveilher S, Ryan N, Burns J, Semba K. Social and Environmental Contexts Modulate Sleep Deprivation-Induced c-Fos Activation in Rats. *Behav Brain Res.* 2013;256:238-249.

Table D.2. The number of Iba1-ir cells and the density of Iba1 immunoreactivity (percent Iba1-ir area) in brain regions for which there were no statistically significant effect of chronic sleep restriction.

		Treatment Group										
Brain Region	**Variable**	**LW**	n	**SD**	n	**SR2**	n	**SR5**	n	**REC**	n	**ANOVA**
ACC	Number of Iba1-ir cells	51.4±7.9	16	70.5±28.8	4	85.8±19.0	9	83.3±28.1	7	66.0±15.1	5	$F_{4,36}$=0.91 p=0.471
	Density of Iba1 immunoreactivity	13.2±1.4	16	15.8±4.2	4	16.6±2.8	9	15.0±2.5	7	17.9±3.4	5	$F_{4,36}$=0.28 p=0.887
PVH	Number of Iba1-ir cells	22.8±10.0	16	3.0±1.0	4	22.8±5.8	8	25.8±13.6	7	16.3±7.6	4	$F_{4,34}$=0.40 p=0.807
	Density of Iba1 immunoreactivity	29.5±3.5	16	15.3±5.0	4	32.0±4.5	8	32.9±5.8	7	32.0±7.2	4	$F_{4,34}$=1.29 p=0.295
DG	Number of Iba1-ir cells	98.9±15.2	16	81.5±15.7	4	129.3±22.1	9	168.2±35.4	8	120.7±26.1	5	$F_{4,37}$=1.69 p=0.172
	Density of Iba1 immunoreactivity	31.1±2.9	16	33.9±4.1	4	35.9±3.2	9	38.7±3.3	8	38.3±4.6	5	$F_{4,37}$=0.97 p=0.438
PB	Number of Iba1-ir cells	18.3±4.6	16	6.3±3.4	4	18.2±4.1	9	15.8±3.4	8	10.2±4.1	5	$F_{4,37}$=0.83 p=0.516
	Density of Iba1 immunoreactivity	18.8±2.0	16	13.4±3.5	4	21.5±2.5	9	15.6±2.2	8	19.9±5.3	5	$F_{4,37}$=1.02 p=0.408
LC	Number of Iba1-ir cells	16.8±4.0	14	13.3±4.2	3	20.6±3.9	9	16.5±4.1	7	9.5±2.7	3	$F_{4,31}$=0.52 p=0.720
	Density of Iba1 immunoreactivity	28.0±2.0	14	31.1±6.6	3	36.2±2.6	9	25.5±4.0	7	22.7±4.9	3	$F_{4,31}$=2.36 p=0.0752
NTS	Number of Iba1-ir cells	30.8±4.9	15	22.9±6.8	4	26.1±3.9	8	39.1±9.3	8	46.7±7.2	5	$F_{4,35}$=1.48 p=0.231
	Density of Iba1 immunoreactivity	26.2±1.7	15	28.6±4.7	4	25.8±2.0	8	29.6±2.1	8	31.5±3.9	5	$F_{4,35}$=0.90 p=0.473

Values represent means ± SEM of unilateral measures (cell counts and density) obtained from two adjacent sections (200 µm apart) in each brain region. Rats in the two time-matched locked wheel groups (LW2 and LW5) were combined into a single control group (LW) as there was no significant group difference for either variable in any of the brain regions examined ($p>0.05$). Within each treatment group, damaged tissue or missing sections resulted in a lower number of

animals (n) for the ACC, PVH, LC, and NTS. Although the density of Iba1 immunoreactivity in the LC showed a trend towards significance, the SR2 and SR5 groups were not significantly different from the LW control group. See Section 2.2.3 for further technical details. Abbreviations: see Appendix D, Table D.1. Reprinted from Hall, S., Deurveilher, S., Robertson, G.S., Semba, K. Homeostatic state of microglia in a rat model of chronic sleep restriction, SLEEP, 2020, 1–16 and used by permission of Oxford University Press.

APPENDIX E: IBA1 EXPRESSION IN THE FRONTAL CORTEX FOLLOWING CSR

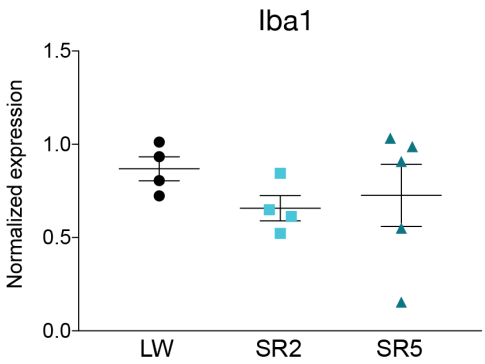

Figure E.1. Iba1 mRNA expression in the frontal cortex under CSR and control conditions. Mean (± SEM) normalized mRNA levels of Iba1 are shown for the LW (n = 4), SR1 (n = 4) and SR5 (n = 5) groups. Each symbol represents a rat. The two time-matched LW groups (LW2 and LW5) were combined into a single LW control group. Iba1 mRNA levels were not significantly affected by CSR.

APPENDIX F: MICROGLIA MORPHOLOGY IN THE PRELIMBIC CORTEX FOLLOWING CSR

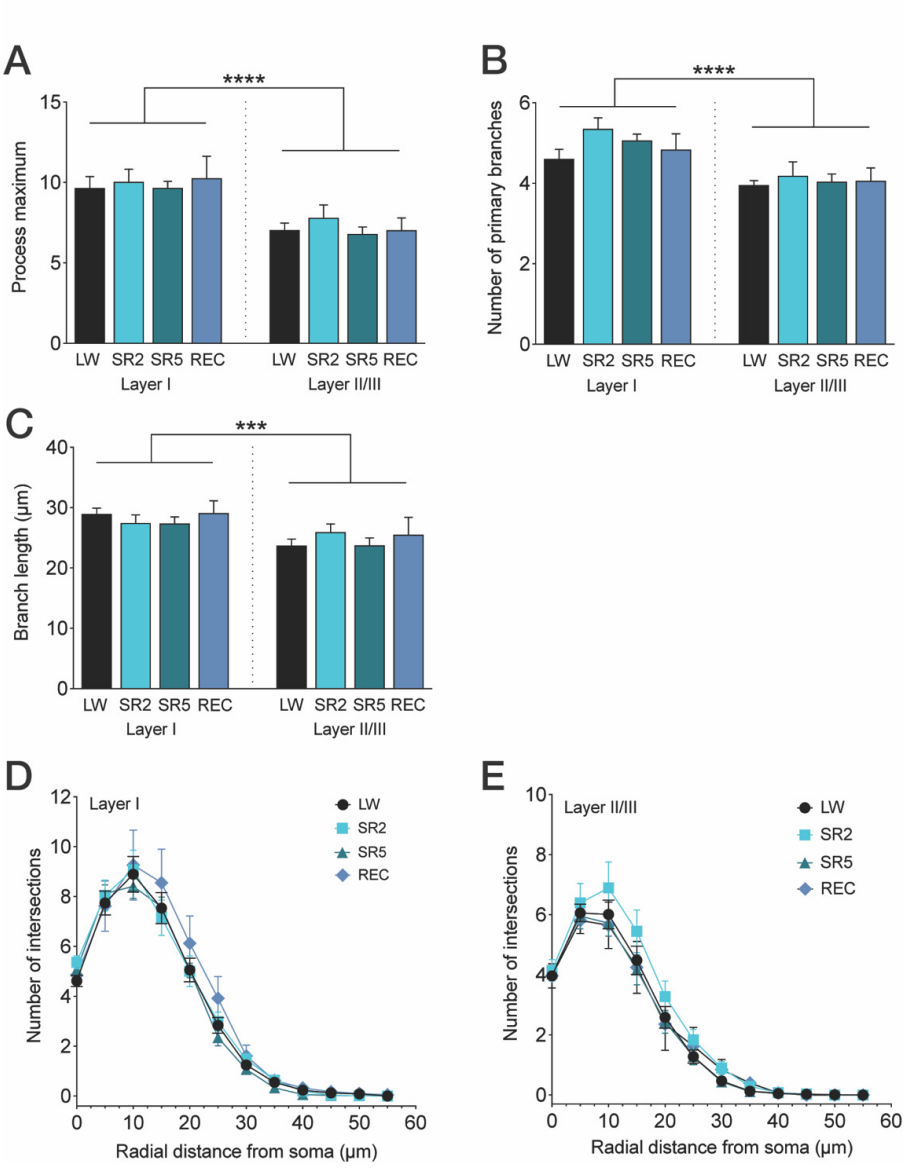

Figure F.1. Microglia morphology in layers I and II/III of the prelimbic cortex, which showed a significant increase in Iba1 immunoreactivity in response to CSR (see Figure 2.2). Mean values (± SEM) are shown for the LW (n = 9), SR2 (n = 9), and SR5 (n = 8) groups. Microglia (n = 8-

10/layer/rat) were randomly selected for Sholl analyses (see Chapter 2, Section 2.2.4 for further details). There was no significant effect of CSR on any parameters measured. However, the following parameters were significantly greater in layer I than in layer II/III across all treatment groups: process maximum (A), number of primary branches (B), the longest branch length (C), and number of intersections at increasing distance from the soma in layers I (D) and II/III (E). Additional measures are shown in Figure 2.3. ***$p<0.001$, ****$p<0.0001$ (main effect of Layer, two-way repeated ANOVA).

APPENDIX G: BLOOD-BRAIN BARRIER PERMEABILITY IN THE PRELIMBIC CORTEX (PRL) AFTER CSR ASSESSED USING EVANS BLUE DYE AND SODIUM FLUORESCEIN: A PILOT STUDY

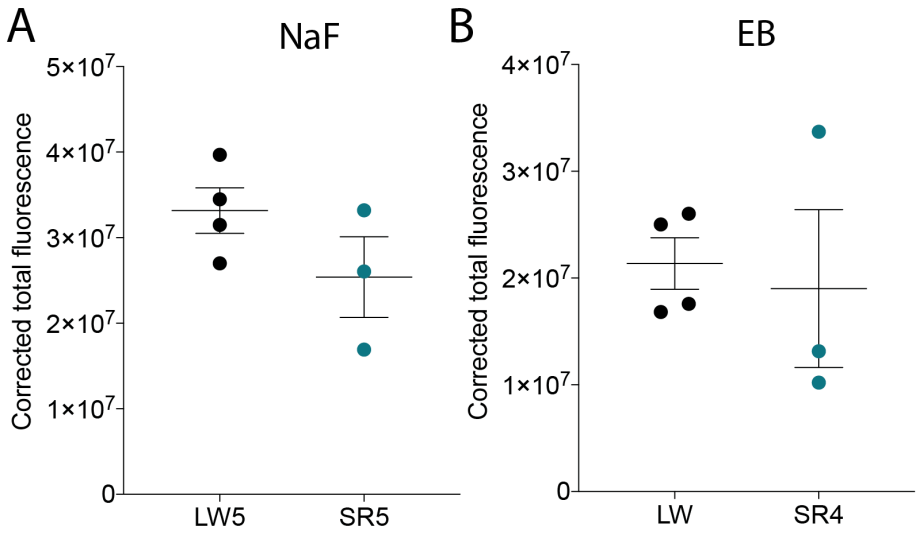

Figure G.1. Sodium fluorescein (NaF) and Evans Blue dye (EB) corrected total fluorescence in the PrL following CSR. Corrected total fluorescence values are expressed per section per side of the brain (2 sections per rat; see Section 2.2.6.1 for further details) and are shown as means ± SEM for the LW5 (n = 4) and SR5 (n = 3) groups and are expressed per section per side of the brain (2 sections analyzed per rat). CSR did not significantly change either NaF or EB fluorescence in the PrL (Student's t-test).

APPENDIX H: RAT BODY WEIGHTS

Table H.1. Body weights in all treatment groups for Chapter 2, Experiment 1 (Iba1 immunohistochemistry) and Experiment 2 (Microglia morphology).

Treatment Group	n	Initial Body Weight (g)	Final Body Weight (g)	Change in Body Weight (%)
LWD	3	408 ± 2	419 ± 4	+2.7 ± 0.4
SD	4	424 ± 19	432 ± 17	+1.8 ± 1.4
LW2	5	438 ± 13	454 ± 15	+3.7 ± 0.7
SR2	9	431 ± 16	415 ± 12	-3.3 ± 1.4**
LW5	4	418 ± 17	457 ± 13	+9.5 ± 1.4
SR5	8	421 ± 15	387 ± 12	-7.7 ± 2.3***
LWR	4	349 ± 13	426 ± 21	+22 ± 3.4
REC	5	358 ± 9	391 ± 11	+9.2 ± 3.6*

All values are reported as means ± SEM. Rats underwent either 3 h (SD), 27 h (SR2), or 99 h (SR5) of the 3/1 CSR protocol, or 99 h followed by 6 days of recovery (REC). Animals in the LWD, LW2, LW5, and LWR control groups were housed in locked wheels for a time period matched to that of their respective sleep-restricted group. The initial body weight of each rat was recorded on the last day of habituation before the start of experimental protocols. The final body weights were recorded at the end of the respective protocols. Change (%) in body weight was calculated in each rat and averaged in each group. *$p<0.05$, **$p<0.01$, ***$p<0.001$ vs. respective locked wheel control group (unpaired t-tests).

Table H.2. Chapter 2: Body weights in the LW5 and SR5 groups for Chapter 2, Experiment 3 (Microglia proliferation).

Treatment Group	n	Initial Body Weight (g)	Final Body Weight (g)	Change in Body Weight (%)
LW5	8	367 ± 16	404 ± 14	+10.5 ± 2.3
SR5	8	374 ± 10	353 ± 9	-5.4 ± 1.2****

All values are reported as means ± SEM. See Appendix H, Table H.1. for further details.

****p<0.0001 vs. LW5 (unpaired t-test).

Table H.3. Chapter 2: Body weights in the LW5 and SR5 groups for Chapter 2, Experiment 4 (Blood-brain barrier permeability).

Treatment Group	n	Initial Body Weight (g)	Final Body Weight (g)	Change in Body Weight (%)
LW5	6	384 ± 12	404 ± 17	+5.1 ± 3.4
SR5	6	364 ± 21	325 ± 17	-10.5 ± 6.2***

All values are reported as means ± SEM. See Appendix H, Table H.1 for further details.

***p<0.001 vs. LW5 (unpaired t-test).

Table H.4. Body weights in the LW2, SR2, LW5, and SR5 groups for Chapter 3, Experiment 1 (Cytokine mRNA expression).

Treatment Group	n	Initial Body Weight (g)	Final Body Weight (g)	Change in Body Weight (%)
LW2	2	375 ± 12	396 ± 6	+5.5 ± 1.9
SR2	4	367 ± 5.6	351 ± 10	-4.3 ± 1.8*
LW5	2	343 ± 15	386 ± 18	+12.5 ± 0.3
SR5	5	351 ± 7	353 ± 5	+0.7 ± 1.6**

All values are reported as means ± SEM. Rats underwent either 27 h (SR2) or 99 h (SR5) of the 3/1 CSR protocol. Animals in the LW2 and LW5 control groups were housed in locked wheels for a time period matched to that of their respective sleep-restricted group. The initial body weight of each rat was recorded on the last day of habituation before the start of experimental protocols. The final body weights were recorded at the end of the respective protocols. Change (%) in body weight was calculated in each rat and averaged in each group. *$p<0.05$ vs. LW2, **$p<0.01$ vs. LW5 (unpaired t-tests).

Table H.5. Body weights in the LW2, SR2, LW5, and SR5 groups for Chapter 3, Experiment 2 (inflammatory microglia phenotype).

Treatment Group	n	Initial Body Weight (g)	Final Body Weight (g)	Change in Body Weight (%)
LW2	1	405	420	+3.7
SR2	3	407 ± 17	407 ± 17	+0.1 ± 2.2
LW5	2	408 ± 8	437 ± 12	+7.3 ± 1.0
SR5	3	393 ± 2	352 ± 16	-10.4 ± 4.1*

All values are reported as means ± SEM (except for the LW2 group). See Appendix H, Table H.1 for further details. *$p<0.05$ vs. LW5 (unpaired t-test).

Table H.6. Body weights in the EC, LW2, SR2, LW5, and SR5 groups for Chapter 3 Experiment 3 (homeostatic microglia phenotype) and Chapter 4 (microglia apposition).

Treatment Group	n	Initial Body Weight (g)	Final Body Weight (g)	Change in Body Weight (%)
EC	9	369 ± 6	393 ± 8	+6.7 ± 0.6
LW2	4	416 ± 8$^{\#}$	430 ± 6	+3.4 ± 0.7
SR2	9	407 ± 5$^{\#}$	400 ± 6*	-1.7 ± 1.2$^{*,\#}$
LW5	4	402 ± 12$^{\#}$	437 ± 14	+8.6 ± 0.9
SR5	9	393 ± 3$^{\#}$	372 ± 9*	-5.3 ± 2.1$^{*,\#}$

All values are reported as means ± SEM. See Appendix H, Table H.1 for details. Animals in the EC group were housed in unlocked wheels the rats could rotate freely. Rats in the EC group had a smaller initial body weight compared to the other four treatment groups; this difference was likely due to the availability of unlocked wheels for voluntary wheel running during the habituation period. $^{\#}$ Different from EC; *Different from respective LW control group ($p<0.05$, Fischer's LSD post-hoc tests).

APPENDIX I: PRIMER SEQUENCES USED FOR QRT-PCR

Table I.1. Primer sequences used for qRT-PCR.

Gene	Forward primer	Reverse primer	Length (bp)	GenBank Accession
Iba1	GCCTCATCGTCATCTCCCCA	AGGAAGTGCTTGTTGATCCCA	142	NM_017196.3
IL1β	CCCTGCAGCTGGAGAGTGTGG	TGTGCTCTGCTTGAGAGGTGCT	153	NM_031512.2
IL6	CCCAACTTCCCAATGCTCTCCTA	GCTTTCAAGATGAGTTGGATGGT	88	NM_012589.2
IL10	GGGAGAGAAGCTGA AGACCC	GTCCAGTAGATGCCGGGTG	223	NM_012854.2
TNFα	GACCCTCACACTCAGATCATCTTCT	TGCTACGACGTGGGCTACG	64	NM_012675.3
β2M	CGAGACCGATGTATATGCTTGC	GTCCAGATGATTCAGAGCTCCA	114	NM_012512.2
GAPDH	ATGATTCTACCCACGGCAAG	CTGGAAGATGGTGATGGGTT	89	M17701.1
HPRT	CCCAGCGTCGTGATTAGTGATG	TTCAGTCCTGTCCATAATCAGTCC	126	NM_012583.2

β2M, β2-microglobulin; GAPDH, Glyceraldehyde 3-phosphate dehydrogenase; HPRT, hypoxanthine phosphoribosyl transferase; Iba1, ionized calcium-binding adaptor molecule-1; IL1β, interleukin-1β; IL6, interleukin-6; IL10, interleukin-10; TNFα, tumor necrosis factor-α.

APPENDIX J: IBA1 AND P2Y12 IMMUNOFLUORESCENCE IN RESPONSE TO CSR

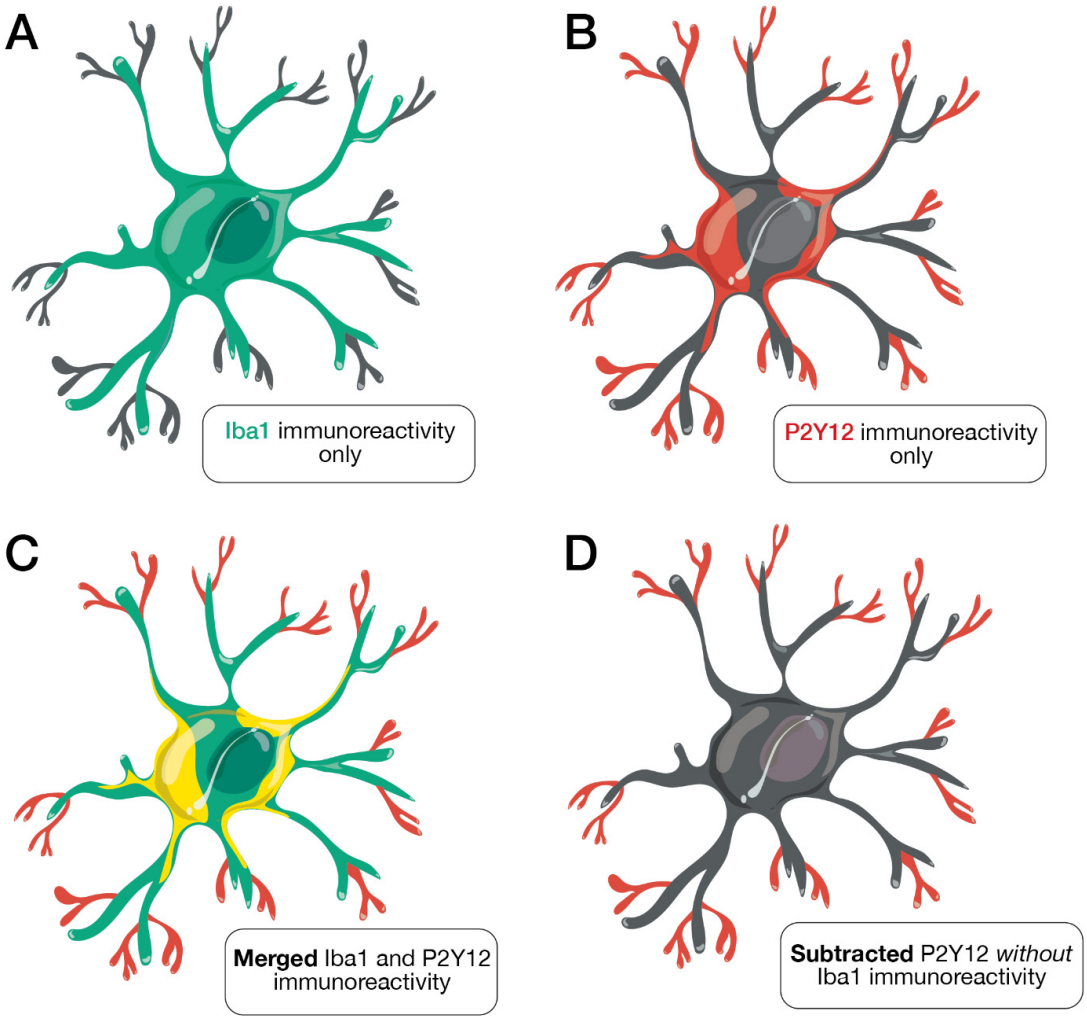

Figure J.1 Conceptual illustration of microglia immunostained for the microglia markers Iba1 (green) and P2Y12 (red). Four measures of the density of Iba1 and/or P2Y12 immunoreactivity were taken: (A) the density of total Iba1 immunoreactivity only, (B) the density of total P2Y12 immunoreactivity only, (C) the density of merged Iba1 and P2Y12 immunoreactivity (i.e., including overlapping [yellow] or non-overlapping [green or red] immunopositive areas), and

(D) the density of P2Y12 immunoreactivity without Iba1 co-localization using a subtracted image.

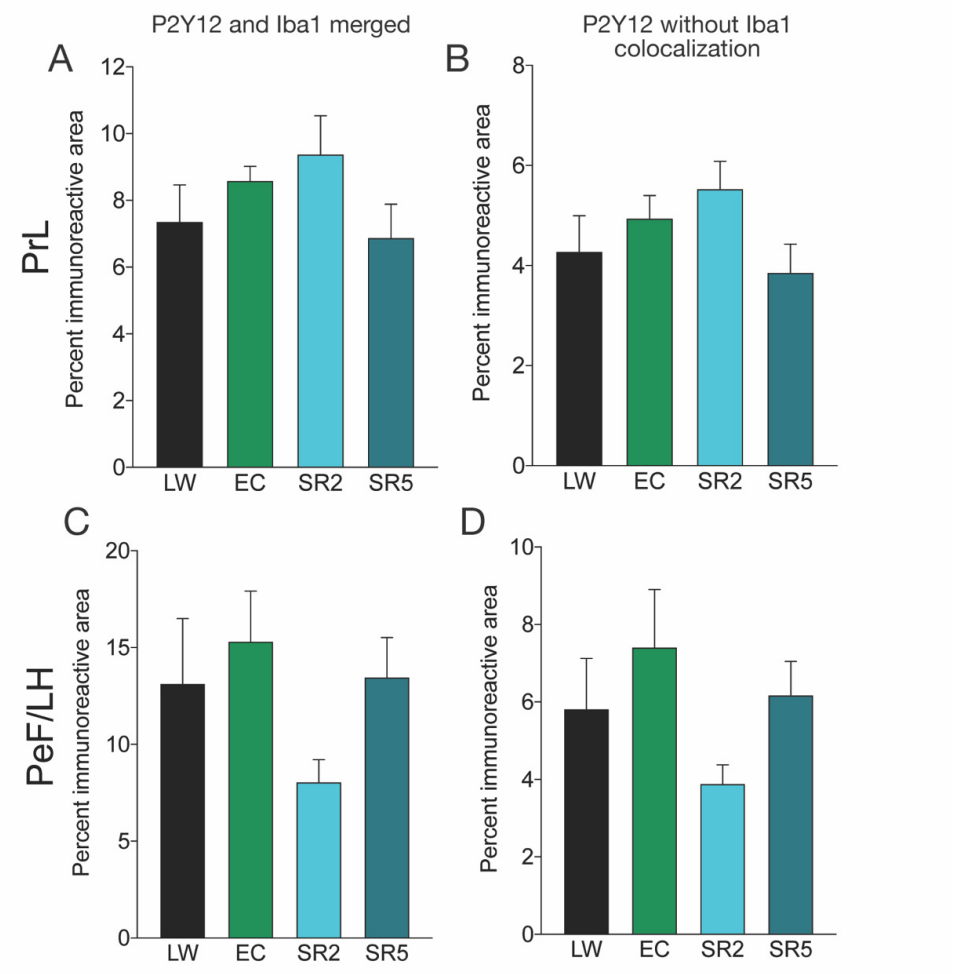

Figure J.2. The density (percent immunoreactive area) of Iba1 and P2Y12 merged (A,C) and P2Y12 excluding Iba1 (B,D) in the prelimbic cortex (PrL; A,B) and perifornical lateral hypothalamic area (PeF/LH; C,D) in the control groups (LW and EC) and following CSR (SR2 and SR5).

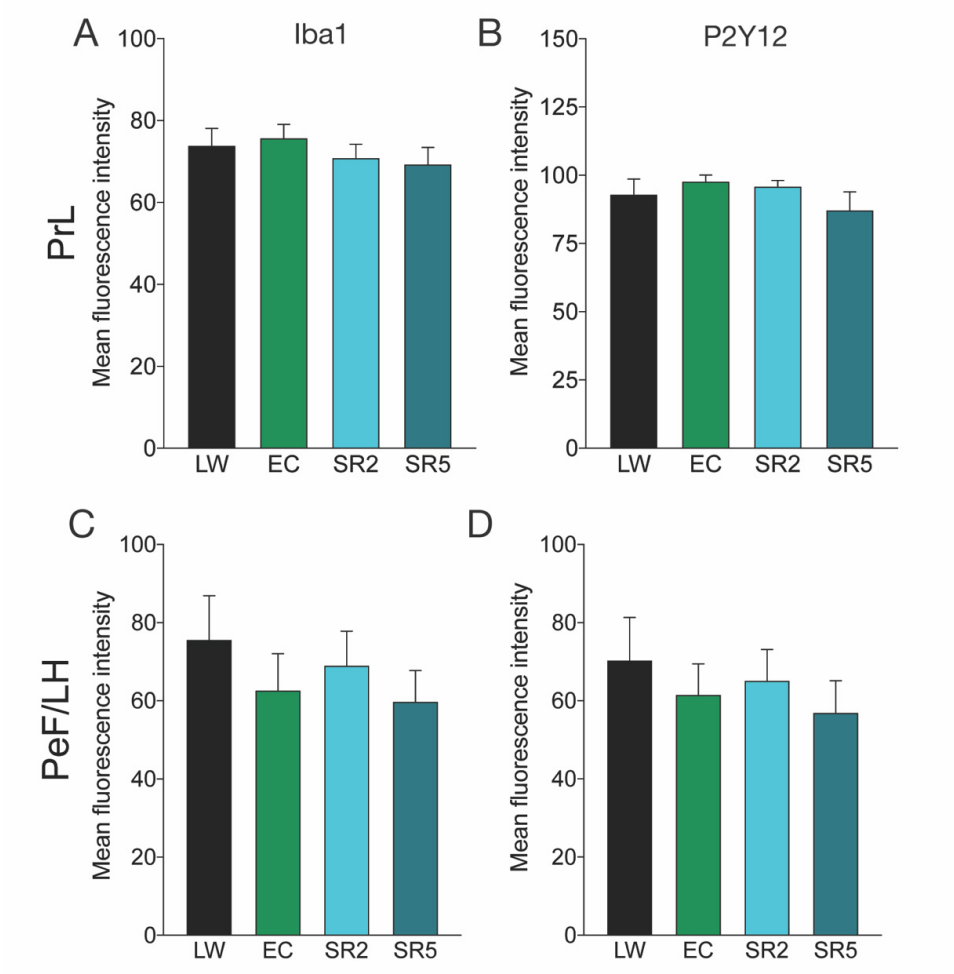

Figure J.3. The mean fluorescence intensity of Iba1- (A,C) and P2Y12-ir (B,D) area in the prelimbic cortex (PrL; A,B) and the perifornical lateral hypothalamic area (PeF/LH; C,D) in the control groups (LW and EC) and following CSR (SR2 and SR5).

APPENDIX K: SOMATIC CONTOUR LENGTH OF MCH AND ORX NEURONS IN THE LATERAL HYPOTHALAMUS

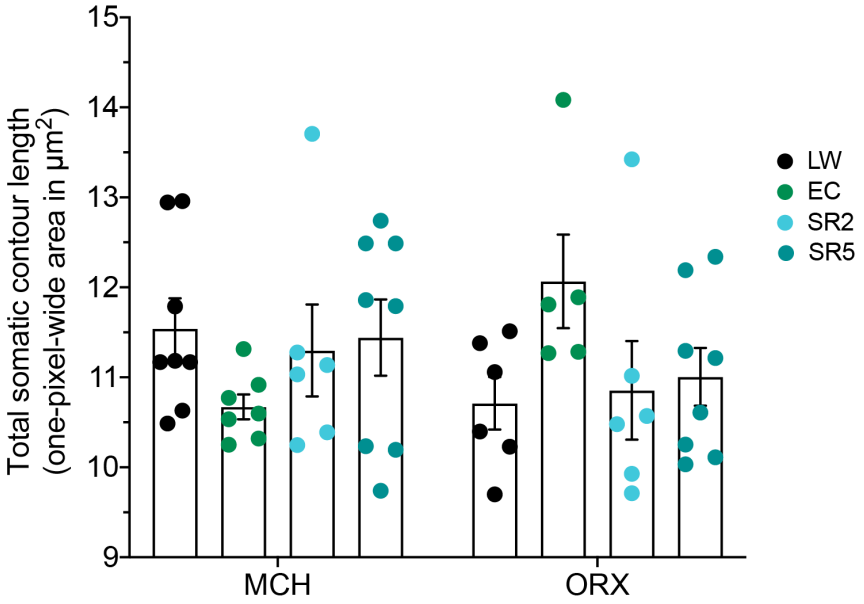

Figure K.1. The total somatic contour length of MCH (*left*) and ORX (*right*) neurons in the PeF/LH following CSR. The total somatic contour length was measured as the area (μm^2) occupied by the one-pixel-wide somatic contour (see section 4.2.6 for further details). The LW2 and LW5 control groups were combined into a single LW control group. Each symbol represents a rat. Data are shown as means ± SEM for the LW (n = 6–8), EC (n = 5–7), SR2 (n = 6), and SR5 (n = 8) groups. No significant change in the total somatic contour of MCH or ORX neurons was found following CSR, and no significant difference was found between neuronal phenotypes (Mixed Effects Model).

APPENDIX L: AVERAGE NUMBER OF DAILY WHEEL ROTATIONS IN THE EXERCISE CONTROL GROUP

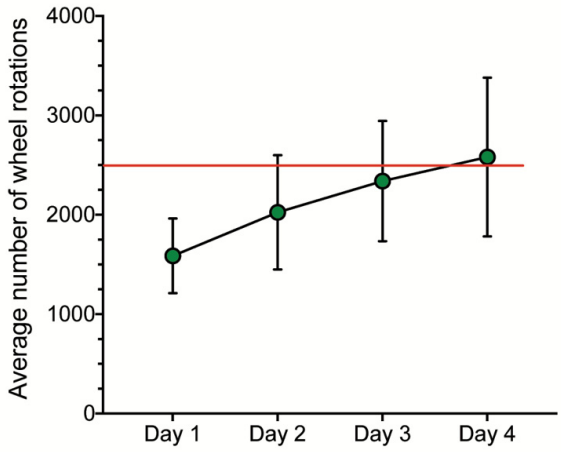

Figure L.1. The average number of daily wheel rotations (mean ± SEM) of animals in the EC group (n = 9). Rats in the EC group were housed in unlocked wheels which they could rotate freely for a time period matched to the SR5 group (i.e., 10 days, including habituation). The average daily number of wheel rotations is shown for the last 4 days of the protocol (Day 1−4, corresponding to SR1−4 in the SR5 group). The red line indicates the number of daily rotations imposed on rats in the SR2 and SR5 groups (2,454 rotations).

APPENDIX M: COPYRIGHT PERMISSIONS

OXFORD UNIVERSITY PRESS LICENSE
TERMS AND CONDITIONS

Jul 03, 2020

This Agreement between Shannon Hall ("You") and Oxford University Press ("Oxford University Press") consists of your license details and the terms and conditions provided by Oxford University Press and Copyright Clearance Center.

License Number	4861371423730
License date	Jul 03, 2020
Licensed content publisher	Oxford University Press
Licensed content publication	SLEEP
Licensed content title	Homeostatic state of microglia in a rat model of chronic sleep restriction
Licensed content author	Hall, Shannon; Deurveilher, Samüel
Licensed content date	Jun 1, 2020
Type of Use	Thesis/Dissertation
Institution name	
Title of your work	Microglia Responses in a Rat Model of Chronic Sleep Restriction

Publisher of your work	Dalhousie University
Expected publication date	Jul 2020
Permissions cost	0.00 CAD
Value added tax	0.00 CAD
Total	0.00 CAD
Title	Microglia Responses in a Rat Model of Chronic Sleep Restriction
Institution name	Dalhousie University
Expected presentation date	Jul 2020
Portions	Figures 1, 3, 4, 5, 7, Supplementary Figure 2, Supplementary Tables 1, 2, 3, 6, 7, 8, 9
Requestor Location	Shannon Hall 5850 College Street PO Box 15000 Room 13MN Halifax, NS B3H4R2 Canada Attn: Shannon Hall
Publisher Tax ID	GB125506730
Total	0.00 CAD

Terms and Conditions

STANDARD TERMS AND CONDITIONS FOR REPRODUCTION OF MATERIAL FROM AN OXFORD UNIVERSITY PRESS JOURNAL

1. Use of the material is restricted to the type of use specified in your order details.

2. This permission covers the use of the material in the English language in the following territory: world. If you have requested additional permission to translate this material, the terms and conditions of this reuse will be set out in clause 12.

3. This permission is limited to the particular use authorized in (1) above and does not allow you to sanction its use elsewhere in any other format other than specified above, nor does it apply to quotations, images, artistic works etc that have been reproduced from other sources which may be part of the material to be used.

4. No alteration, omission or addition is made to the material without our written consent. Permission must be re-cleared with Oxford University Press if/when you decide to reprint.

5. The following credit line appears wherever the material is used: author, title, journal, year, volume, issue number, pagination, by permission of Oxford University Press or the sponsoring society if the journal is a society journal. Where a journal is being published on behalf of a learned society, the details of that society must be included in the credit line.

6. For the reproduction of a full article from an Oxford University Press journal for whatever purpose, the corresponding author of the material concerned should be informed of the proposed use. Contact details for the corresponding authors of all Oxford University Press journal contact can be found alongside either the abstract or full text of the article concerned, accessible from www.oxfordjournals.org Should there be a problem clearing these rights, please contact journals.permissions@oup.com

7. If the credit line or acknowledgement in our publication indicates that any of the figures, images or photos was reproduced, drawn or modified from an earlier source it will be necessary for you to clear this permission with the original publisher as well. If this permission has not been obtained, please note that this material cannot be included in your publication/photocopies.

8. While you may exercise the rights licensed immediately upon issuance of the license at the end of the licensing process for the transaction, provided that you have disclosed complete and accurate details of your proposed use, no license is finally effective unless and until full payment is received from you (either by Oxford University Press or by Copyright Clearance Center (CCC)) as provided in CCC's Billing and Payment terms and conditions. If full payment is not received on a timely basis, then any license preliminarily granted shall be deemed automatically revoked and shall be void as if never granted. Further, in the event that you breach any of these terms and conditions or any of CCC's Billing and Payment

terms and conditions, the license is automatically revoked and shall be void as if never granted. Use of materials as described in a revoked license, as well as any use of the materials beyond the scope of an unrevoked license, may constitute copyright infringement and Oxford University Press reserves the right to take any and all action to protect its copyright in the materials.

9. This license is personal to you and may not be sublicensed, assigned or transferred by you to any other person without Oxford University Press's written permission.

10. Oxford University Press reserves all rights not specifically granted in the combination of (i) the license details provided by you and accepted in the course of this licensing transaction, (ii) these terms and conditions and (iii) CCC's Billing and Payment terms and conditions.

11. You hereby indemnify and agree to hold harmless Oxford University Press and CCC, and their respective officers, directors, employs and agents, from and against any and all claims arising out of your use of the licensed material other than as specifically authorized pursuant to this license.

12. Other Terms and Conditions:

v1.4

Questions? customercare@copyright.com or +1-855-239-3415 (toll free in the US) or +1-978-646-2777.